A New Library of Stellar Model Atmospheres and Spectra

DAVID JONATHAN HYDER

A thesis submitted in partial fulfilment of the requirements of Liverpool John Moores University for the degree of Master of Philosophy

March 2019

Declaration

The work presented in this thesis was carried out at the Astrophysics Research Institute, Liverpool John Moores University. Unless otherwise stated, it is the original work of the author.

While registered as a candidate for the degree of Master of Philosophy, for which submission is now made, the author has not been registered as a candidate for any other award. This thesis has not been submitted in whole, or in part, for any other degree.

David Hyder
Astrophysics Research Institute
Liverpool John Moores University
146 Brownlow Hill
Liverpool
L3 5RF
UK

Abstract

The information we can gather about chemical composition and evolutionary status of stars comes from the detection and analysis of the photons that are emitted, and comparisons with theoretical predictions. The relative abundances of elements within the Sun provide the baseline against which the elemental abundances of all other stars, galaxies and the interstellar medium are based upon. Libraries of model atmospheres and stellar spectra have been previously computed using ATLAS9 based upon the solar metallicity and chemical composition values calculated by Grevesse & Sauval (1998), used as the standard until Asplund *et al.* (2009) produced a new determination of the chemical composition of the Sun. This new value for the total metallicity of the Sun is lower than that which was previously determined, and the abundances of elements such as carbon, oxygen and nitrogen are different, which has significant implications for the analysis of the spectroscopy of stellar populations.

In this project new opacity distribution functions have been calculated using the Asplund *et al* (2009) abundances for several metallicities ranging from -2.5 to +0.5, and these have been used to produce new grids of ATLAS9 model atmospheres and synthetic spectra for stars with effective temperatures of 3500 K to 100000 K and log g from 0.0 dex to 0.5 dex, for both normal and alpha enhanced stars. Comparisons of the synthetic spectra produced by the old and new models show that there is very little difference in the energy distribution in stars hotter than 4500 K. Investigations into the bolometric corrections and colour indices show some differences with the U-B, B-V and u-b indices from the new ODFs being slightly redder for effective temperatures below 4500K, but above this there are no significant differences. Comparisons between the bolometric corrections and colour indices calculated using the new abundances and the empirically derived values show a good general agreement for main sequence stars regardless of the metallicity, but less so for giant stars.

Acknowledgements

I would like to sincerely offer my thanks to my supervisor Maurizio Salaris for his support over the years and also to Alessio Mucciarelli for his invaluable assistance and guidance with the installation and usage of the ATLAS9 software; their input was extremely useful and much appreciated. I would also like to thank my thesis examiners, Andrew Newsam, Santi Cassisi and Emanuele Dalessandro for their insightful comments and questions.

I would also like to extend my thanks to Elaine Hyder for her continued support during the course of this project.

Contents

Declaration	ii
Abstract	iii
Acknowledgements	iv
List of Figures	vi
List of Tables	ix
Chapter 1: Introduction	1
Chapter 2: ATLAS9 and the production of synthetic spectra	10
Chapter 3: Comparisons of old and new synthetic spectra	27
Chapter 4: Comparisons of bolometric corrections and colours	47
Chapter 5: Conclusions and Further Work	78
References	80

List of Figures

2.1.1. Schematic absorption coefficient of overlapping spectral lines. 12

2.1.2. Schematic ODF of the spectrum shown in figure 2.1.1. 12

2.5.1. Grid showing the log g and Teff (K) values of each calculated model at [Fe/H]=0.0. 21

2.5.2. Grid showing the log g and Teff (K) values of each calculated model at [Fe/H]=-2.0. 21

3.2.1. Comparison of fluxes from the old ODF and the new ODF model with parameters T_{eff}=40000 K, logg=4.0, [Fe/H]=0.0. 29

3.2.2. Comparison of fluxes from the old ODF and the new ODF model with parameters T_{eff}=20000 K, logg=4.5, [Fe/H]=0.0. 30

3.2.3. Comparison of fluxes from the old ODF and the new ODF model with parameters T_{eff}=20000 K, logg=3.0, [Fe/H]=0.0. 31

3.2.4. Comparison of fluxes from the old ODF and the new ODF model with parameters T_{eff}=10000 K, logg=4.5, [Fe/H]=0.0. 32

3.2.5. Comparison of fluxes from the old ODF and the new ODF model with parameters T_{eff}=10000 K, logg=3.0, [Fe/H]=0.0. 33

3.2.6. Comparison of fluxes from the old ODF and the new ODF model with parameters T_{eff}=8000 K, logg=1.0, [Fe/H]=0.0. 34

3.2.7. Comparison of fluxes from the old ODF and the new ODF model with parameters T_{eff}=6000 K, logg=4.5, [Fe/H]=0.0. 35

3.2.8. Comparison of fluxes from the old ODF and the new ODF model with parameters T_{eff}=45000 K, logg=5.0, [Fe/H]=0.0. 36

3.2.9. Comparison of fluxes from the old ODF and the new ODF model with parameters T_{eff}=4000 K, logg=4.5, [Fe/H]=0.0. 37

3.2.10. Comparison of fluxes from the old ODF and the new ODF model with parameters T_{eff}=4000 K, logg=3.0, [Fe/H]=0.0. 38

3.2.11. Comparison of fluxes from the old ODF and the new ODF model with parameters T_{eff}=4000 K, logg=1.0, [Fe/H]=0.0. 39

3.2.12. Comparison of fluxes from the old ODF and the new ODF model with parameters T_{eff}=3500 K, logg=4.5, [Fe/H]=0.0. 40

3.2.13. Comparison of fluxes from the old ODF and the new ODF model with 41

parameters T_{eff}=3500 K, logg=4.5, [Fe/H]=0.0.

3.2.14. Comparison of fluxes from the old ODF and the new ODF model with parameters T_{eff}=3500 K, logg=4.5, [Fe/H]=0.0. 42

3.3.1. Comparison of fluxes from the old alpha enhanced ODF and the new alpha enhanced ODF model with parameters T_{eff}=4500 K, logg=5.0, [Fe/H]=0.0. 43

3.3.2. Comparison of fluxes from the old ODF and the new ODF model with parameters T_{eff}=5500 K, logg=4.5, [Fe/H]=-1.0. 44

3.3.3. Comparison of fluxes from the old ODF and the new ODF model with parameters T_{eff}=5750 K, logg=4.5, [Fe/H]=-2.5. 45

3.3.4. Comparison of fluxes from the old ODF and the new ODF model with parameters T_{eff}=8000 K, logg=2.5, [Fe/H]=-2.5. 46

4.0.1. Response functions for filters of various photometric systems. 49

4.2.1. Johnson T_{eff}-colour relations for old ODF and new ODF models with parameters logg=4.5 and [Fe/H]=0.0. 53

4.2.2. Stromgren T_{eff}-colour relations for old ODF and new ODF models with parameters logg=4.5 and [Fe/H]=0.0. 55

4.2.3. f300w filter T_{eff}-colour relations for old ODF and new ODF models with parameters logg=4.5 and [Fe/H]=0.0. 55

4.2.4. Johnson T_{eff}-colour relations for old ODF and new ODF models with parameters logg=1.5 and [Fe/H]=0.0. 57

4.2.5. Stromgren T_{eff}-colour relations for old ODF and new ODF models with parameters logg=1.5 and [Fe/H]=0.0. 58

4.3.1. T_{eff}-colour relations for new ODF, new alpha enhanced ODF models and empirical data with parameters logg=4.5 and [Fe/H]=0.0. 64

4.3.2. T_{eff}-colour relations for new ODF, new alpha enhanced ODF models and empirical data with parameters logg=3.0 and [Fe/H]=0.0. 65

4.3.3. T_{eff}-colour relations for new ODF, new alpha enhanced ODF models and empirical data with parameters logg=1.5 and [Fe/H]=0.0. 66

4.3.4. T_{eff}-colour relations for new ODF, new alpha enhanced ODF models and empirical data with parameters logg=0.0 and [Fe/H]=0.0. 67

4.3.5. T_{eff}-colour relations for new ODF, new alpha enhanced ODF models and empirical data with parameters logg=4.5 and [Fe/H]=-1.0. 68

4.3.6. T_{eff}-colour relations for new ODF, new alpha enhanced ODF models and empirical data with parameters logg=3.0 and [Fe/H]=-1.0. 69

4.3.7. T_{eff}-colour relations for new ODF, new alpha enhanced ODF models and empirical data with parameters logg=1.5 and [Fe/H]=-1.0. 70

4.3.8. T_{eff}-colour relations for new ODF, new alpha enhanced ODF models and empirical data with parameters logg=0.0 and [Fe/H]=-1.0. 71

4.3.9. T_{eff}-colour relations for new ODF, new alpha enhanced ODF models and empirical data with parameters logg=4.5 and [Fe/H]=-2.0. 72

4.3.10. T_{eff}-colour relations for new ODF, new alpha enhanced ODF models and empirical data with parameters logg=3.0 and [Fe/H]=-2.0. 73

4.3.11. T_{eff}-colour relations for new ODF, new alpha enhanced ODF models and empirical data with parameters logg=1.5 and [Fe/H]=-2.0. 74

4.3.12. T_{eff}-colour relations for new ODF, new alpha enhanced ODF models and empirical data with parameters logg=0.0 and [Fe/H]=-2.0. 75

List of Tables

2.4.1. Metallicity number density values from Grevesse & Sauval (1998) and Asplund *et al.* (2009). 18

2.4.2. Values for alpha enhanced elements. 19

2.4.3. X, Y and Z values for each global metallicity of the solar mixture and alpha enhanced mixture. 19

2.5.1. Grid of models for the new scaled solar metallicity. 22-23

2.5.2. Grid of models for the new alpha enhanced metallicity. 24-25

4.1.1. Comparisons of Johnson-Cousins-Bessell colour relations of a synthetic Solar star created using the new and old chemical abundances. 50

4.1.2. Comparisons of Strömgren colour relations of a synthetic Solar star created using the new and old chemical abundances. 51

4.2.1. Comparisons of Johnson-Cousins-Bessell colour relations of sample synthetic spectra for main sequence stars created using the new and old chemical abundances. 52

4.2.2. Comparisons of Strömgren colour relations of sample synthetic spectra for main sequence stars created using the new and old chemical abundances. 54

Chapter 1

Introduction

1.1 Stellar Modelling

A detailed understanding of stars is of vital importance in astrophysics, and the modelling and observation of stars is of fundamental significance in studying both the nature of the stars themselves and the larger systems that they occur in, such as galaxies and globular clusters, and the way that these systems evolve over time.

The information we can gather about chemical composition and evolutionary status of stars comes from the detection and analysis of the photons that are emitted, and the comparisons of this empirical data with theoretical predictions. Stars emit a continuous featureless blackbody spectrum of photons from their photosphere, the deepest visible layer. The photosphere is surrounded by a thinner, optically thin, atmosphere and the chemical elements present within these layers produce absorption lines that show up in the observed flux distribution superimposed over the continuous spectrum emitted by the photosphere. The theoretical modelling of these atmospheric layers is therefore a crucial part of the tools aimed at understanding the evolution of cosmic structures such as star clusters and galaxies.

Theoretical studies of stellar populations make use of both stellar evolution models and stellar model atmospheres. In stellar evolution models the evolution of a star with a specified initial mass and chemical composition can be calculated by solving the equations of stellar structure and evolution (e.g. Salaris & Cassisi, 2005). The output of these models is the prediction of the physical (pressure, temperature and density) and chemical (abundances of chemical elements) quantities at each layer of the model, from the core to

the photosphere, and the changes of these quantities over time. These can then be compared with the observations taken of real stars, based on the detection and analysis of the photons that they emit.

To permit the comparison of the observed data and the theoretical predictions, the luminosity and effective temperature created by the output of stellar models needs to be converted into the magnitudes and colours observed from real stars, and this conversion can be calculated by using bolometric corrections and effective temperature-colour relationships (Girardi *et al.,* 2002).

Once the properties of a model star have been calculated, or the characteristics of a real star observed, then the star can be positioned on a Colour Magnitude Diagram (CMD) – this is a plot of the magnitude of the star in a given photometric band versus the difference between the magnitudes in two different photometric bands. The difference between the apparent magnitudes of a single star in two different bands is termed the colour index.

Model atmosphere calculations, on the other hand, predict physical and chemical quantities throughout the atmospheric layers, starting from the photosphere, for a specified photospheric chemical composition, effective temperature and surface gravity (that is determined by the mass and radius of the underlying stellar model). Once the model atmosphere structure is calculated, one can calculate the outgoing spectrum of photons, that include all spectral lines produced by the atomic transitions of the ions (and eventually molecules) present in the atmospheric layers. It is important to notice that stellar evolution and model atmosphere calculations employ different sets of equations because of the necessarily different treatment of radiative transport, due to the different temperature/density regime of the atmospheric layers compared to the stellar interior and the lack of energy generation and negligible mass in the atmospheres.

Once these calculations are available it is then possible to predict the detailed spectrum of a star, and from this the magnitude, bolometric correction and colour of that star in a given photometric band. This can be then done for, in principle, any system of photometric filters, for any age or combination of ages of stellar populations, and this can then produce a library of stellar spectra that can be used for a variety of purposes.

Although they can be limited by the parameters and assumptions used, producing a stellar synthetic spectral library has a number of advantages over using an empirical library; they are less limited in the wavelength covered and the spectral resolution, and can cover different physical and chemical compositions of stars (Husser *et al.*, 2013). The majority of the current spectral libraries used are based on the model atmospheres that were created by Kurucz (1970) and specific spectral libraries, such as MARCS for late-type model atmospheres (Gustafsson *et al.*, 2008) and one based on the PHOENIX code, have been created for comparisons with specific sets of observations taken from X-Shooter on the VLT and CRIRES (Husser *et al.*, 2013). The TLUSTY code has been used to create grids of stellar models and synthetic spectra for one-dimensional, plane-parallel, non-LTE hot stars with effective temperatures of over 10,000 K (Lanz & Hubeny, 2003) which has more recently been expanded to cover cooler stars (Hubeny & Lanz, 2017).

There are two main shortcomings of current theoretical model atmospheres (Salaris & Cassisi, 2005); the accuracy of the stellar spectra produced, and approximations used in calculating the energy transport. In the first case, although the broad features of stars with solar chemical compositions can be reproduced to a reasonable degree; there are differences in both the number and relative strength of the spectral lines when compared to the Sun. While this will have less of an impact in the calculation of broadband colours, when considering narrowband filters these differences in individual metallic lines can have a significant effect on the bolometric corrections. With regard to the second shortcoming;

two and three dimensional hydrodynamical simulations of stellar spectra have begun to be produced, but have not so far built up a sufficiently large database covering the full range of masses, chemical compositions and evolutionary phases (Salaris & Cassisi, 2005).

1.2 Stellar Spectra

Stars are not perfect black-bodies, the spectra that they produce is modified by the emission and absorption processes within the stellar atmosphere. The effective temperature of a star is a physical quantity related to the stellar luminosity and radius, and is the temperature of an equivalent black body that gives the same total power per unit area (Smalley, 2005). This can be expressed as

$$\sigma T_{eff}^4 \equiv \int_0^\infty F_v dv = F_{star} = L/4\pi R^2$$

Where L is the bolometric luminosity, σ is Boltzmann's constant, and R is the radius of the star. The value of the stellar radius used in determining the effective temperature can be taken as the depth of the formation of the spectral continuum (Smalley, 2005). If measurements of the angular diameter (θ) of a star can be taken, and allowances made for any interstellar reddening or limb-darkening (the gradual decrease in the observed brightness from the centre of its star to its edge), then the effective temperature can be calculated for real stars by measuring the total observed flux at the Earth.

$$F_{Star} = \frac{\theta^2}{4} f_{Earth}$$

The modifications to the black-body spectra caused by the lines created by absorption in the stellar atmosphere can reveal a great deal of information about the star. The relative strengths of some lines can give an indication of the temperature of the star and the chemical abundances of the elements that make up the atmosphere. In addition, the broadening of the spectral lines give an indication of the surface pressure and gravity.

The surface gravity (g) of a star is a measure of the photospheric pressure of the stellar atmosphere (Smalley, 2005) and can be calculated by using the stellar mass (M) and the radius (R) of the star and expressed logarithmically as:

$$\log g = \log M - 2\log R + 4.437$$

The spectra also gives information regarding the colour of a star as the temperature of the star is directly related to the peak of the spectral energy distribution; a hotter star will have its peak flux at shorter wavelengths, and hence be 'bluer' than a 'redder' cool star with a peak flux at longer wavelengths.

1.3 Population Synthesis Models

It also becomes possible to predict the integrated spectra, magnitude and colours of stellar populations that cannot be resolved into individual stars (unresolved distant galaxies or star clusters, for example). These predictions (that go under the general name of population synthesis models – PSMs, see e.g. Salaris *et al.,* 2009) have led to the development of a wide variety of techniques that can be used to determine the ages and star formation histories of both resolved and unresolved stellar populations. PSMs are currently one of the main tools for investigating the formation and evolution of galaxies, and can be utilised in one of two ways. In the first approach, photometric and spectroscopic observations of, for example, unresolved galaxies provide empirical integrated spectra, colours and/or magnitudes that can be used to constrain the star formation history of the population by comparisons with the results from PSMs. The second, more direct approach starts with a theoretical model of the formation of the galaxy that predicts a specific star formation history of the stellar population. Using a PSM, it is possible to convert this theoretical history into expected integrated photometric and spectroscopic properties, that can then by compared to the observations taken of the real

object. Any differences between the model and the observations can be used to refine the theoretical galaxy formation model, and the model may be run again.

There are a number of large stellar population synthesis databases, such as the BaSTI (Bag of Stellar Tracks and Isochrones) project, that cover the evolution of stars over a wide range of masses and chemical compositions (Pietrinferni *et al.*, 2004, 2006, Cordier *et al.,* 2007, Salaris *et al.,* 2010). The continued expansion and update of these databases with stellar models and spectra for ever larger ranges of chemical composition, mass and evolutionary stages is a great asset to further research into the timescales of the evolution of both resolved and unresolved stellar populations, which can then be used to provide further information on galaxy formation and evolution. In this respect, there have been some crucial new developments in the recent years that require a major update to take into account the new solar chemical composition and the latest updates in the stellar input physics.

1.4 Solar Metallicity

The chemical composition of the Sun is of fundamental importance in astronomical research and understanding as it provides the reference values relative to which the metal content of all other stars in the universe are determined. It is therefore vital to accurately determine the solar total mass fraction (metallicity) and the measured individual abundances of metals – elements heavier than hydrogen and helium - along with values of the elemental abundances of planets and the interstellar medium. In all cases, X+Y+Z must equal 1. The mass fractions of the hydrogen (X), helium (Y) and metals (Z) present in the stellar atmosphere are defined as:

$$X \equiv \frac{total\ mass\ of\ hydrogen}{total\ mass\ of\ gas}$$

$$Y \equiv \frac{total\ mass\ of\ helium}{total\ mass\ of\ gas}$$

$$Z \equiv \frac{total\ mass\ of\ metals}{total\ mass\ of\ gas}$$

$$\left[\frac{Fe}{H}\right] \equiv log_{10}\left(\frac{N_{Fe}}{N_H}\right) - log_{10}(\frac{N_{Fe}}{N_H})_{\odot}$$

The metallicity of a star is usually defined by the ratio of iron to hydrogen (Fe/H) in the atmosphere which is compared to the Sun's value:

$$\left[\frac{Fe}{H}\right] \sim \log(\frac{Z_{star}}{Z_{\odot}})$$

A star with a ratio of iron to hydrogen equal to that of the Sun would have an [Fe/H] of 0.0. The old, extremely metal poor stars can have a value as low as -4.5 and the youngest, metal rich stars can have a value up to +1.0. If a universal scaled solar distribution of heavy elements is not assumed, then the relationship between [Fe/H] and the X, Y and Z values changes, as the ratio between the abundance of iron and the total metal abundance would be different from that of the Sun.

The solar metallicity abundance cannot be determined solely by observations of the solar spectrum; the spectrum must be observed and the abundances are then calculated by modelling (Scott et al., 2014). The development of three dimensional hydrodynamic codes have driven new determinations of the solar metal mixture, which have then enabled a more accurate determination of the overall solar metallicity and the relative abundances of the elements within it.

In the previous decade Asplund *et al.* (2005) determined a new value of the metal composition of the Sun, which has more recently been refined further (Asplund *et al.,* 2009). The new value for the total metallicity of the Sun is lower than has previously determined, and the abundances of oxygen relative to nitrogen and carbon is also lower,

which can have a significant impact on some of the stellar models and spectra used in population synthesis models. These models are calculated based on the solar metallicity and the solar metal distribution, and changes in the values of the relative abundances of metals used will cause changes in the subsequent models. Changing the relative abundances can have different effects depending on the temperature of the star as the elements have differing opacities at different temperatures. For example changes in the abundances of magnesium and silicon can have a significant effect on the spectra of red giant stars because at low temperatures they are strong sources of opacities, where as carbon, oxygen and nitrogen are not (VandenBerg *et al.,* 2012). However, changes in the relative abundance of carbon, nitrogen and especially oxygen can affect the turnoff luminosity-age relations of main sequence stars, as they are responsible for the operation of the CNO cycle that affects the structure of the star (VandenBerg *et al.,* 2012). One particularly important group of stars that have a significantly different metal mixture to the scaled solar is the case of the α-enhanced metal distribution that occurs in old, metal poor ([Fe/H] below around -0.6) stars in the haloes of spiral galaxies and within the Magellanic Clouds. The α elements are oxygen, neon, magnesium, silicon, sulphur, calcium and titanium, and these are enhanced with respect to Fe compared to the scaled solar distributions, usually by an approximately constant factor for every element (Salaris & Cassisi, 2005). Although these stellar objects are metal poor, the ratio of α/Fe is larger than the equivalent scaled solar ratio at a given iron abundance.

1.5 Project Aims

Previous grids of model atmospheres have been calculated using the ATLAS9 code (Kurucz, 1992, Castelli *et al.*, 1997, and Castelli & Kurucz, 2004), using the most accurately determined solar abundances at the time. The most recent extensive grids of model atmospheres (Castelli & Kurucz, 2004) were calculated using the opacity distribution

functions based on the Grevesse & Sauval (1998) abundances. The effects of changing the solar metal distribution to the Asplund *et al.* (2009) values has been studied with regard to the effects on stellar evolution, but there are currently no libraries of stellar spectra and bolometric corrections available based on these new abundances, and this project aims to update the model atmosphere and spectral libraries available, taking into account these latest determinations of the solar chemical composition. This project utilised the ATLAS9 suite of software to create a grid of stellar spectra for a range of surface gravities, effective temperatures and metallicities, based upon the most recent standard determination of the metal distribution of the Sun (Asplund *et al.,* 2009).

Chapter 2

ATLAS9 and the production of synthetic spectra

2.1 ATLAS9

R. L. Kurucz (1970, 1993, 2005) developed one of the most popular tools for the calculation of stellar atmospheres and synthetic spectra that currently includes the ATLAS9 and ATLAS12 codes. These are used for the calculation of model atmospheres and make a number of assumptions and approximations in the calculations (Kurucz, 1970). The atmosphere is assumed to be thin relative to the radius of the star, and can thus be regarded as plane layers instead of concentric shells. ATLAS9 can therefore produce one dimensional plane parallel atmosphere models that split the atmosphere into a number of homogenous layers that are in hydrostatic equilibrium. Each layer is in local thermodynamic equilibrium and the state of the atmosphere depends only on the local values, and is not influenced by the state of the other layers (Castelli, 1988). The flux and radiative and convective energy is constant with the depth of the atmosphere, and the abundances of the elements are also constant throughout the atmosphere (Castelli, 1988).

In 1992 Kurucz, used the ATLAS9 code and published a group of extended grids of model atmospheres calculated for several metallicities, covering a range of effective temperatures and gravities. These were later extended by Castelli who calculated the grids for the alpha enhanced elements (Castelli & Kurucz, 2004). The Kurucz and Castelli models were computed by using Kurucz's (1990) model atmospheres and were are all based on the solar abundances from Anders & Grevesse (1989). In 2004 Castelli and Kurucz updated their model grids with the revised solar abundances published by Grevasse and Sauval (1998)

and with some replacement to the molecular lines for TiO and H_2O (Castelli & Kurucz, 2004).

The two most widely used methods for sampling the large amounts of molecular and atomic line data are utilising either Opacity Distribution Functions (ODF) or Opacity Sampling (OS), which are both based upon using an absorption coefficient that has a sufficient number of frequency points that would allow a full synthetic spectrum to be computed (Jørgensen, 1992). When using the ODF technique the opacity is not explicitly calculated at every frequency, taking advantage of the fact that the atmospheric structure depends upon the average properties of the spectrum rather than its specific details (Kurucz, 1970). Rather than calculate the opacity for each wavelength, the spectrum is split into a number of smaller intervals and the spectral line opacities are represented by simplified distribution functions over each subsection of the spectra as a function of temperature and electron density (pressure). For each of these small subsections a distribution function is calculated that computes the fraction of that interval having an opacity less than a given value (Kurucz, 1996), illustrated in figure 2.1.1., that shows the absorption coefficient of an idealised section of a spectrum, with an arbitrary opacity value - line Xi(v) – indicated. The fraction of this subsection of spectra with a line opacity less than the value Xi(v) can then be determined, and then plotted on a graph of this fraction against frequency (Hubeny & Mihalas, 2015). In each such ODF subsection, the frequency points with a larger absorption value are moved towards one side of the interval, and the points with a smaller absorption value are moved towards the other (Jørgensen, 1992) as shown in figure 2.1.2.

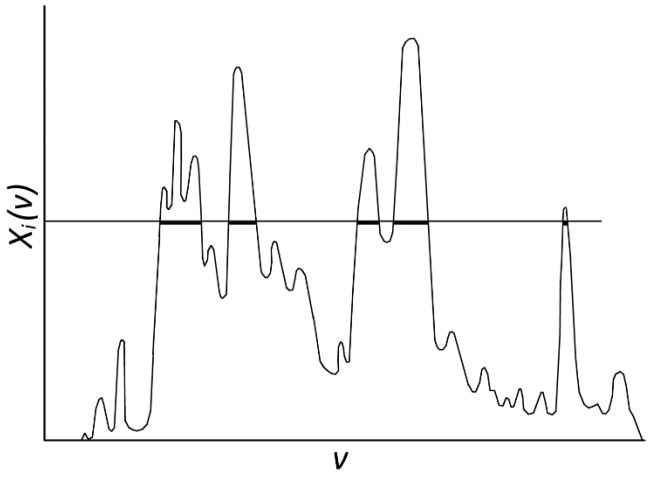

Figure 2.1.1. Schematic absorption coefficient of overlapping spectral lines of an idealised subsection of a spectrum. After Hubeny & Mihalas (2015).

This allows the spectra to be well approximated by a relatively small number of subsections containing constant opacities. Inside each of these subsections, the absorption coefficient is selected at a limited number of frequency points, which are then used for calculating the model atmosphere. During each calculation, the opacity of a particular atom or molecule can be calculated based on these ODFs and pressures.

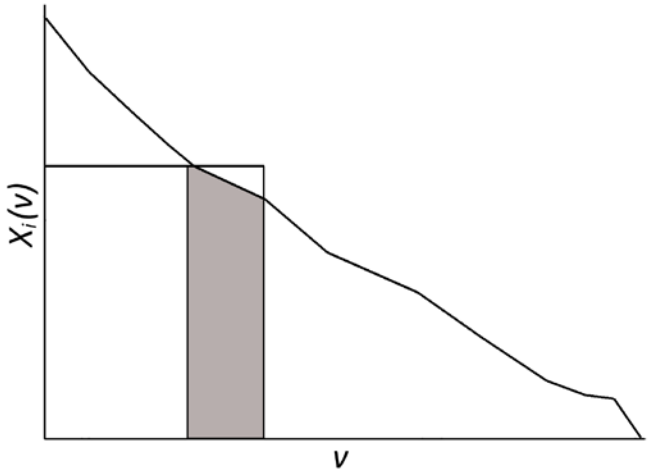

Figure 2.1.2. Schematic opacity distribution function (ODF) of a spectrum with the subsection from figure 2.1.1. shown as the shaded area. After Hubeny & Mihalas (2015).

A limitation to this method is that it assumes the wavelength position of a given line remains constant with optical depth, which may not be the case if the wavelength bands of two different elements or molecules overlap (Hubeny & Mihalas, 2015).

For ATLAS9 the opacity of the model atmosphere is treated with the ODF technique and each ATLAS ODF file contains the line opacity data for different values of electron density and temperature within the required wavelength range. While the ATLAS9 code utilises well-tested pre-computed ODFs to calculate the transfer of radiation, ATLAS12 uses the alternate Opacity Sampling method to calculate the atomic and molecular opacities on the run, by choosing a small number of random wavelength points that does not resolve the spectrum in detail (Kurucz, 1996) and then computing the model by using the integral over the spectrum at a particular depth to determine the energy flowing through this level of the model atmosphere, alleviating the problems that can occur with variations with depth in complex spectra (Hubeny & Mihalas, 2015).

This second method allows a greater flexibility and the use of arbitrary atmospheric compositions at the cost of a greatly increased processing time. However, for the creation of a large number of models it will be more efficient to create a specific ad-hoc ODF for the chosen metal distribution, and use ATLAS9 (Sbordone *et al.,* 2006). Grids of ODFs and model atmospheres have been computed by Castelli and Kurucz (2004) using the solar abundances from Grevesse and Sauval (1998) for effective temperatures from 3500K to 50000K and log g from 0.0 dex to 5.0 dex and these were used as the basis for comparisons with the models produced by this project.

2.2 Usage of ATLAS 9

ATLAS (Kurucz, 1979) is an atmospheric modelling code that has been widely used to produce synthetic spectra from a single dimension plane parallel atmosphere model (Meszaros *et al.*, 2012). A number of extensive grids of model atmospheres have been

calculated using ATLAS9 (Castelli & Kurucz, 2003; Meszaros *et al.*, 2012) for a variety of metallicities. A variety of solar abundances have been used to create these models, including those from Grevesse and Sauval (1998) by Castelli and Kurucz (2004), Anders and Grevesse (1989) by Kirby (2011) and Asplund *et al.,* (2005) by Meszaros *et al.* (2012). The ATLAS9 version of the ATLAS code reduces the computation time of the model by calculating the line opacity with the ODF (Castelli, 2005) and given the large number of models required by this project, ATLAS9 was chosen over the more flexible, but slower, ATLAS12 version of the software. The calculations for this project are using the solar composition values published by Asplund *et al.,* (2009), which required new ODF and Rosseland opacity calculations to produce the model atmospheres and then the synthetic spectra based on those atmospheres. In addition to the abundance and opacity files, producing the model atmosphere also requires an input of the effective temperature, log g value, and a value for the global metallicity that is used to select a base model to start the calculations from. ATLAS9 works by taking the specified input values, and selecting a 'starting model' of the relationship with similar input parameters, and then calculates the temperature and optical depth for each layer within the simulated photosphere (Kurucz, 2005). The programme then iterates the calculation of the equation of state, line opacity and flux in each layer until the model converges and the flux and temperature become constant in each layer.

2.3 Other parameters: microturbulence, overshooting and rotation.

In the one-dimensional model atmospheres calculated using ATLAS9, there is a free parameter of microturbulence that is introduced into the models which will cause a broadening of the spectral lines produced in a synthetic spectrum (Casagrande & VandenBerg, 2014), which can conserve the width of the weaker lines and reduce the saturation of the stronger lines. The grids of synthetic spectra produced by Castelli &

Kurucz (2004) assume a constant value of ξ = 2kms^{-1} in the model atmospheres generated, as do the synthetic spectra in the MARCS library (Casagrande & VandenBerg, 2014), so for direct comparison, the models generated here maintained the same constant value.

Casagrande and VandenBerg (2014) report that there is no clear correlation between the microturbulence value and the observed stellar parameters, although there are indications that the value increases with luminosity. The microturbulence value is thought to represent the physical property of the non-thermal, small scale motion that occurs in a stellar atmosphere and the value of 1.5 to 2.5 kms^{-1} is considered typical for dwarf, subgiant and RGB stars.

ATLAS9 requires a parameter to be set for the "mixing-length" which deals with the treatment of convection within the stellar atmosphere, and also allows for the computation of stellar models with an "overshooting" factor, representing the processes within a star that can extend the mixing effect of convection extending beyond its Schwarzschild convective boundary, and into a stable region of the atmosphere. Castelli (1999) and Bessell *et al.* (1997) discussed the differences between the models produced with this option included or not, and concluded that in general, the no-overshoot models agree better with observations (although not in the case of the solar spectra), and as such this option was not included in any of the models produced in this study. Previous calculations by Kirby (2011) and Castelli & Kurucz (2004) have used the mixing length value of 1.25 and for consistency with the prior models this value was also used in this project.

ATLAS9 also has the capacity to simulate the effect of stellar rotation within the produced synthetic spectra. If a star is observed at any orientation other than directly pole-on, then there will be broadening of the spectral lines due to the rotation of the star, as the spectrum emitted from each point on the surface is Doppler shifted by the projected rotation velocity of the star at that point, and the total flux of the spectrum consists of a

combination of the spectra emitted at all points (Kurucz, 2005). To enable comparison between the new abundances and the previous work, this option was set to 0 for this project.

2.4 Calculation of the ODF and Rosseland opacities

As a test of the software a new ODF and Rosseland Opacity was computed using the Grevesse and Sauval (1998) values. The spectra produced using this model was tested against the Grevesse and Sauval (1998) based spectra available on the website of F.Castelli to determine that the model was calculated correctly, giving the same output spectra with the same input parameters.

A second test was conducted by producing a model that used the values of Grevesse and Sauval (1998), but with the alpha elements enhanced by +0.4. The spectra produced using this model was tested against the alpha enhanced spectra available on the website of F.Castelli to determine that the model was calculated correctly. Testing the models and comparing to the parameters of the models calculated by Castelli allowed the determination of the range of effective temperatures at which models could be successfully calculated for each log g (shown in figures 2.5.1. and 2.5.2. later).

As a general overview, an ODF was calculated for each chemical composition required (the new scaled solar, and the new alpha enhanced) which was then used within ATLAS9 to create a database of model atmospheres based upon an input grid of effective temperature and gravity. The complete grid produced covers appropriately the evolutionary phases of stellar populations with the widest possible stellar parameters that could be calculated with ATLAS9. Once a model atmosphere has been calculated, a synthetic stellar spectrum was calculated, and compared with the synthetic spectrum produced by a star with the same metallicity, gravity and effective temperature but with the older abundances of Grevesse and Sauval (1998).

More specifically, ODFs have been be produced for seven different [Fe/H] values (+0.5, 0, -0.5, -1.0, -1.5, -2.0 and -2.5) and two different metal mixtures - solar metal abundances from Asplund *et al.* (2009) and the same mixture with the alpha elements enhanced by +0.4 dex (whereby at a given metallicity the abundances of elements like O, Mg, Ne, Ca are increased compared to Fe, with respect to the reference solar metal mixture, as observed in the halo of our galaxy and elliptical galaxies), to cover the full range of chemical compositions observed in the universe. Each ODF then became the input used to run calculations to produce a grid of model atmospheres and synthetic spectra of stars with surface gravities of log g between 0 and 5 (in cgs units), and with an effective temperatures between 3500 and 100000 kelvin. A grid of spectra for both the scaled solar and alpha-enhanced metal distributions were produced and added to the database.

The DFSYNTHE, KAPPA9 and ATLAS9 codes produced by Kurucz (1993) were used to create grid of plane-parallel model atmospheres that are in local thermodynamic equilibrium. The Opacity Distribution Functions were first calculated with DFSYNTHE (described by Castelli, 2005) using the scaled solar abundances given by Asplund *et al.* (2009) for each element that they listed and the Rosseland opacity was calculated using the KAPPA9 code. The codes were compiled using the Intel Fortran compiler in Linux.

For elements not listed in Asplund *et al.* (2009), the values given by Grevesse and Sauval (1998) were used (see Table 2.3.1). A total of eight ODFs and Rosseland opacities were calculated using this solar abundance with global metallicity values of -2.5, -2.0, -1.5, -1.0, -0.5, 0.0, 0.5 and 1.0 to cover a large range of scaled solar abundances and chemical compositions.

No.	Element	G&S (1998)	Asplund et al (2009)		No.	Element	G&S (1998)	Asplund et al (2009)
1	Hydrogen				47	Silver	0.94	0.94
2	Helium				48	Cadmium	1.77	[1.77]
3	Lithium	1.10	1.05		49	Indium	1.66	0.80
4	Beryllium	1.40	1.38		50	Tin	2.00	2.04
5	Boron	2.55	2.70		51	Antimony	1.00	[1.00]
6	Carbon	8.52	8.43		52	Tellurium	2.24	[2.24]
7	Nitrogen	7.92	7.83		53	Iodine	1.51	[1.51]
8	Oxygen	8.83	8.69		54	Xenon	2.17	2.24
9	Fluorine	4.56	4.56		55	Caesium	1.13	[1.13]
10	Neon	8.08	7.93		56	Barium	2.13	2.18
11	Sodium	6.33	6.24		57	Lanthanum	1.17	1.10
12	Magnesium	7.58	7.60		58	Cerium	1.58	1.58
13	Aluminium	6.47	6.45		59	Praseodymium	0.71	0.72
14	Silicon	7.55	7.51		60	Neodymium	1.5	1.42
15	Phosphorus	5.45	5.41		61	Promethium	-10	[-10]
16	Sulphur	7.33	7.12		62	Samarium	1.01	0.96
17	Chlorine	5.50	5.50		63	Europium	0.51	0.52
18	Argon	6.40	6.40		64	Gadolinium	1.12	1.07
19	Potassium	5.12	5.03		65	Terbium	0.35	0.30
20	Calcium	6.36	6.34		66	Dysprosium	1.14	1.10
21	Scandium	3.17	3.15		67	Holmium	0.26	0.48
22	Titanium	5.02	4.95		68	Erbium	0.93	0.92
23	Vanadium	4.00	3.93		69	Thulium	0.00	0.10
24	Chromium	5.67	5.64		70	Ytterbium	1.08	0.84
25	Manganese	5.39	5.43		71	Lutetium	0.06	0.10
26	Iron	7.50	7.50		72	Hafnium	0.88	0.85
27	Cobalt	4.92	4.99		73	Tantalum	-0.13	[-0.13]
28	Nickel	6.25	6.22		74	Tungsten	1.11	0.85
29	Copper	4.21	4.19		75	Rhenium	0.28	[0.28]
30	Zinc	4.60	4.56		76	Osmium	1.45	1.40
31	Gallium	2.88	3.04		77	Iridium	1.35	1.38
32	Germanium	3.41	3.65		78	Platinum	1.80	[1.80]
33	Arsenic	2.37	[2.37]		79	Gold	1.01	0.92
34	Selenium	3.41	[3.41]		80	Mercury	1.13	[1.13]
35	Bromine	2.63	[2.63]		81	Thallium	0.90	0.90
36	Krypton	3.31	3.25		82	Lead	1.95	1.75
37	Rubidium	2.60	2.52		83	Bismuth	0.71	[0.71]
38	Strontium	2.97	2.87		84	Polonium	-10	[-10]
39	Yttrium	2.24	2.21		85	Astatine	-10	[-10]
40	Zirconium	2.60	2.58		86	Radon	-10	[-10]
41	Niobium	1.42	1.46		87	Francium	-10	[-10]
42	Molybdenum	1.92	1.88		88	Radium	-10	[-10]
43	Technetium	-10	[-10]		89	Actinium	-10	[-10]
44	Ruthenium	1.84	1.75		90	Thorium	0.09	0.02
45	Rhodium	1.12	0.91		91	Protactinium	-10	[-10]
46	Palladium	1.69	1.57		92	Uranium	-0.5	[-0.5]

Table 2.4.1. Metallicty number density values (log (NL/NH)+12 from Grevesse & Sauval (1998) and Asplund et al. (2009). Values in square brackets are not given in Asplund et al. (2009), so values from Grevesse & Sauval (1998) are substituted.

The global metallicity was specified (e.g. -0.5) along with the mass fraction of hydrogen and helium. For the other elements, the values were given as a number density log. The abundances are given as log (N_X/N_H) + 12 where N_X is the number density of the element and N_H is the number density of hydrogen, in the same way as Asplund *et al.* (2009). For elements in which the value is unknown or not given, then a number density of -10 was used.

The input values were then modified to produce a further seven ODFs and Rosseland opacities with the alpha enhanced mixture (see Table 2.3.3). The values for the alpha enhanced elements were each increased by 0.4 dex.

No.	Element	Values for solar mixture	Values for alpha enhanced mixture
8	Oxygen	8.69	9.09
10	Neon	7.93	8.33
12	Magnesium	7.60	8.00
14	Silicon	7.51	7.91
16	Sulphur	7.12	7.52
18	Argon	6.40	6.80
20	Calcium	6.34	6.74
22	Titanium	4.95	5.35

Table 2.4.2. Values for alpha enhanced elements (Asplund et al. (2009)) mixture increased by 0.4.

The model atmospheres produced by the calculations had the following X. Y and Z values for each global metallicity.

Global Metallicity	X	Y	Z		X	Y	Z (a)
-2.5	0.75146	0.24850	0.00004		0.75141	0.28450	0.00009
-2.0	0.75136	0.24850	0.00014		0.75123	0.24850	0.00027
-1.5	0.75107	0.24850	0.00043		0.75064	0.24850	0.00086
-1.0	0.75014	0.24850	0.00136		0.74879	0.24850	0.00271
-0.5	0.74722	0.24850	0.00428		0.74299	0.24850	0.00851
+0.0	0.73812	0.24850	0.01338		0.72525	0.24850	0.02625
+0.5	0.71075	0.24850	0.04075		0.67431	0.24850	0.07719
+1.0	0.63615	0.24850	0.11535				

Table 2.4.3. X, Y, and Z values for each global metallicity of solar mixture and alpha enhanced mixture based on the abundances of Asplund et al. (2009).

2.5 Calculation of the stellar model atmospheres

Using the output files from the previous code, the ODF and Rosseland opacities were used as the input to create the model atmospheres and synthetic spectra produced using the SYNTHE code of the ATLAS9 suite. The criteria for the acceptance of an atmospheric model followed that suggested by Meszaros *et al.* (2012) in that a model was accepted if it successfully converged throughout the full 72 layers of the atmosphere, or if four or less layers did not converge. (As suggested by Alessio Mucciarelli, the presence of less than five unconverged layers at either of the topmost or bottommost five layers would not result in an unacceptable model). A model was rejected if the calculation failed to converge at all, or if there were five or more unconverged layers in the model. The metallicity of the calculations in the grid varied from $Z/Z_{\odot}$ =-2.5 to +1.0 to cover a large range of scaled solar abundances and chemical compositions, with the acceptable models having effective temperatures ranging from 3500 to 60000 kelvin, and log g from 0.0 to 5.0.

To match the grid produced by Castelli and Kurucz (2004) and to give good coverage of the parameters without creating an excessive number of models, the step size for log (g) was kept at 0.5 while the temperature of the calculated models was as follows:

3500K – 13000K	Step size: 250K
13000K – 40000K	Step size: 1000K
>40000K	Step size: 10000K

This gave a total of around 500 models for each of the eight metallicity values. A grid showing each of the successfully calculated models in presented in table 2.4.1. In some cases, at the highest and lowest effective temperatures for each value of log g, ATLAS9 failed to produce acceptable models for every one of the metallicity values calculated, and these are clearly indicated in the table. In particular, the extreme metallicity value of +1.0 failed to produce a number of viable models, especially at temperatures below 4250K.

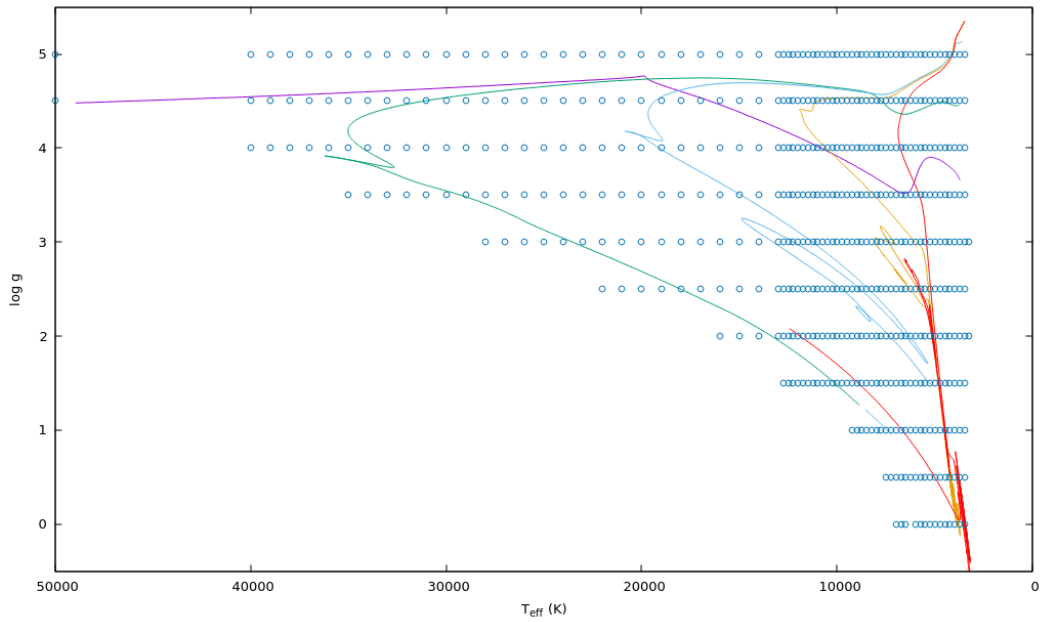

Figure 2.5.1. Grid showing the log g and T_{eff} (K) values of calculated models up to 50000K (blue circles) with isochrones of stars with [Fe/H]=0.0 at ages of 10^6Myr (purple), 10^7Myr (green), 10^8Myr (blue), 10^9Myr (yellow), 10^{10}Myr (red). (Isochrones MIST v. 1.0, MESA revision, 7503, Dotter, 2016).

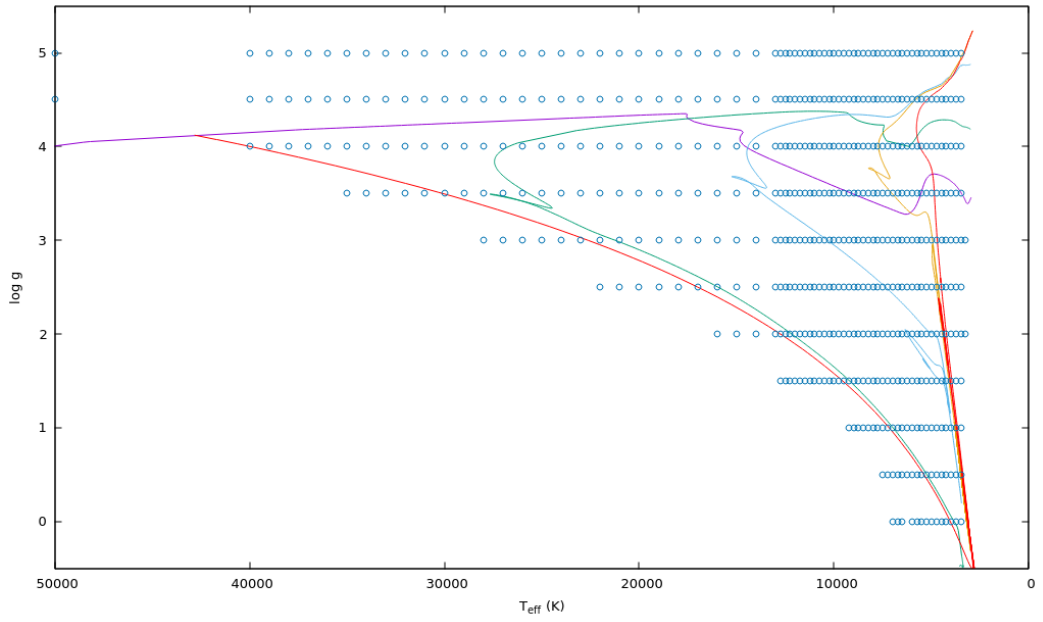

Figure 2.5.2. Grid showing the log g and T_{eff} (K) values of calculated models up to 50000K (blue circles) with isochrones of stars with [Fe/H]=-2.0 at ages of 10^6Myr (purple), 10^7Myr (green), 10^8Myr (blue), 10^9Myr (yellow), 10^{10}Myr (red). (Isochrones MIST v. 1.0, MESA revision, 7503, Dotter, 2016).

Figures 2.5.1 and 2.5.2 above show a plot of the effective temperature values and log g of each calculated model along with isochrones of various ages of stars to illustrate that the grid of calculated models gives good coverages of the evolutionary phases of different masses of stars.

Teff/ logg	0.0	0.5	1.0	1.5	2.0	2.5	3.0	3.5	4.0	4.5	5.0
3500	X [abh]	X [abh]	X [abh]	X [ab]	X [ab]	X [ab]	X [ah]	X [ah]	X [gh]	X [fgh]	X [gh]
3750	X	X [a]	X [a]	X	X	X	X [a]	X [a]	X [a]	X [a]	X [ah]
4000	X [a]	X	X [a]	X [a]	X [a]	X [a]	X	X	X	X	X [ah]
4250	X [a]	X	X	X [a]	X [a]	X [a]	X [a]	X	X	X	X [a]
4500	X	X [a]	X	X [a]	X	X	X	X	X [a]	X	X
4750	X [a]	X [a]	X [a]	X [a]	X [a]	X [a]	X	X	X	X	X
5000	X [a]	X [a]	X [a]	X	X [a]	X	X [a]	X	X	X	X
5250	X [a]	X [a]	X [a]	X	X	X	X	X	X	X	X
5500	X [a]	X	X [a]	X [a]	X	X	X	X	X	X	X
5750	X	X [a]	X	X	X	X [a]	X	X	X [a]	X	X
6000	X	X	X [a]	X	X	X	X	X	X	X	X
6250	X [abc]	X	X	X [a]	X	X	X	X	X	X	X
6500	X [ad]	X	X	X	X [a]	X	X	X	X	X	X
6750	X [bfg]	X	X	X	X	X [a]	X	X	X	X	X
7000	X [abf]	X	X	X	X	X	X [a]	X	X	X	X
7250		X	X	X	X	X	X [a]	X [a]	X	X	X
7500		X [a]	X	X	X	X	X	X	X	X	X
7750			X	X	X	X	X	X	X	X	X
8000			X	X	X	X	X	X	X	X [a]	X
8250			X	X	X	X	X	X	X	X	X [a]
8500			X	X	X	X	X	X	X	X	X [d]
8750			X	X	X	X	X	X	X	X	X
9000			X	X	X	X	X	X [a]	X	X	X
9250			X [a]	X	X	X	X	X	X	X	X
9500				X	X	X	X	X	X	X	X
9750				X	X	X	X	X	X	X	X
10000				X	X	X	X	X	X	X	X
10250				X	X	X	X	X	X	X	X
10500				X	X	X	X	X	X	X	X
10750				X [a]	X	X	X	X	X	X	X
11000				X [a]	X	X	X	X	X	X	X
11250				X [ab]	X	X	X	X	X	X	X
11500				X [ab]	X	X	X	X	X	X	X
11750				X [ab]	X	X	X	X	X	X	X
12000				X [ab]	X	X	X	X	X	X	X
12250				X [ab]	X [a]	X	X	X	X	X	X
12500				X [ab]	X [a]	X	X	X	X	X	X
12750				X [abc]	X	X	X	X	X	X	X
13000					X	X	X	X	X	X	X
14000					X	X	X	X	X	X	X
15000					X	X	X	X	X	X	X

16000	X [ab]	X	X	X	X	X	X
17000		X	X	X	X	X	X
18000		X	X	X	X	X	X
19000		X	X	X	X	X	X
20000		X	X	X	X	X	X
21000		X	X	X	X	X	X
22000		X [b]	X	X	X	X	X
23000			X	X	X	X	X
24000			X	X	X	X	X
25000			X [a]	X	X	X	X
26000			X [a]	X	X	X	X
27000			X [a]	X	X	X	X
28000			X [ab]	X	X	X	X
29000				X	X	X	X
30000				X	X	X	X
31000				X [a]	X	X	X
32000				X	X	X	X
33000				X [ab]	X	X	X
34000				X [ab]	X [a]	X	X
35000				X [ab]	X [a]	X	X
36000					X [a]	X [a]	X
37000					X [a]	X [a]	X
38000					X [ab]	X [a]	X
39000					X [ab]	X [a]	X
40000					X [ab]	X [a]	X
50000						X [ab]	X
60000							X [ab]

Table 2.5.1 Grid of models for the new scaled solar metallicity. X indicates an acceptable model atmosphere was created at the given effective temperature and gravity for all global metallicity values (+1.0 to -2.5) with the following exceptions; no acceptable model produced for [a] +1.0, [b] +0.5, [c] +0.0, [d] -0.5, [e] -1.0, [f] -1.5, [g] -2.0 [h] -2.5.

The process was repeated for the alpha enhanced abundances, and the grid of acceptable models is shown in table 2.4.2. Attempting to calculate models with an alpha enhanced global metallicity of +1.0 failed to produce any acceptable models, and hence these are not included in the table.

Teff/ logg	0.0	0.5	1.0	1.5	2.0	2.5	3.0	3.5	4.0	4.5	5.0
3500	X [b]	X [bch]	X [bch]	X [bcg]	X [bcgf]	X [bcf]	X [bh]	X [befgh]	X [efgh]		
3750	X	X [h]	X [gh]	X	X	X [bf]	X [bf]	X [bgh]	X [efgh]	X [defgh]	X [cdefgh]
4000	X	X	X	X	X	X	X	X	X [h]	X [fg]	X [defg]
4250	X	X	X	X	X	X	X	X	X	X [gh]	X [fgh]
4500	X [b]	X	X	X	X	X	X	X	X	X	X [h]
4750	X	X	X	X	X	X	X	X	X	X	X
5000	X	X	X	X	X	X	X	X	X	X	X
5250	X	X	X	X	X	X	X	X	X	X	X
5500	X	X	X	X	X	X	X	X	X	X	X
5750	X	X	X	X	X	X	X	X	X	X	X
6000	X	X	X	X	X	X	X	X	X	X	X
6250	X	X	X	X	X	X	X	X	X	X	X
6500	X [df]	X	X	X	X	X	X	X	X	X	X
6750	X [bdfgh]	X	X	X	X	X	X	X	X	X	X
7000	X [bdfgh]	X	X	X	X	X	X	X	X	X	X
7250		X	X	X	X	X	X	X	X	X	X
7500		X [b]	X	X	X	X	X	X	X	X	X
7750			X	X	X	X	X	X	X	X	X
8000			X	X	X	X	X	X	X	X	X
8250			X	X	X	X	X	X	X	X	X
8500			X	X	X	X	X	X	X	X	X [d]
8750			X	X	X	X	X	X [b]	X	X	X
9000			X	X	X	X	X	X	X	X	X
9250			X	X	X	X	X	X	X	X	X
9500				X	X	X	X	X	X	X	X
9750				X	X	X	X	X	X	X	X
10000				X	X	X	X	X	X	X	X
10250				X	X	X	X	X	X	X	X
10500				X	X	X	X	X	X	X	X
10750				X	X	X	X	X	X	X	X
11000				X	X	X	X	X	X	X	X
11250				X [b]	X	X	X	X	X	X	X
11500				X [b]	X	X	X	X	X	X	X
11750				X [b]	X	X	X	X	X	X	X
12000				X [b]	X	X	X	X	X	X	X
12250				X [b]	X	X	X	X	X	X	X
12500				X [b]	X	X	X	X	X	X	X
12750				X [bc]	X	X	X	X	X	X	X
13000					X	X	X	X	X	X	X
14000					X	X	X	X	X	X	O
15000					X	X	X	X	X	X	X
16000					X	X	X	X	X	X	X
17000						X	X	X	X	X	X
18000						X	X	X	X	X	X
19000						X	X	X	X	X	X
20000						X	X	X	X	X	X
21000						X	X	X	X	X	X
22000						X [b]	X	X	X	X	X
23000							X	X	X	X	X

24000		**X**	**X**	**X**	**X**	**X**
25000		**X**	**X**	**X**	**X**	**X**
26000		**X**	**X**	**X**	**X**	**X**
27000		**X**	**X**	**X**	**X**	**X**
28000		**X** [b]	**X**	**X**	**X**	**X**
29000			**X**	**X**	**X**	**X**
30000			**X**	**X**	**X**	**X**
31000			**X**	**X**	**X**	**X**
32000			**X**	**X**	**X**	**X**
33000			**X** [b]	**X**	**X**	**X**
34000			**X** [b]	**X**	**X**	**X**
35000			**X** [bc]	**X**	**X**	**X**
36000				**X**	**X**	**X**
37000				**X**	**X**	**X**
38000				**X** [b]	**X**	**X**
39000				**X** [b]	**X**	**X**
40000				**X** [bc]	**X** [b]	**X**
50000					**X** [bc]	**X**
60000						**X**

Table 2.5.2 Grid of models for new alpha enhanced metallicity. X indicates an acceptable model atmosphere was created at the given effective temperature and gravity for all global metallicity values (+0.5α to -2.5α) with the following exceptions; no acceptable model produced for [b] *+0.5α,* [c] *+0.0α,* [d] *-0.5α,* [e] *-1.0α,* [f] *-1.5α,* [g] *-2.0α* [h] *-2.5α.*

2.6 Calculation of the synthetic spectra

The calculation of a synthetic spectrum between a minimum and maximum wavelength requires the corresponding linelist files to be provided. The linelists of atomic and molecular transitions, (including H2,HD, CH, C2, CN, CO, NH, OH, MgH, SiH,and SiO) were those of Kurucz (1990) and obtained from the following website http://wwwuser.oat.ts.astro.it/castelli/sources/dfsynthe.html in the same manner as Kirby (2011) and Meszaros *et al.* (2012). Each of these linelist files covers a set range of wavelengths and contain details of the atomic transitions between those wavelengths (Sbordone & Bonifacio, 2005). The files themselves contain the details of the element and/or isotope, the wavelength of the line and the oscillator strength (log gf) which determines the probability of the emission or absorption in the transition between energy levels.

The linelist files that cover the atomics and molecular lines over the wavelengths used were as follows:

gf0300.fc covers the lines from 2000 to 3000 A

gf0400.fc covers the lines from 3000 to 4000 A

gf0500.fc covers the lines from 4000 to 5000 A

gf0600.fc covers the lines from 5000 to 6000 A

gf0800.fc covers the lines from 6000 to 8000 A

gf1200.fc covers the lines from 8000 to 12000 A

gf3000.am covered the lines from 12000 to 30000 A

The Autokur programme that creates the synthetic spectra required a number of input parameters; the effective temperature, the surface gravity and an input model atmosphere as an initial estimate (produced by the ODF). The MOLECULES option includes the above molecular transitions within the calculated spectra, and the TIO option includes the transitions of Titanium Oxide. Including Titanium Oxide within the calculations significantly increased the runtime of the calculation so was only included in cool stars (T_{eff} <4500K). To make direct comparisons and maintain consistency with the spectra and models produced by Castelli and Kurucz, the convective overshoot option was switched off and rotation was set to zero.

Chapter 3

Comparisons of old and new synthetic spectra

3.1 Introduction

Castelli and Kurucz (2004) produced a set of synthetic spectra and model atmospheres based upon the then new Grevesse and Sauval (1998) abundances along with new line lists for H_2O and TiO and compared them to the earlier Anders and Grevesse (1989) abundances. They reported that their newer models only produced significant differences in the energy distributions in the spectra of stars with temperatures below 4500K, and Castelli and Kurucz (2004) indicated that the primary source of the changes in the models is due to the addition of the new line lists, rather than the differences in solar abundances. For this current study, the ODFs and model atmospheres created with the old (Grevesse & Sauval, 1998) and new (Asplund *et al.,* 2009) abundances were used to create synthetic spectra for simulated stars of various metallicities, effective temperatures and gravities between 2000 and 30000 Angstroms. The new abundances of Asplund *et al.* (2009) have somewhat less carbon (log (N_X/N_H) + 12 = 8.56 compared to 8.43), nitrogen (7.92 to 7.83) and oxygen (8.83 to 8.69) compared to the older abundances (see table 2.3.1 previously), which may alter the relative strength of some of the indicative spectral lines. In addition, there are reductions in other significant elements such as sodium (6.33 to 6.24), calcium (6.36 to 6.34) and titanium (5.02 to 4.95). Very few elements have a greater abundance in the new model, the most significant of which is the small increase in magnesium (7.58 to 7.60).

The line lists are identical in the old and new ODFs used in this model, the only variation was in the abundances, so any differences were likely to be smaller than those identified in

the earlier study, and the synthetic spectra produced by using the Asplund *et al.* (2009) abundances are very similar to those created with the Grevesse and Sauval (1998) abundances, with the greatest difference being in the cooler stars below 4500K.

3.2 Comparison of Synthetic Spectra at solar metallicity

A sample of the produced synthetic spectra at various effective temperatures, gravities and metallicities are given in the following sections, and differences in particular spectral lines identified from the literature (Allard *et al.,* 2010, Kramida *et al.,* 2018) are highlighted. At temperatures above 6000K, the new and old model spectra are almost identical, regardless of the values of the gravity (figures 3.2.1 to 3.2.7) although though there are some discrepancies identified below.

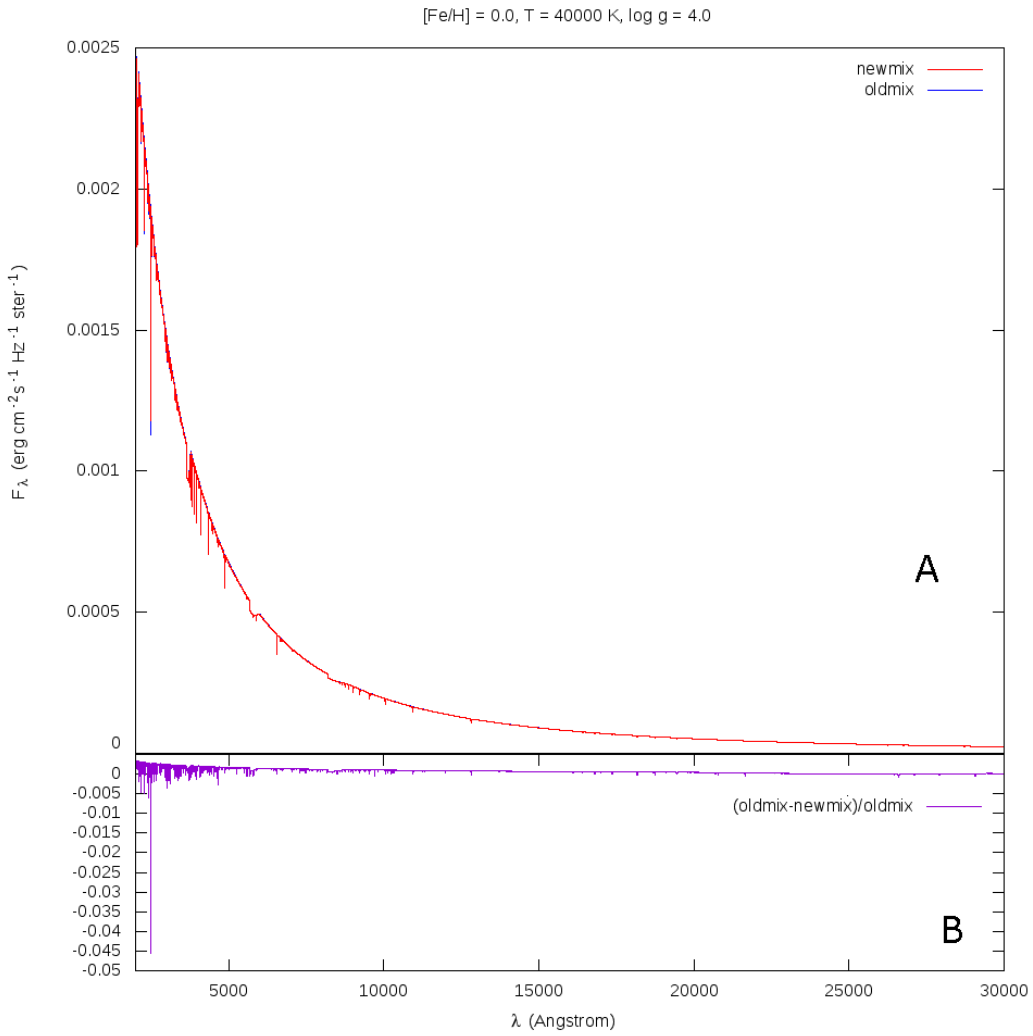

Figure 3.2.1. ***A****. Comparison of fluxes from the old ODF (blue) and the new ODF model (red) with parameters* T_{eff}*=40000 K, logg=4.0, [Fe/H]=0.0.* ***B****. Difference between the fluxes (oldmix - newmix) / oldmix.*

For hot main sequence stars with an effective temperature of 40,000 K, the spectra produced by the old and the new models are almost identical (figure 3.2.1.A), with the two lines being almost indistinguishable. The comparison of the ratios between the fluxes shows that the total flux of the new mixture is very slightly lower (within 0.5%) at wavelengths shorter than 5000 Å with the exception of a single He line at 2495 Å.

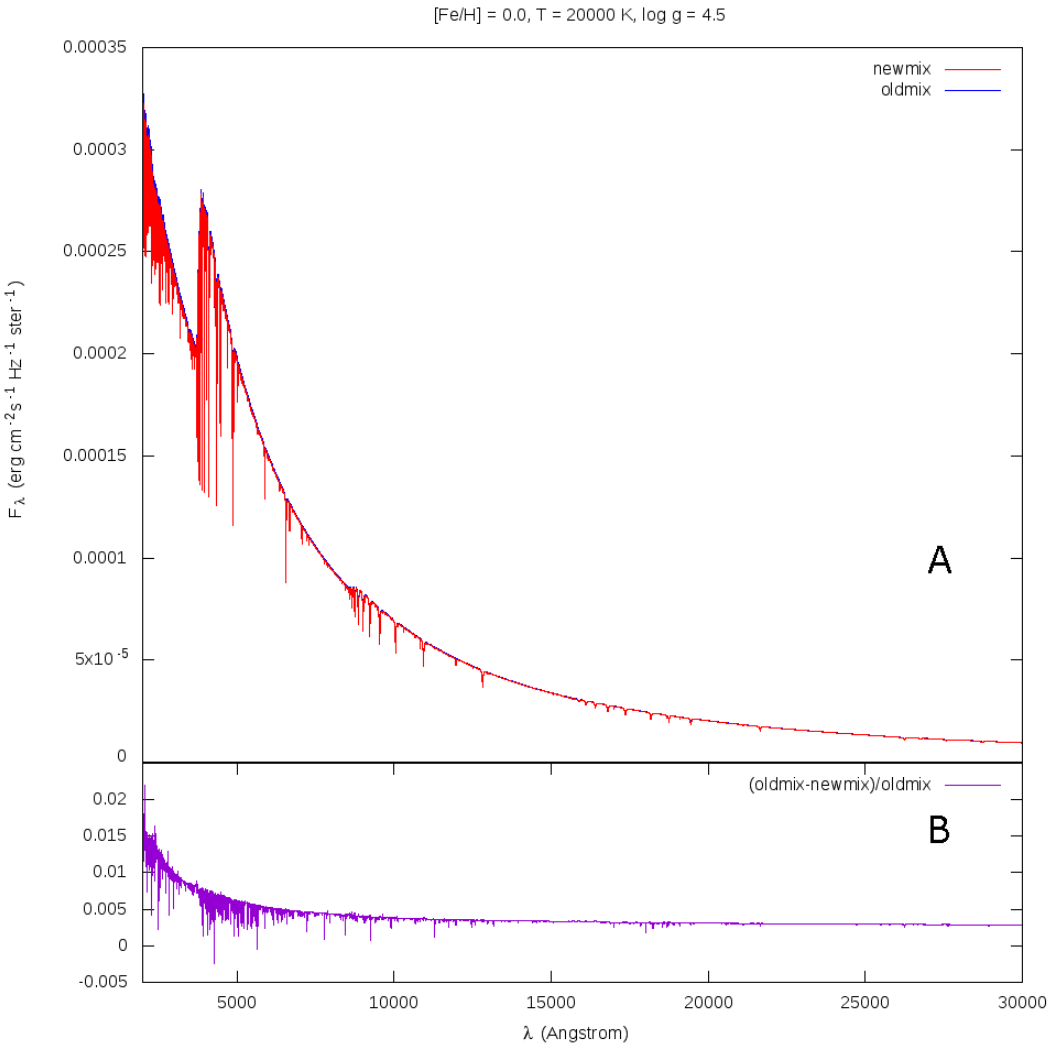

Figure 3.2.2. ***A.*** *Comparison of fluxes from the old ODF (blue) and the new ODF model (red) with parameters* T_{eff}*=20000 K, logg=4.5, [Fe/H]=0.0.* ***B.*** *Difference between the fluxes (oldmix - newmix) / oldmix.*

The spectra produced for B type main sequence stars with an effective temperature of 20,000 K by the new mixture have a lower flux (up to 1.5%) in wavelengths shorter than 5000 Å, and a slightly lower flux (around 0.3%) at longer wavelengths compared to that produced by the old mixture (figure 3.2.2).

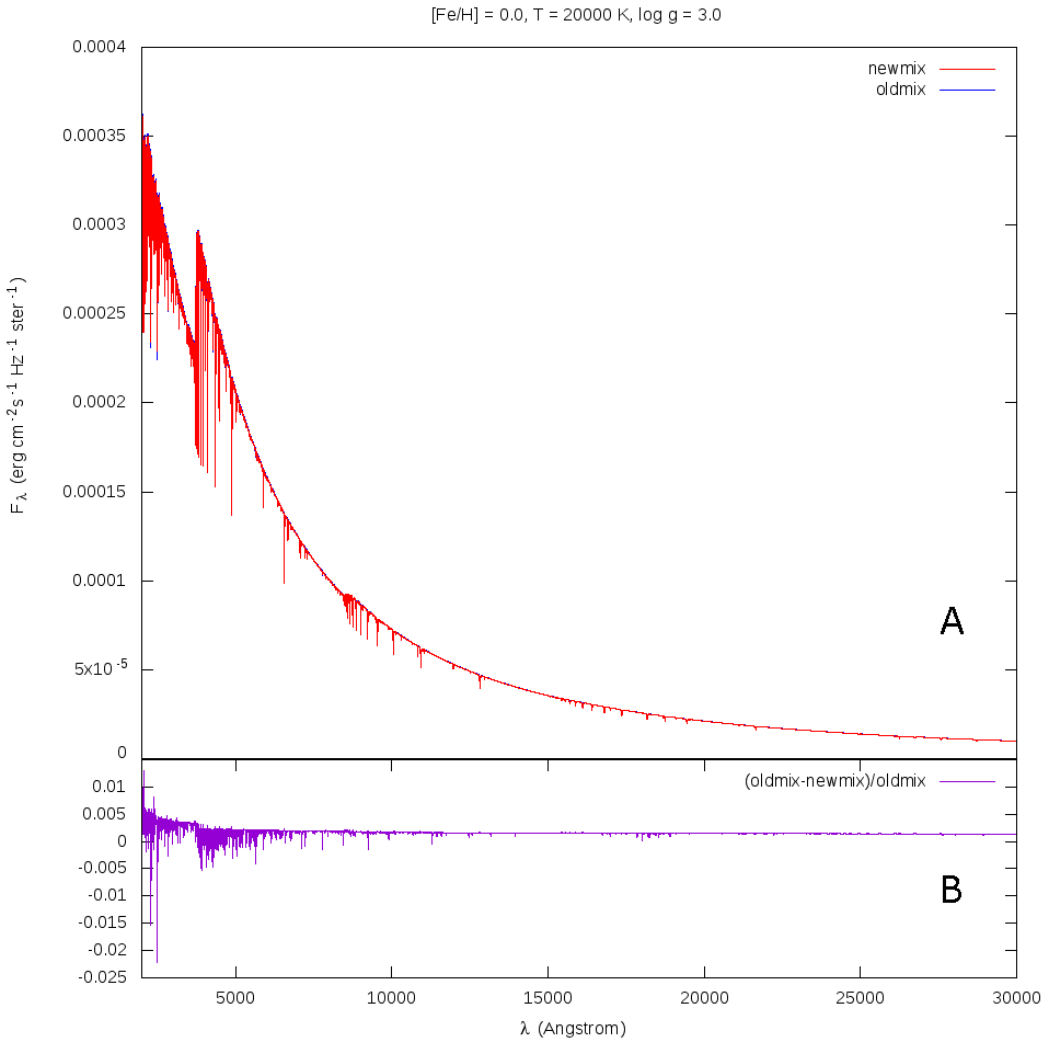

Figure 3.2.3. ***A.*** *Comparison of fluxes from the old ODF (blue) and the new ODF model (red) with parameters* T_{eff}*=20000 K, logg=3.0, [Fe/H]=0.0.* ***B.*** *Difference between the fluxes (oldmix - newmix) / oldmix.*

With decreasing gravity, the difference between the flux of the spectra produced by the old and the new models for stars with an effective temperature of 20000K decreases. The comparison of the ratios between the old and new model fluxes for blue giant stars shows that the total flux of the new mixture is very slightly lower (within 0.5%) at wavelengths shorter than 5000 Å with the exception of a two He lines below 2500 Å, where the depth of the lines is 1-2% higher (figure 3.2.3).

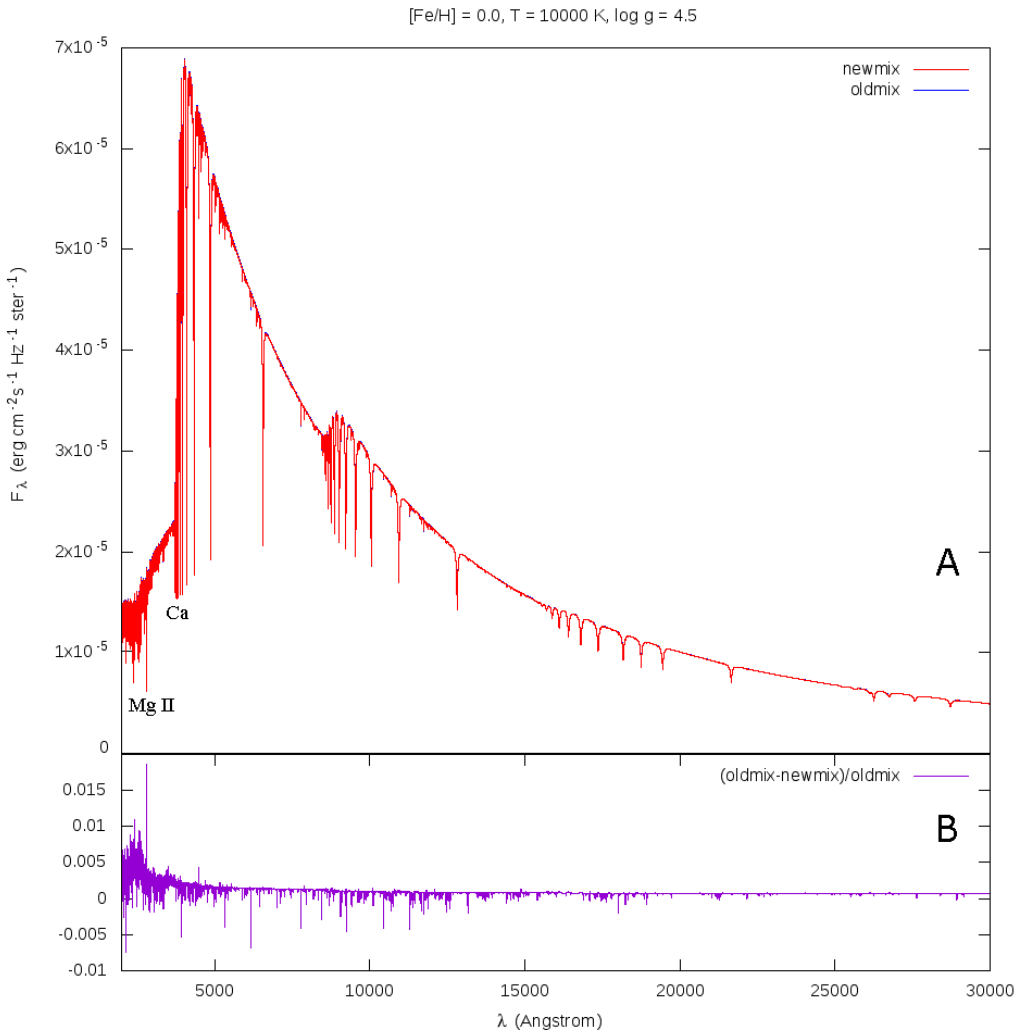

Figure 3.2.4. ***A.*** *Comparison of fluxes from the old ODF (blue) and the new ODF model (red) with parameters* T_{eff}*=10000 K, logg=4.5, [Fe/H]=0.0.* ***B.*** *Difference between the fluxes (oldmix - newmix) / oldmix.*

The synthetic spectra for A type main sequence stars produced by the old and new models are almost identical with only a small differences in the total flux at wavelengths less than 3000 Å. Magnesium is one of the few elements that has a higher abundance in the new mixture, and this can explain the differences in the flux at around 2800 and 4480 Å due to the Mg II absorption lines (figure 3.2.4).

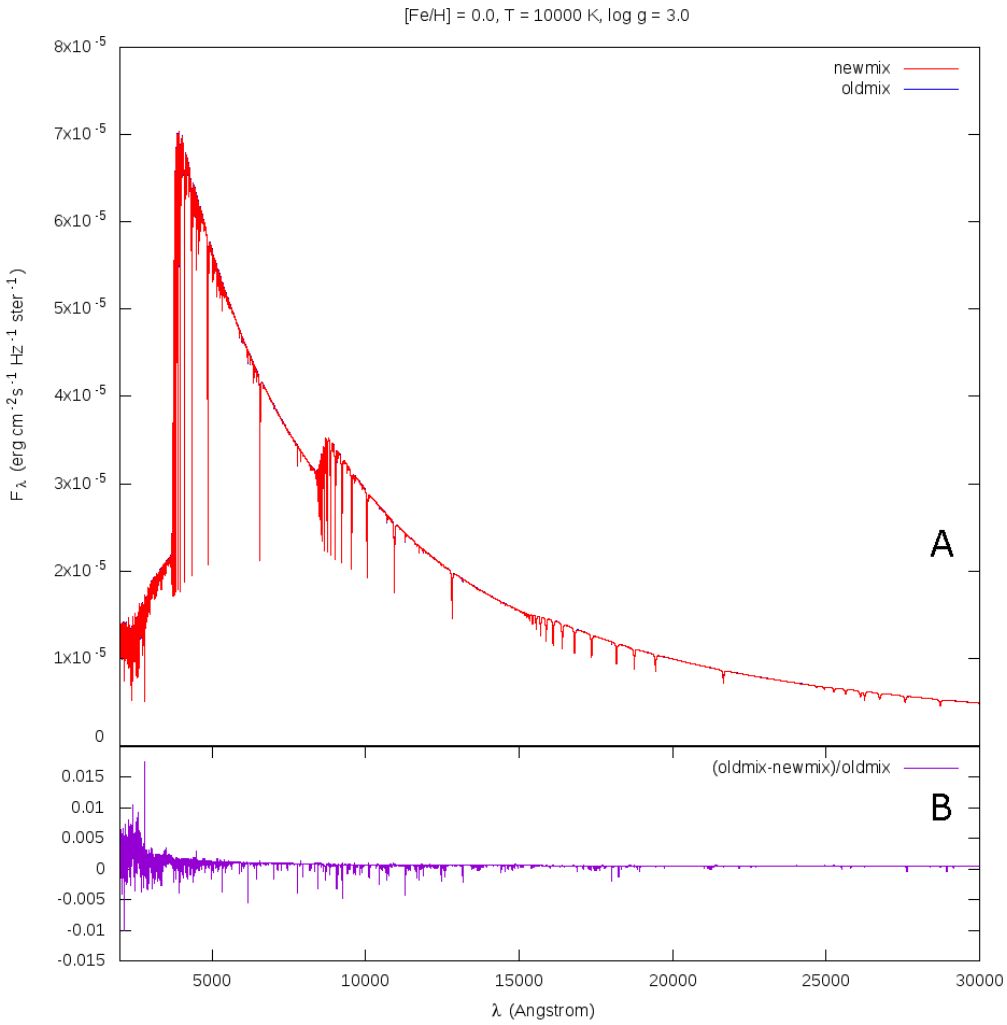

Figure 3.2.5. ***A.*** *Comparison of fluxes from the old ODF (blue) and the new ODF model (red) with parameters* T_{eff}*=10000 K, logg=3.0, [Fe/H]=0.0.* ***B.*** *Difference between the fluxes (oldmix - newmix) / oldmix.*

With decreasing gravity there is little change in the differences between the spectra produced by the old and new models for A type stars (unlike the synthetic spectra for B type stars - figures 3.2.2 and 3.2.3). The differences in fluxes are very similar to the log g 4.5 model (figure 3.2.4).

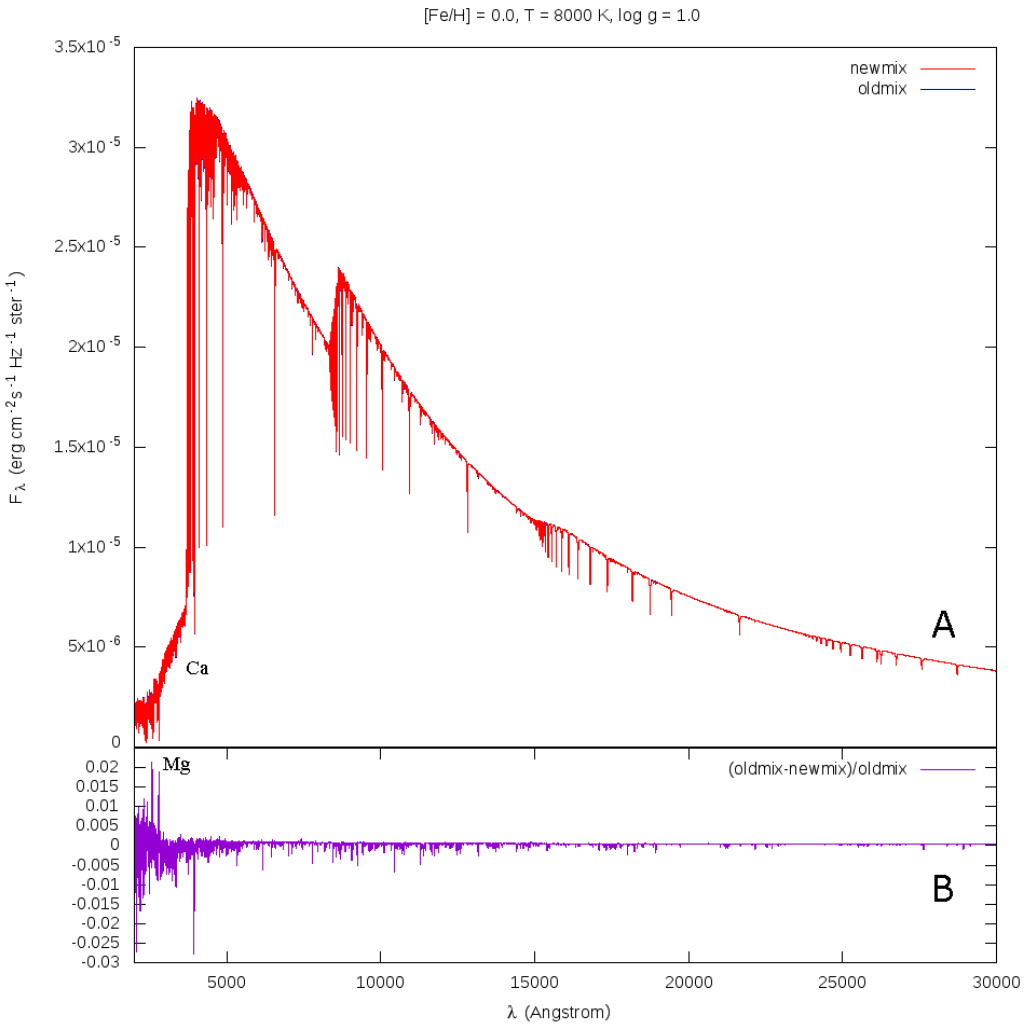

Figure 3.2.6. ***A.*** *Comparison of fluxes from the old ODF (blue) and the new ODF model (red) with parameters* T_{eff}*=8000 K, logg=1.0, [Fe/H]=0.0.* ***B.*** *Difference between the fluxes (oldmix - newmix) / oldmix.*

The main differences between the spectra produced by the old and the new mixtures for stars with an effective temperature of 8000K is in the region below 5000 Å (figure 3.2.6). The higher magnesium and lower calcium abundance in the new model can be the cause of the differences in the lines at 2800 Å and 3933 Å respectively.

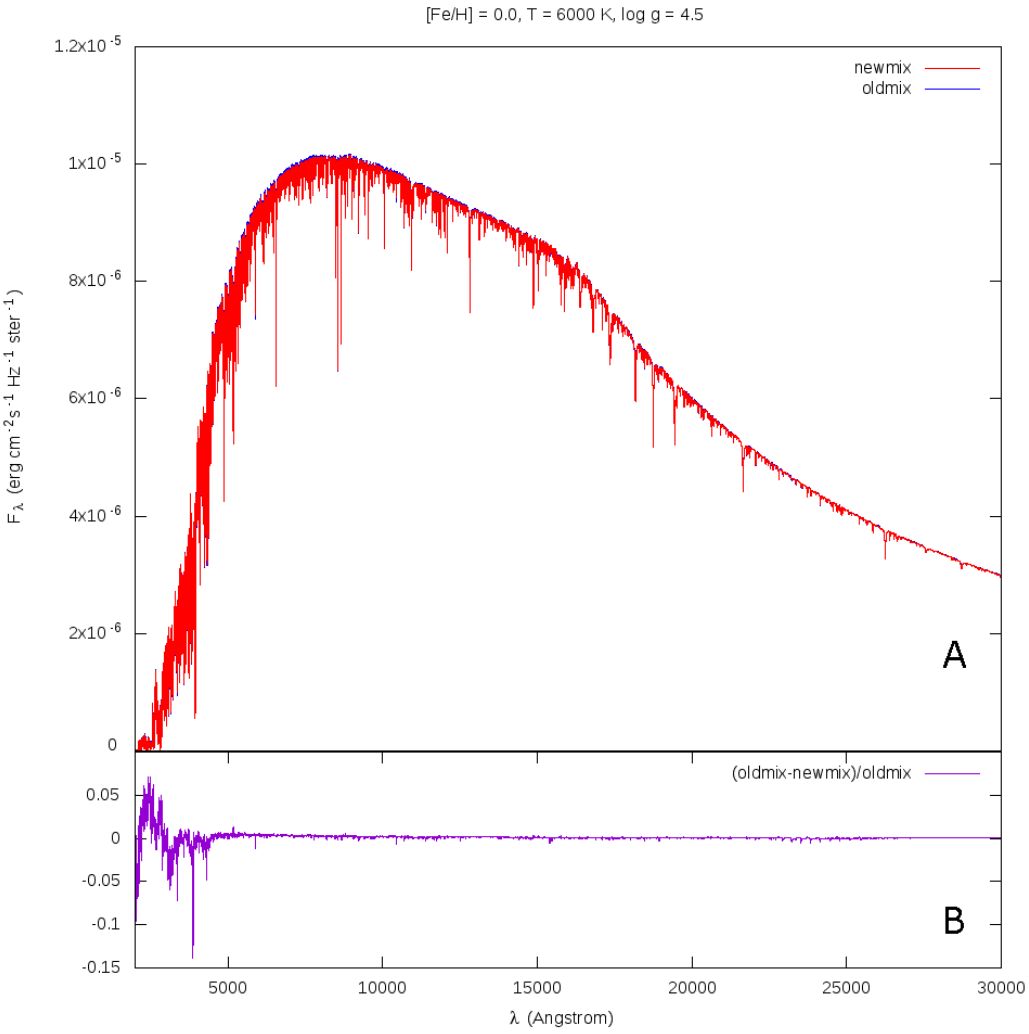

Figure 3.2.7. ***A.*** *Comparison of fluxes from the old ODF (blue) and the new ODF model (red) with parameters* T_{eff}*=6000 K, logg=4.5, [Fe/H]=0.0.* ***B.*** *Difference between the fluxes (oldmix - newmix) / oldmix.*

At 6000K, while there are differences of up to 5% in the flux below 5000 Å, there is much less flux in this region of the spectra for G-type main sequence stars compared to the hotter stars shown earlier, and at wavelengths above 5000 Å the spectra produced by the old and the new models are almost identical (figure 3.2.7).

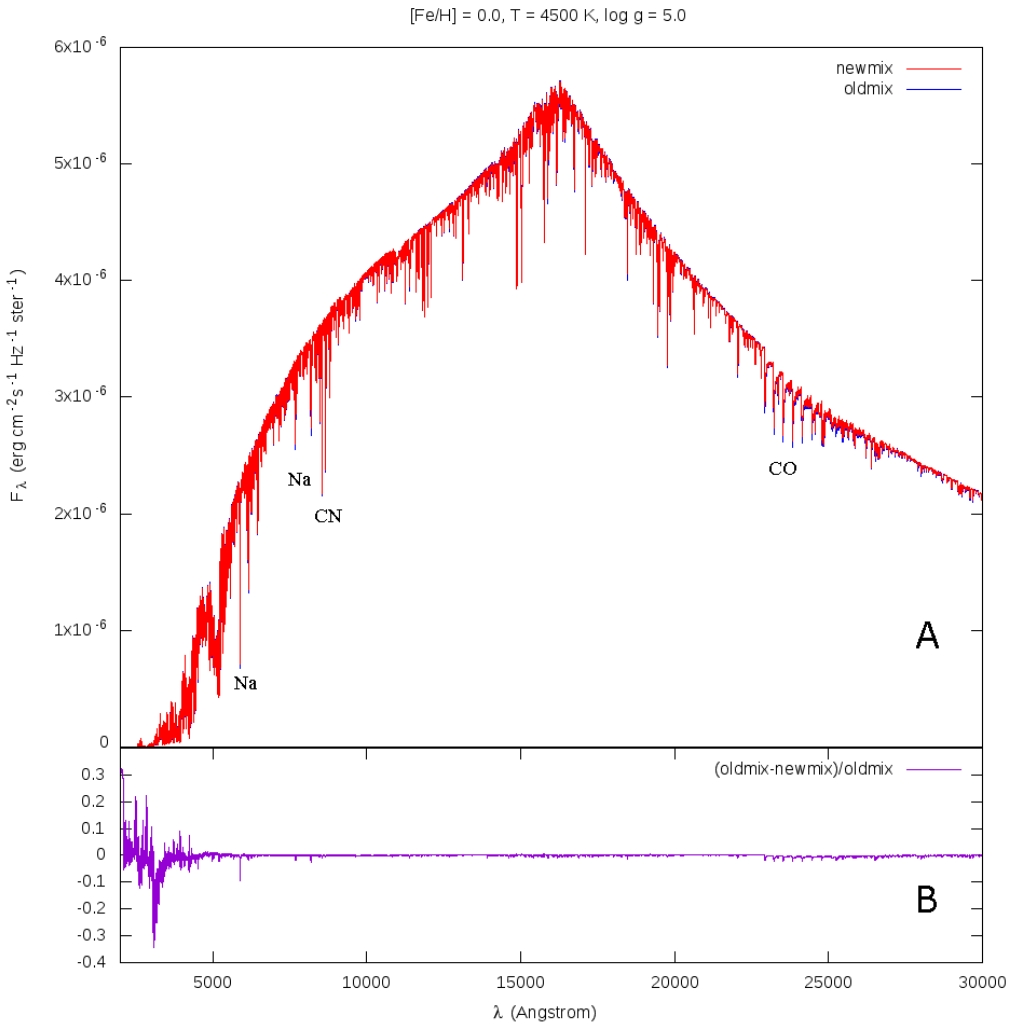

Figure 3.2.8. ***A.*** *Comparison of fluxes from the old ODF (blue) and the new ODF model (red) with parameters* T_{eff}*=4500 K, logg=5.0, [Fe/H]=0.0.* ***B.*** *Difference between the fluxes (oldmix - newmix) / oldmix.*

At 4500K, while there are differences of up to 30% in the flux below 5000 Å, there is much less flux in this region of the spectra compared to the hotter stars shown earlier, and at wavelengths above 5000 Å the spectra produced by the old and the new models are almost identical (figure 3.2.8). The depth of the sodium lines at 5900 Å and 8200 Å are between 2 and 10% greater, and the CN and CO molecular lines indicated also begin to show a greater depth.

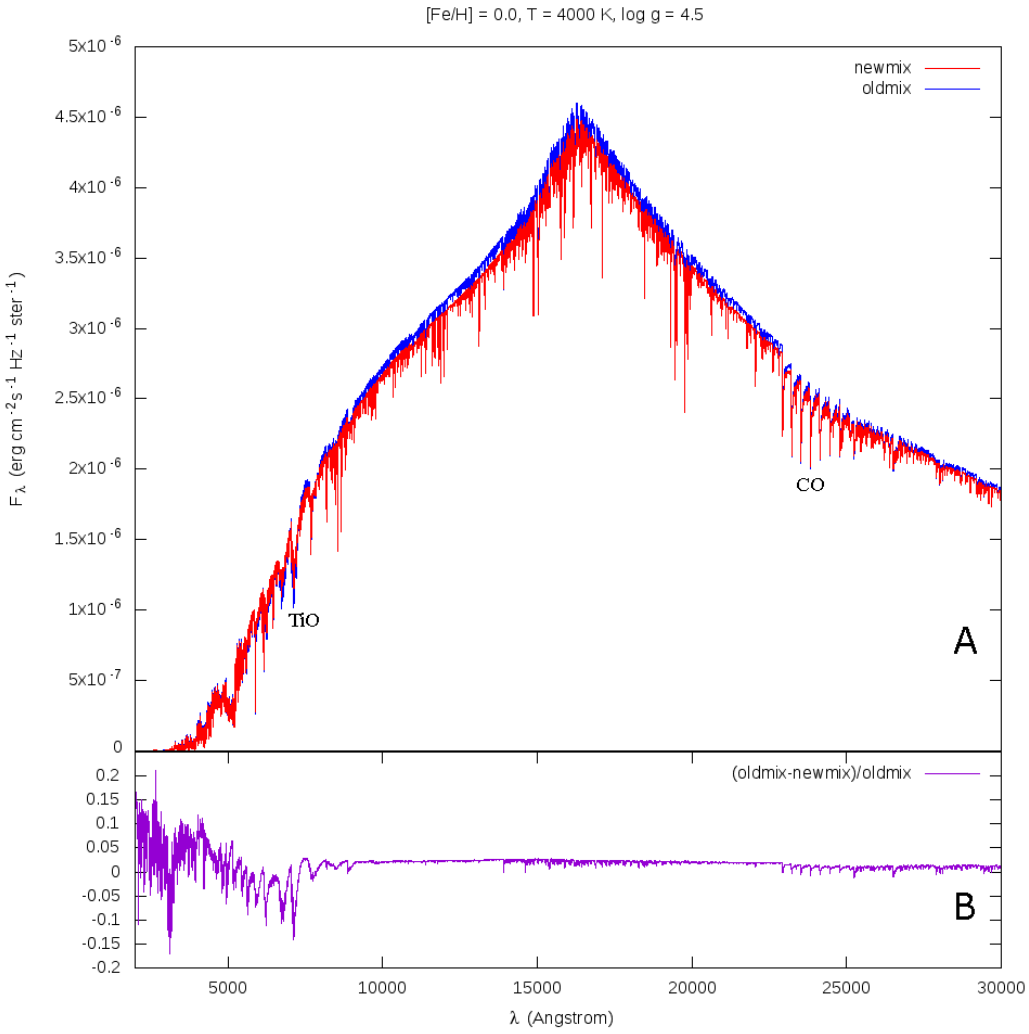

Figure 3.2.9. ***A.*** *Comparison of fluxes from the old ODF (blue) and the new ODF model (red) with parameters* T_{eff}*=4000 K, logg=4.5, [Fe/H]=0.0.* ***B.*** *Difference between the fluxes (oldmix - newmix) / oldmix.*

For red main sequence stars at a temperature of 4000K the spectra between 5000 and 9000 Å becomes dominated by the TiO spectral lines (figure 3.2.9). The old ODF has higher abundances of both Ti and O and these lines being 10-15% deeper. The overall flux for the spectra produced by the new ODF abundances is around 1% less than that produced by the old abundances.

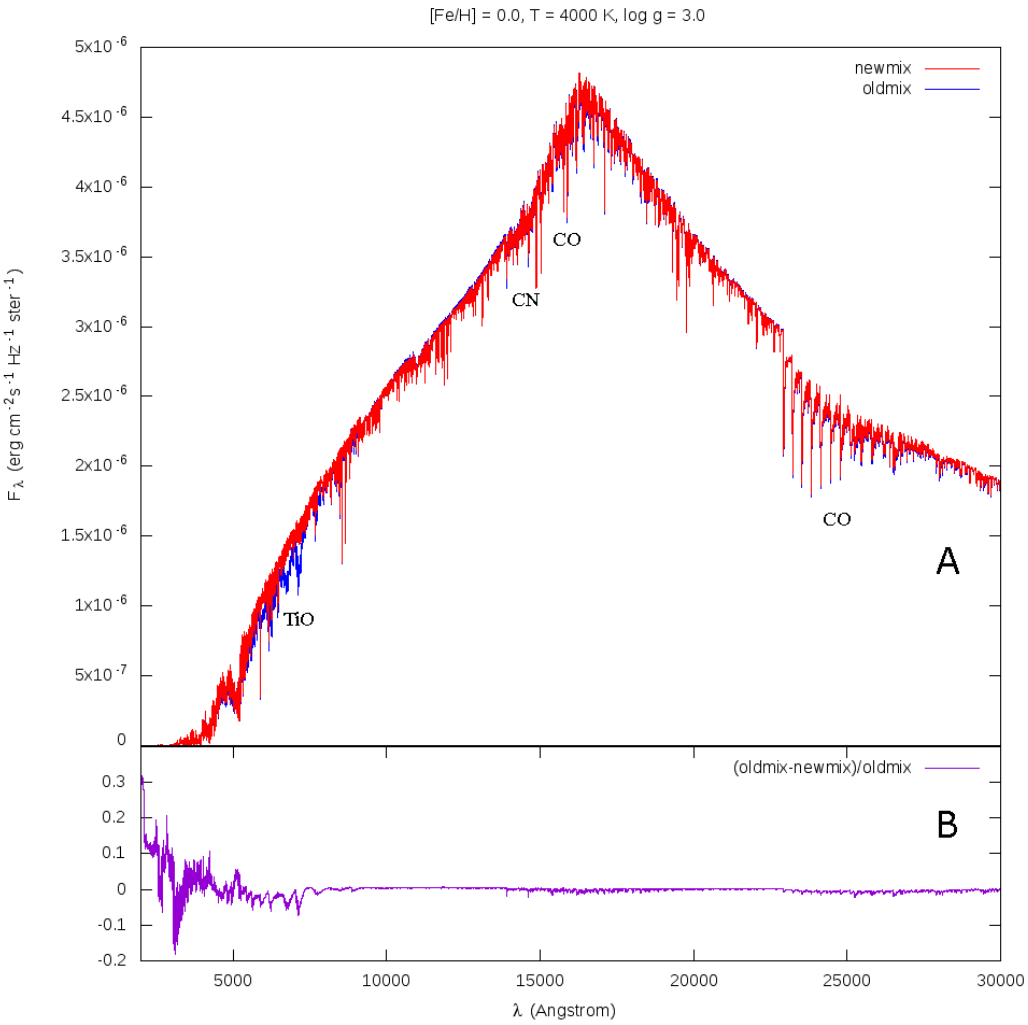

Figure 3.2.10. A. Comparison of fluxes from the old ODF (blue) and the new ODF model (red) with parameters T_{eff}=4000 K, logg=3.0, [Fe/H]=0.0. B. Difference between the fluxes (oldmix - newmix) / oldmix.

With decreasing gravity the differences in the old and new model spectra for cool red stars between 5000 and 9000 Å become less as the depth of the TiO spectral lines become more similar; 10% for log g 4.5, 5% for log g 3.0 and 2% for log g 1.0 (compare figures 3.2.9, 3.2.10 and 3.2.11). The differences at longer wavelengths seem to remain fairly constant with decreasing gravity; the CN lines at 1460 Å and the CO lines at 1560 Å and 25000 Å are slightly deeper (1 to 2%) in the spectra produced by the old ODF abundances.

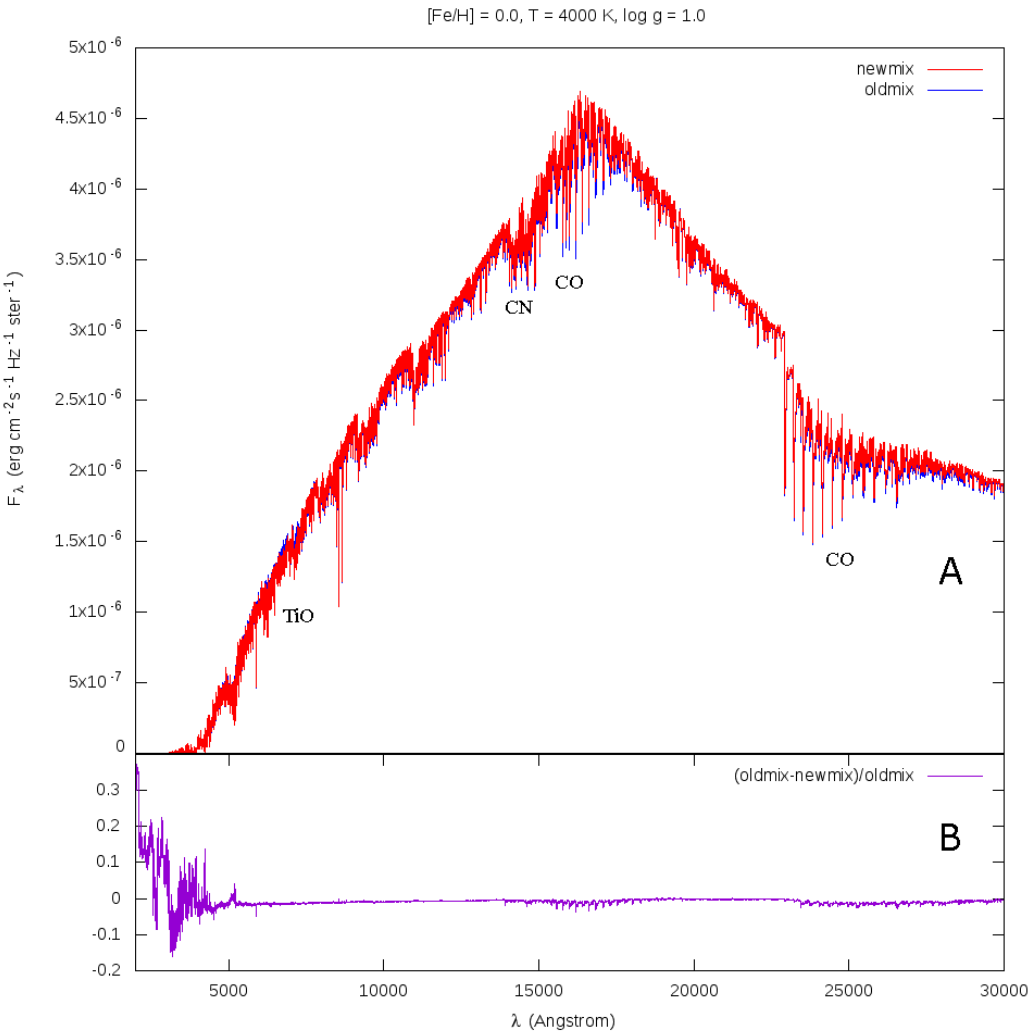

Figure 3.2.11. ***A.*** *Comparison of fluxes from the old ODF (blue) and the new ODF model (red) with parameters* T_{eff}*=4000 K, logg=1.0, [Fe/H]=0.0.* ***B.*** *Difference between the fluxes (oldmix - newmix) / oldmix.*

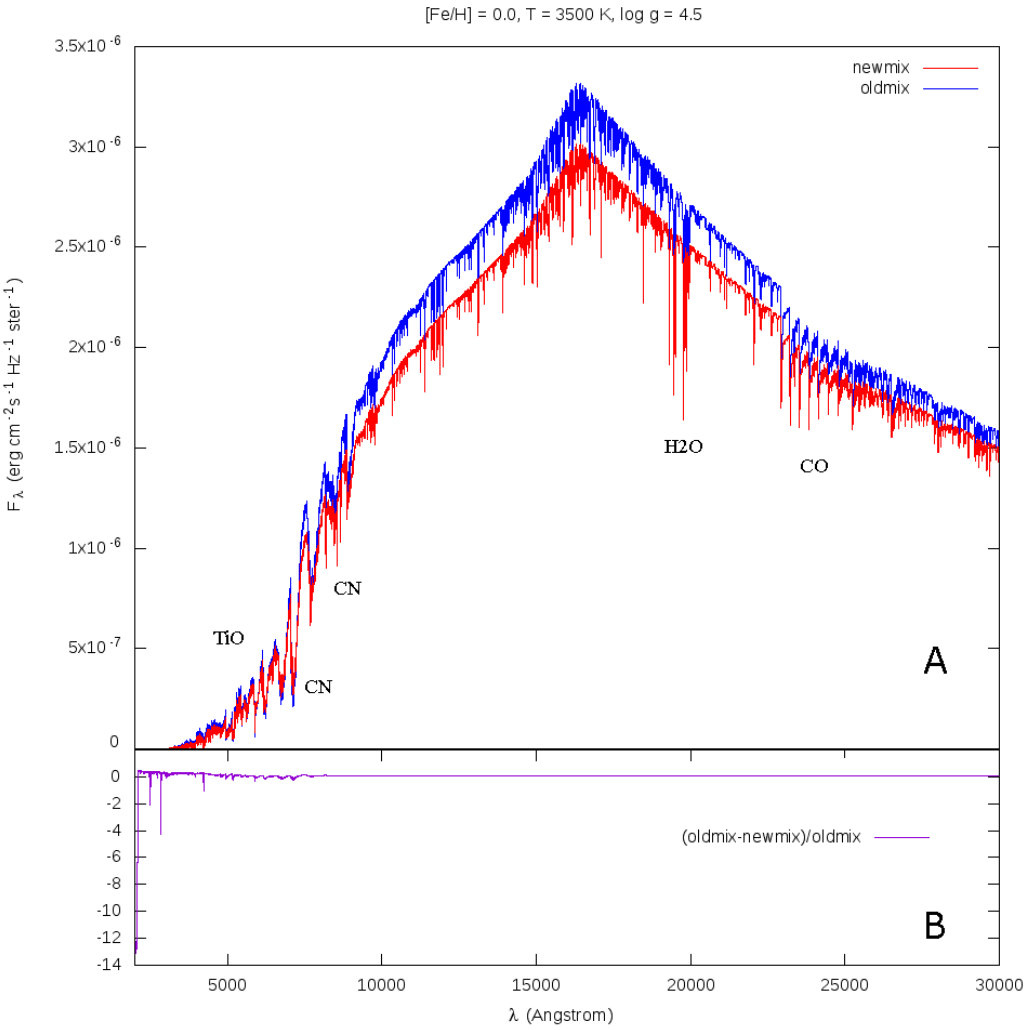

Figure 3.2.12. ***A.*** *Comparison of fluxes from the old ODF (blue) and the new ODF model (red) with parameters* T_{eff}*=3500 K, logg=4.5, [Fe/H]=0.0.* ***B.*** *Dfference between the fluxes (oldmix - newmix) / oldmix.*

At temperatures of 3500 K; the lowest that can be produced by the ATLAS 9 programme, the overall shape of the energy distribution remains the same between the old and the new models, but there is considerable variation in the amount of flux in the synthetic spectra. This varies by wavelength (see figure 3.2.12) and it is worth examining the different regions of the spectra more closely.

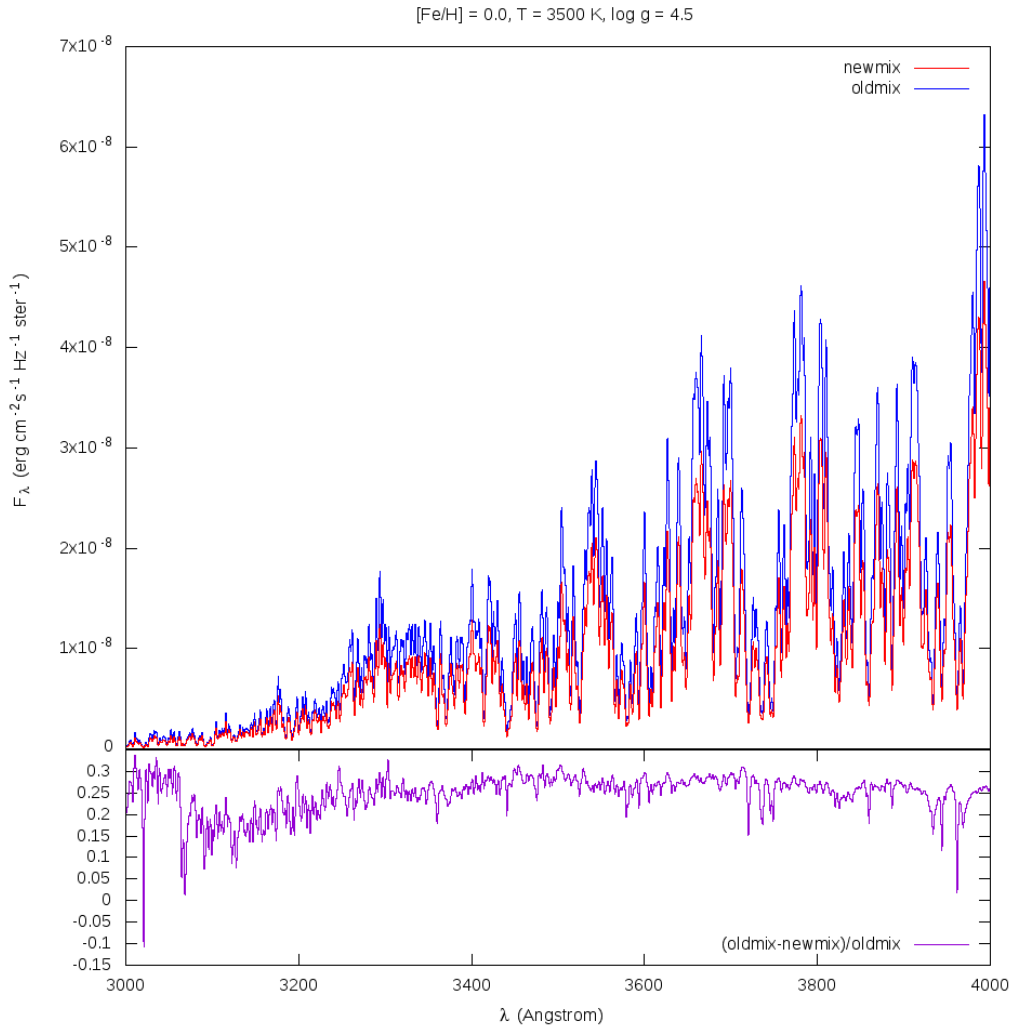

Figure 3.2.13. Same as figure 3.2.12, but for the smaller wavelength region (3000-4000 Å) plotted on a larger scale. ***A.*** *Comparison of fluxes from the old ODF (blue) and the new ODF model (red) with parameters* T_{eff}*=3500 K, logg=4.5, [Fe/H]=0.0.* ***B.*** *Difference between the fluxes (oldmix - newmix) / oldmix.*

Between 3000 and 4000 Å, the flux produced by the old mixture is about 25% greater (figure 3.2.13) and differences in some lines, such as the Ca line at 3933 Å are evident, with the majority of the lines in the old mixture being up to 20% deeper.

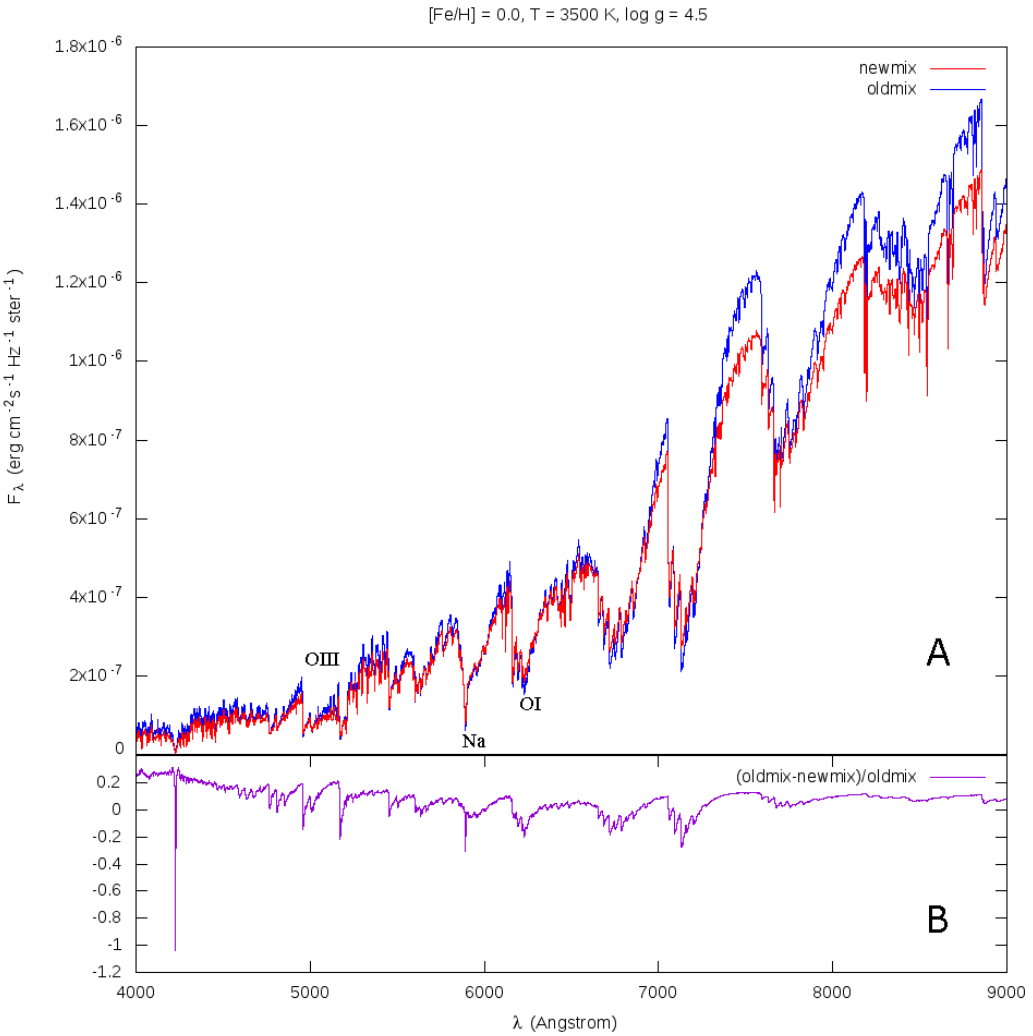

Figure 3.2.14. Same as figure 3.2.12, but for the smaller wavelength region (4000-9000 Å) plotted on a larger scale. ***A.*** *Comparison of fluxes from the old ODF (blue) and the new ODF model (red) with parameters* T_{eff}*=3500 K, logg=4.5, [Fe/H]=0.0.* ***B.*** *Difference between the fluxes (oldmix - newmix) / oldmix.*

Between 4000 and 9000 Å, the flux produced by the old mixture is about 10% greater (figure 3.2.14) and differences in some lines, such as the titanium oxide, oxygen and sodium lines can be seen, with again the majority of the lines in the spectrum produced by the old mixture being up to 20% deeper.

3.3 Comparison of Synthetic Spectra at other metallicities

The previous spectra have all been calculated using a scaled solar metallicity with [Fe/H] = 0.0. A grid of model atmospheres and synthetic spectra have also been calculated for metallicities of [Fe/H] of 1.0, 0.5, -0.5, -1.0, -1.5, -2.0 and -2.5, and for alpha enhanced metallicities (+0.4 dex) of [Fe/H] of 0.5, 0.0, -0.5, -1.0, -1.5, -2.0 and -2.5. A selection of these synthetic spectra is shown below, highlighting any differences between those produced by the old and new abundance mixtures.

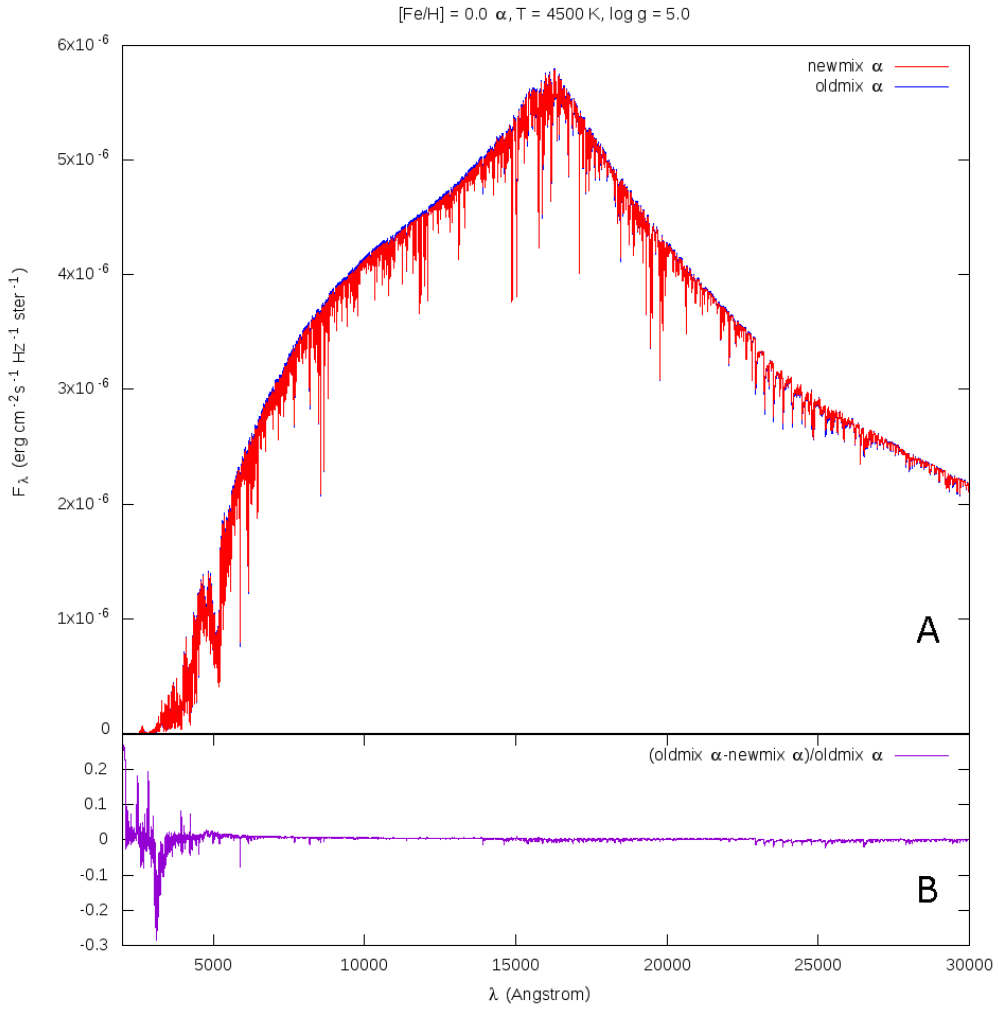

Figure 3.3.1. ***A.*** *Comparison of fluxes from the old alpha enhanced (+0.4 dex) ODF (blue) and the new alpha enhanced (+0.4 dex) ODF model (red) with parameters T_{eff}=4500 K, logg=5.0, [Fe/H]=0.0.* ***B.*** *Difference between the fluxes (oldmix alpha – newmix alpha) / oldmix alpha.*

Comparisons between the synthetic spectra produced by the alpha enhanced ODFs made with the old and new abundance mixtures follow the same pattern and show almost identical variations as between the scaled solar ODFs (compare figure 3.3.1 above with figure 3.2.8 in the previous section). This is true regardless of the effective temperature, global metallicity and gravity used in producing the models.

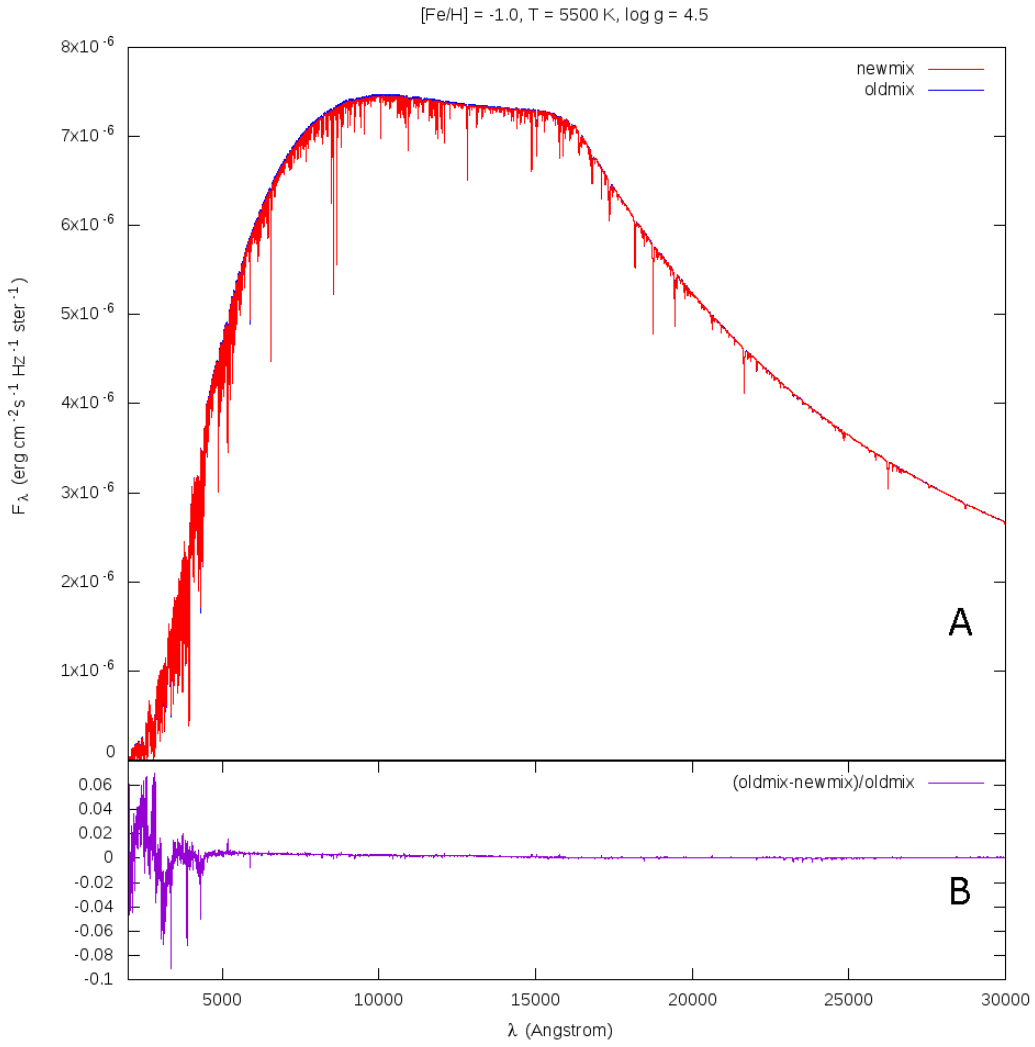

Figure 3.3.2. ***A.*** *Comparison of fluxes from the old ODF (blue) and the new ODF model (red) with parameters* T_{eff}*=5500 K, logg=4.5, [Fe/H]=-1.0.* ***B.*** *Difference between the fluxes (oldmix - newmix) / oldmix.*

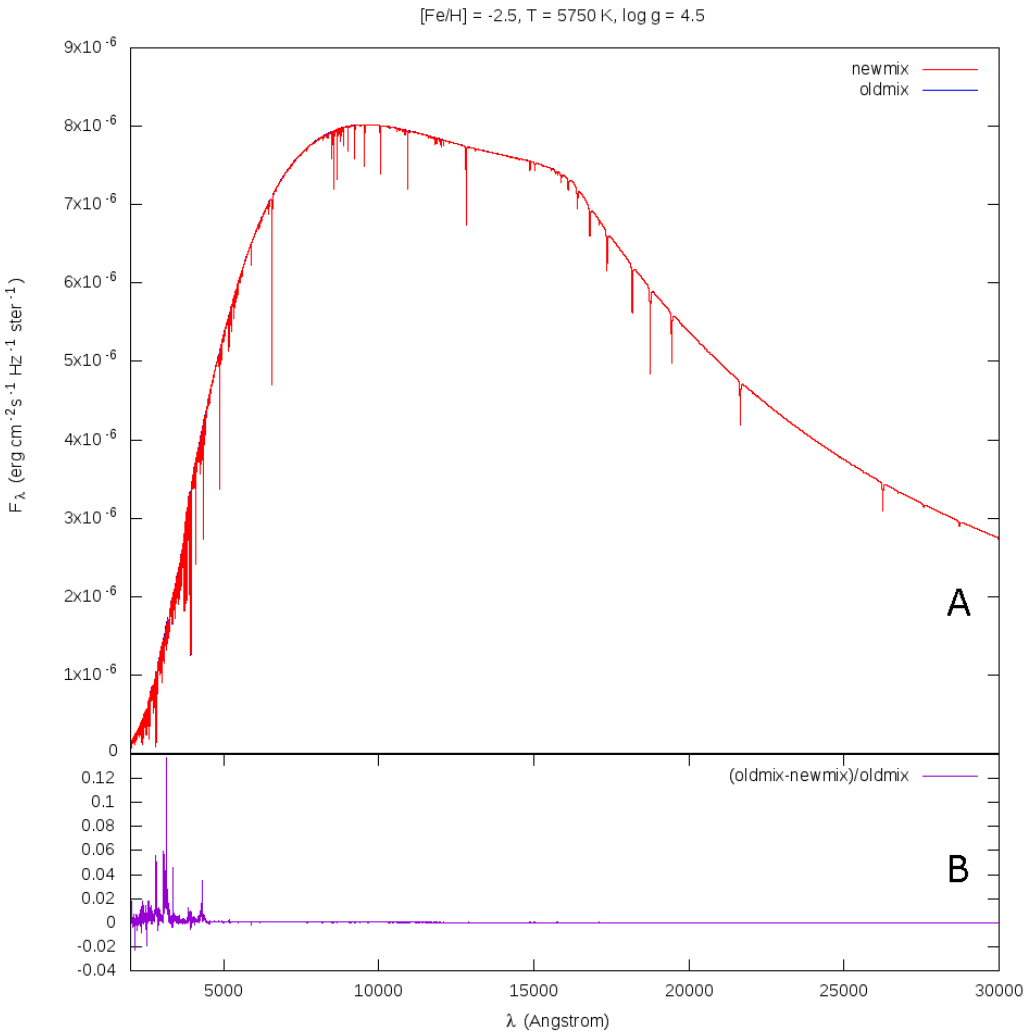

Figure 3.3.3. ***A.*** *Comparison of fluxes from the old ODF (blue) and the new ODF model (red) with parameters* T_{eff}*=5750 K, logg=4.5, [Fe/H]=-2.5.* ***B.*** *Difference between the fluxes (oldmix - newmix) / oldmix.*

Comparing the spectra at lower metallicities than [Fe/H] = 0 (figures 3.3.2 and 3.3.3) show similar patterns to those at higher metallicities – the fluxes in the spectra produced by the old and new ODF models are within 1% of each other for the majority of the spectrum, especially at wavelengths greater than 5000 Å; and the overall difference in the flux decreases with decreasing metallicity.

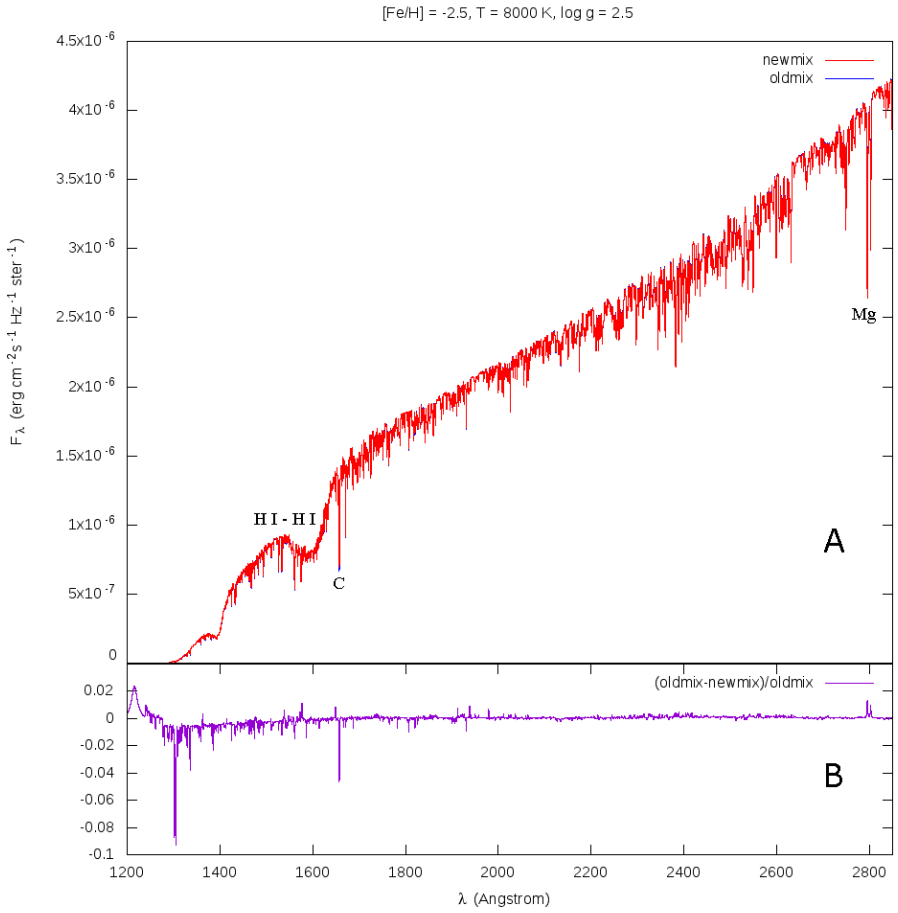

Figure 3.3.4. ***A.*** *Comparison of fluxes from the old ODF (blue) and the new ODF model (red) with parameters* T_{eff}*=8000 K, logg=2.5, [Fe/H]=-2.5.* ***B.*** *Difference between the fluxes (oldmix - newmix) / oldmix.*

One of the key changes between the spectra produced by the older Anders and Grevesse (1989) abundances to the newer Grevesse and Sauval (1998) values reported by Castelli and Kurucz (2004) was in the 1200-2000 Å part of the spectrum for low metallicity stars. As this was primarily due to the inclusion of H I-H I molecular absorption lines, rather than the change in the chemical abundance, a similar change was not expected when the abundances were replaced with those from Asplund *et al.* (2009). This is shown in figure 3.3.4 where the flux in the 1500-1600 Å region is within 1% of the old ODF model. However, there are some differences that are solely due to the changes in abundances, most significantly it can be seen that the depth of the carbon line at 1657 Å is 4.5% greater in the old model spectra compared to the new one.

Chapter 4

Comparisons of bolometric corrections and colours.

4.1 Photometric Systems, Bolometric Corrections and Colour Transformations

The magnitudes and colours of star systems such as globular and open clusters can be analysed by producing integrated CM diagrams that can then be used to derive the ages and metallicities of the stars that comprise the system. Likewise, these integrated colour magnitude diagrams can also be made for galaxies and can then be used to study the proportion and type of the constituent stars.

In order for these studies to be made, it is necessary to calibrate these measurements onto a standard scale of flux, normalised to a star of constant brightness (Bessell, 2005). There have been many photometric systems created by different astronomers using different passbands, instrumentation and detectors which enable the measurement of absolute fluxes of stars. The different systems can be more appropriate for different types of stars, as they are designed to be sensitive to a particular indicator such as temperature, gravity or a particular metal abundance indicator (Casagrande & VandenBerg, 2014). The photometric filter system will be designed to select a region within the stellar spectra that highlights the variation in a particular characteristic trait which will then allow the properties of the observed star to be derived, including effective temperature, gravity and metallicity. Filter systems that cover a large wavelength range of the spectra give broad-band colours, which are mainly dependent on the temperature of a star, while intermediate or narrow-band filters can be focussed on specific spectral features that can be dependent on other parameters.

The absolute magnitude of a star over all wavelengths of light emitted by that star is known as the bolometric magnitude. However, most detectors only measure the flux of a star

within the wavelength band of a given filter, and to convert from the observed magnitude within this filter to the overall magnitude of the star requires a bolometric correction.

The absolute bolometric magnitude of a star M_{bol} can be stated as:

$$M_{bol} = M_{bol\odot} - 2.5 \log\left(\frac{L}{L_{\odot}}\right) = M_{bol\odot} - 2.5 \log(4\pi R^2 F_{bol}/L_{\odot})$$

Where $M_{bol\odot}$ is the bolometric magnitude of the Sun (the value of 4.74 was used in these calculations), and the bolometric flux of a star is equal to the sum of its flux at all wavelengths:

$$F_{bol} = \int_0^{\infty} F_{\lambda} d\lambda$$

The bolometric correction for a given wavelength band is dependent on the stellar energy distribution (calculated from the synthetic spectra based upon the effective temperature, surface gravity and chemical composition), the solar luminosity and bolometric magnitude, along with the spectral energy distribution and magnitude of a reference star.

The Johnson-Cousins-Bessell system has fluxes normalised to the flux of Vega, and this system produces tables of intrinsic colours for various types of stars, along with temperature-colour calibrations and bolometric corrections for stars of different colours (Bessell, 2005). This is a broad-band system with filters that are 800 to 1000 Angstroms wide. The Strömgren uvby system consists of intermediate band filters that had been devised to accurately measure the temperature and gravities of early-type stars (Bessell, 2005). Figure 4.0.1 shows the wavelength ranges covered by the filters in the Johnson-Cousins-Bessell and Strömgren systems used in this study.

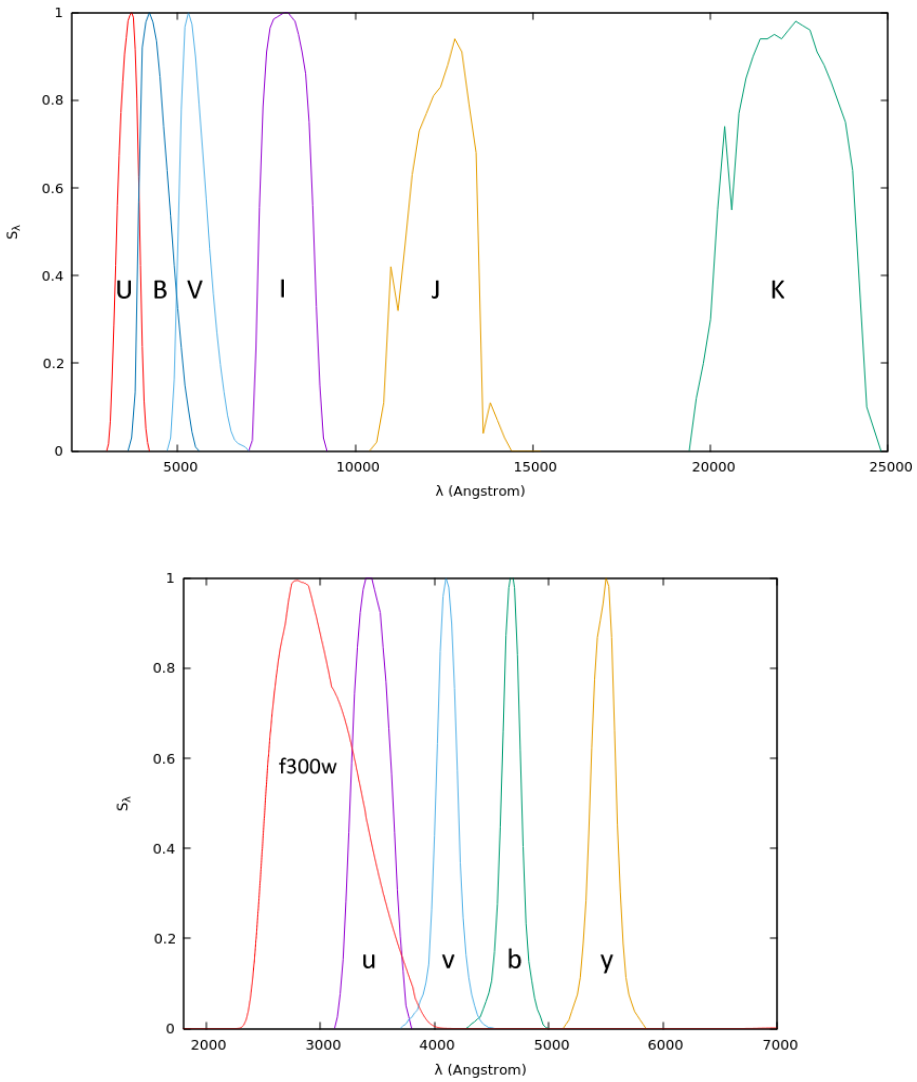

Figure 4.0.1. Response functions S(λ) for filters of various photometric systems. The top panel shows Johnson-Cousins-Bessell filters U,B,V,I,J and K. The bottom panel shows Strömgren filters u, v, b and y, along with the HST/WFPC2 f300w filter.

The bolometric flux at the surface of a star is related to the effective temperature by the following relation

$$F_{bol} = \int_0^\infty F_\lambda \, d\lambda = \frac{ac}{4} T_{eff}^4$$

The bolometric correction for a particular wavelength band A can be calculated from the spectral energy distribution produced by the synthetic spectrum using the following equation (Girardi *et al.*, 2002) dependent on the effective temperature, flux at the stellar

surface (F_λ), solar luminosity ($L_\odot$) and the flux (f_λ^0) and apparent magnitude (m_A^0) of the reference star in that wavelength band.

$$BC_A = M_{bol,\odot} - 2.5\log\left[4\pi(10\,pc)^2\frac{acT_{eff}^4}{4L_\odot}\right] + 2.5\log\left(\frac{\int_{\lambda1}^{\lambda2} F_\lambda S_\lambda\, d\lambda}{\int_{\lambda2}^{\lambda1} f_\lambda^0\, S_\lambda\, d\lambda}\right) - \mathrm{m}_A^0$$

The Johnson system uses the spectra of Vega as a reference system, and assumes that the apparent magnitude of Vega in the V band is equal to zero, and all the colour indicies are also equal to zero (Salaris & Cassisi, 2005).

4.1.1 Comparisons between the bolometric corrections for the Sun

A synthetic spectrum of a star with Solar values of effective temperature, metallicity and gravity was created with the ATLAS9 programme using the Asplund *et al.* (2009) chemical abundance values.

Bolometric corrections and colours were calculated in two widely used photometric systems (Johnson-Cousins-Bessell and Strömgren) from the synthetic spectra produced with the new (Asplund *et al,* 2009) abundances, using and the reference spectra for Vega produced by Castelli and Kurucz (1993). The bolometric corrections and colours from a synthetic spectrum of a similar star with values produced using the older Grevesse and Sauval (1998) mixture was also created and the two sets of results are shown below in Table 4.1.1 and 4.1.2.

	new U-B	old U-B	new B-V	old B-V	new V-I	old V-I	new V-K	old V-K	new J-K	old J-K	new BCV	old BCV
Solar	0.081	0.089	0.621	0.629	0.699	0.696	1.510	1.504	0.380	0.378	0.002	0.008

Table 4.1.1 Comparisons Johnson-Cousins-Bessell colour relations and bolometric corrections in V of a synthetic Solar star created using the new (Asplund et al., 2009) and old (Grevesse & Sauval, 1998) chemical abundances (T_{eff} 5777K, [Fe/H]=0 and log g 4.4).

	new u-b	old u-b	new u-v	old u-v	new b-y	old b-y	new y	old y
Solar	0.069	0.080	-0.410	-0.408	0.377	0.379	0.009	0.015

Table 4.1.2 Comparisons of Strömgren colour relations and bolometric corrections in y of a synthetic Solar star created using the new (Asplund et al., 2009) and old (Grevesse & Sauval, 1998) chemical abundances (T_{eff} 5777K, [Fe/H]=0 and log g 4.4).

In addition, the bolometric correction was also calculated for the HST/WFPCS2 f300w UV filter, giving a value of -1.030 for the new model compared to -1.039 for the old model.

4.2.1 Comparisons between the new and old mixtures for main sequence stars

For each synthetic spectrum created by the ATLAS 9 programme using the Asplund *et al.* (2009) chemical abundances, bolometric corrections and colours were calculated in the Johnson-Cousins-Bessell and Strömgren photometric systems. This was also carried out for synthetic spectra produced using the older Grevesse and Sauval (1998) mixture and the two sets of results are shown below.

Table 4.2.1 and Figure 4.2.1 shows the colour values at different temperatures in passbands in the Johnson-Cousins-Bessell system and Table 4.2.2 and Figure 4.2.2 for passbands in the Strömgren system for synthetic spectra of stars of [Fe/H] = 0 and log g of 4.5. As expected from the similarities in the spectra discussed in the previous chapter, there is very little difference in the T_{eff}-colour relations of the spectra created by the old and the new abundances.

T_{eff}(K)	new U-B	old U-B	new B-V	old B-V	new V-I	old V-I	new V-K	old V-K	new J-K	old J-K	new BCV	old BCV
3500	0.972	0.851	1.342	1.208	2.293	2.309	4.530	4.520	0.983	0.956	-1.712	-1.627
3750	1.053	0.968	1.364	1.260	1.927	1.976	3.951	4.011	0.938	0.928	-1.284	-1.292
4000	1.069	1.039	1.321	1.269	1.646	1.669	3.524	3.553	0.903	0.897	-0.974	-0.984
4250	0.983	0.990	1.213	1.202	1.412	1.423	3.134	3.151	0.838	0.837	-0.715	-0.732
4500	0.818	0.828	1.081	1.081	1.221	1.217	2.753	2.751	0.744	0.744	-0.491	-0.489
4750	0.639	0.645	0.964	0.965	1.073	1.069	2.426	2.419	0.651	0.648	-0.324	-0.317
5000	0.471	0.475	0.871	0.873	0.953	0.946	2.147	2.136	0.570	0.566	-0.198	-0.187
5250	0.318	0.321	0.787	0.790	0.856	0.849	1.910	1.898	0.499	0.496	-0.107	-0.095
5500	0.189	0.189	0.706	0.710	0.777	0.771	1.708	1.697	0.439	0.436	-0.045	-0.034
5750	0.087	0.087	0.630	0.634	0.707	0.702	1.530	1.521	0.386	0.383	-0.003	0.006
6000	0.015	0.012	0.561	0.565	0.644	0.640	1.369	1.362	0.338	0.337	0.026	0.033
6500	-0.056	-0.053	0.445	0.447	0.528	0.528	1.085	1.083	0.257	0.256	0.058	0.060
7000	-0.052	-0.056	0.351	0.351	0.420	0.419	0.834	0.831	0.189	0.188	0.071	0.074
8000	0.027	0.025	0.211	0.211	0.210	0.210	0.396	0.396	0.082	0.082	0.073	0.074
9000	0.043	0.043	0.086	0.085	0.050	0.050	0.092	0.091	0.020	0.020	-0.012	-0.011
10000	-0.056	-0.057	0.009	0.009	-0.027	-0.027	-0.075	-0.076	-0.015	-0.015	-0.197	-0.195
11000	-0.178	-0.178	-0.040	-0.040	-0.067	-0.068	-0.185	-0.186	-0.042	-0.042	-0.403	-0.401
12000	-0.300	-0.301	-0.070	-0.070	-0.090	-0.092	-0.267	-0.268	-0.062	-0.062	-0.602	-0.600
20000	-0.798	-0.800	-0.181	-0.182	-0.209	-0.210	-0.630	-0.632	-0.149	-0.148	-1.901	-1.895

Table 4.2.1 Comparisons of T_{eff} and Johnson-Cousins-Bessell colour relations of sample synthetic spectra for main sequence stars created by the new (Asplund et al., 2009) and old (Grevesse & Sauval, 1998) abundances using [Fe/H]=0 and log g 4.5.

The Johnson colour relations (figure 4.2.1) for the two sets of data for main sequence stars are very similar in the U-B above 5250K, and significant differences only really appear at temperatures below 4250K, with the new models being increasingly redder than the old models with decreasing temperature (Table 4.2.1 and Figure 4.2.1). Similar effects are seen in the B-V and J-K colours, but to a much lesser extent in the V-I and V-K colours and the bolometric correction in V.

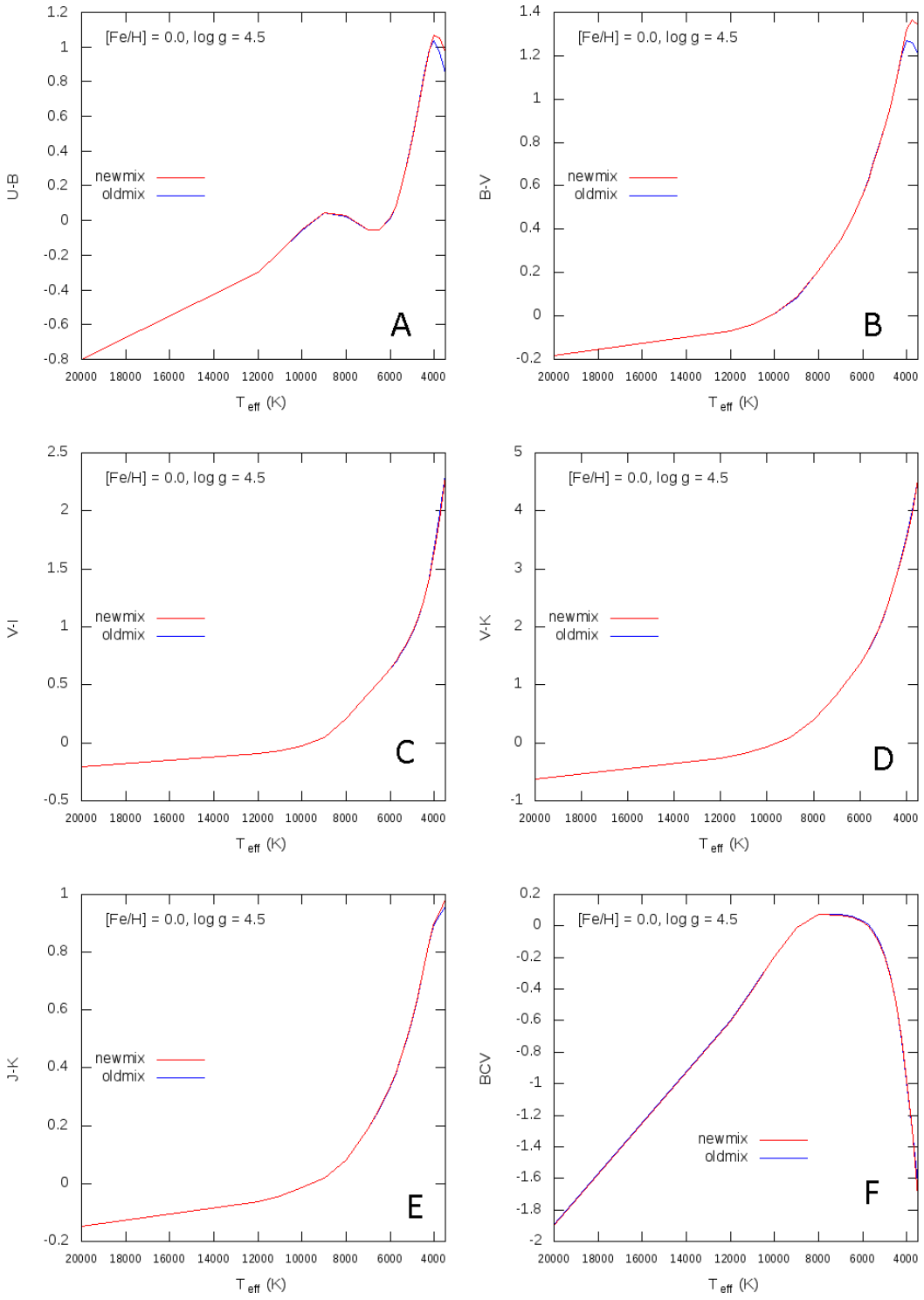

Figure 4.2.1 T_{eff}-colour relations for logg=4.5 and [Fe/H]=0.0 showing old-ODF models (blue) and new-ODF models (red) for five Johnson-Cousins-Bessell colour indices (A: U-B, B: B-V, C: V-I, D: V-K, E: J-K) and F: the bolometric correction in V.

T_{eff}(K)	new u-b	old u-b	new u-v	old u-v	new b-y	old b-y	new y	old y
3500	1.328	1.144	0.515	0.501	1.052	0.997	-1.659	-1.555
3750	1.476	1.344	0.433	0.446	0.959	0.917	-1.242	-1.235
4000	1.493	1.451	0.326	0.354	0.853	0.828	-0.930	-0.933
4250	1.341	1.363	0.167	0.205	0.730	0.726	-0.663	-0.678
4500	1.080	1.106	0.015	0.034	0.629	0.626	-0.442	-0.440
4750	0.807	0.825	-0.114	-0.105	0.556	0.554	-0.288	-0.280
5000	0.569	0.580	-0.226	-0.224	0.501	0.499	-0.175	-0.165
5250	0.366	0.372	-0.314	-0.318	0.456	0.455	-0.093	-0.082
5500	0.201	0.203	-0.376	-0.382	0.416	0.416	-0.036	-0.025
5750	0.074	0.073	-0.416	-0.423	0.381	0.380	0.005	0.013
6000	-0.016	-0.019	-0.436	-0.442	0.347	0.347	0.032	0.039
6500	-0.104	-0.100	-0.422	-0.421	0.285	0.286	0.063	0.066
7000	-0.099	-0.105	-0.351	-0.355	0.227	0.227	0.076	0.079
8000	0.010	0.006	-0.163	-0.166	0.121	0.121	0.078	0.079
9000	0.014	0.014	-0.081	-0.081	0.027	0.027	-0.010	-0.008
10000	-0.139	-0.141	-0.165	-0.167	-0.010	-0.010	-0.196	-0.194
11000	-0.323	-0.323	-0.303	-0.304	-0.030	-0.030	-0.403	-0.401
12000	-0.508	-0.509	-0.461	-0.462	-0.043	-0.043	-0.603	-0.601
20000	-1.239	-1.241	-1.103	-1.105	-0.098	-0.099	-1.905	-1.899

Table 4.2.2 Comparisons of T_{eff} and Strömgren colour relations of sample spectra for main sequence stars created by the new (Asplund et al., 2009) and old (Grevesse and Sauval, 1998) abundances using [Fe/H]=0 and log g 4.5.

The Strömgren colour relations (figure 4.2.2) for the two sets of data for main sequence stars show a similar pattern; there are only significant differences at temperatures below 4250K, with the new models being redder than the old models in u-b and b-y. At temperatures above 4500K, and in u-v at all temperatures, the two models give almost identical results, and there is no difference in the bolometric correction for the y band (figure 4.2.2D). Similarly, the bolometric correction for the f300w UV filter (figure 4.2.3A) for main sequence stars is almost identical at temperatures above 4000K, with the new models being slightly redder than the old models at temperatures below this.

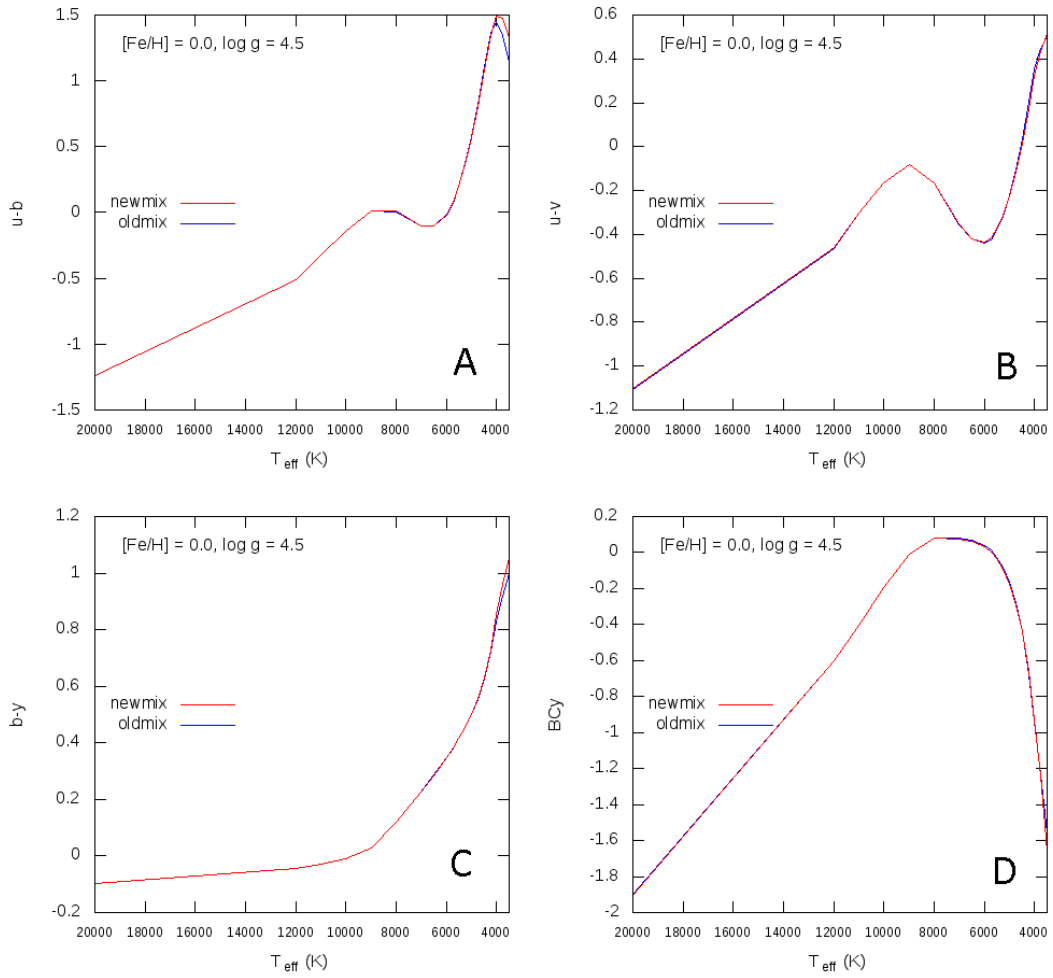

Figure 4.2.2 T_{eff}-colour relations for log g=4.5 and [Fe/H]=0.0 showing old-ODF models (blue) and new-ODF models (red) for three Strömgren colour indices (A: u-b, B: u-v and C: b-y) and D: the bolometric correction in y.

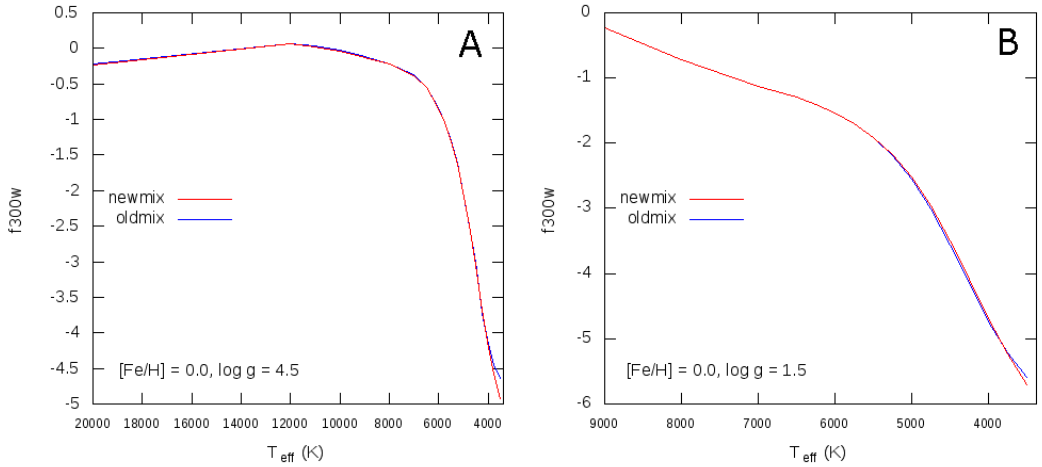

Figure 4.2.3 T_{eff}-colour relations for [Fe/H]=0.0 showing old-ODF models (blue) and new-ODF models (red) for the bolometric correction in the f300w filter for A: stars of log g 4.5 and B: stars of log g 1.5.

4.2.2 Comparisons between the new and old mixtures for giant stars

Figure 4.2.4 shows the colour values at different temperatures in passbands in the Johnson-Cousins-Bessell system and Figure 4.2.5 for passbands in the Strömgren system for synthetic spectra of stars of [Fe/H] = 0 and log g of 1.5.

The Johnson colour relations (figure 4.2.4) for the two sets of data for giant stars are very similar in general, but there are a few key differences. In U-B above 7000K there is no difference, but below 6500K the new models are slightly bluer, giving a discrepancy of around 50K. At temperatures below 4250K however, this reverses with the new models being slightly redder. This is also true in the B-V index, although to a lesser extent. In the J-K colour, there is little difference between the models above 4000K, and at temperatures below this the new models are redder. There are no differences in the V-I and V-K colours and the bolometric correction in V.

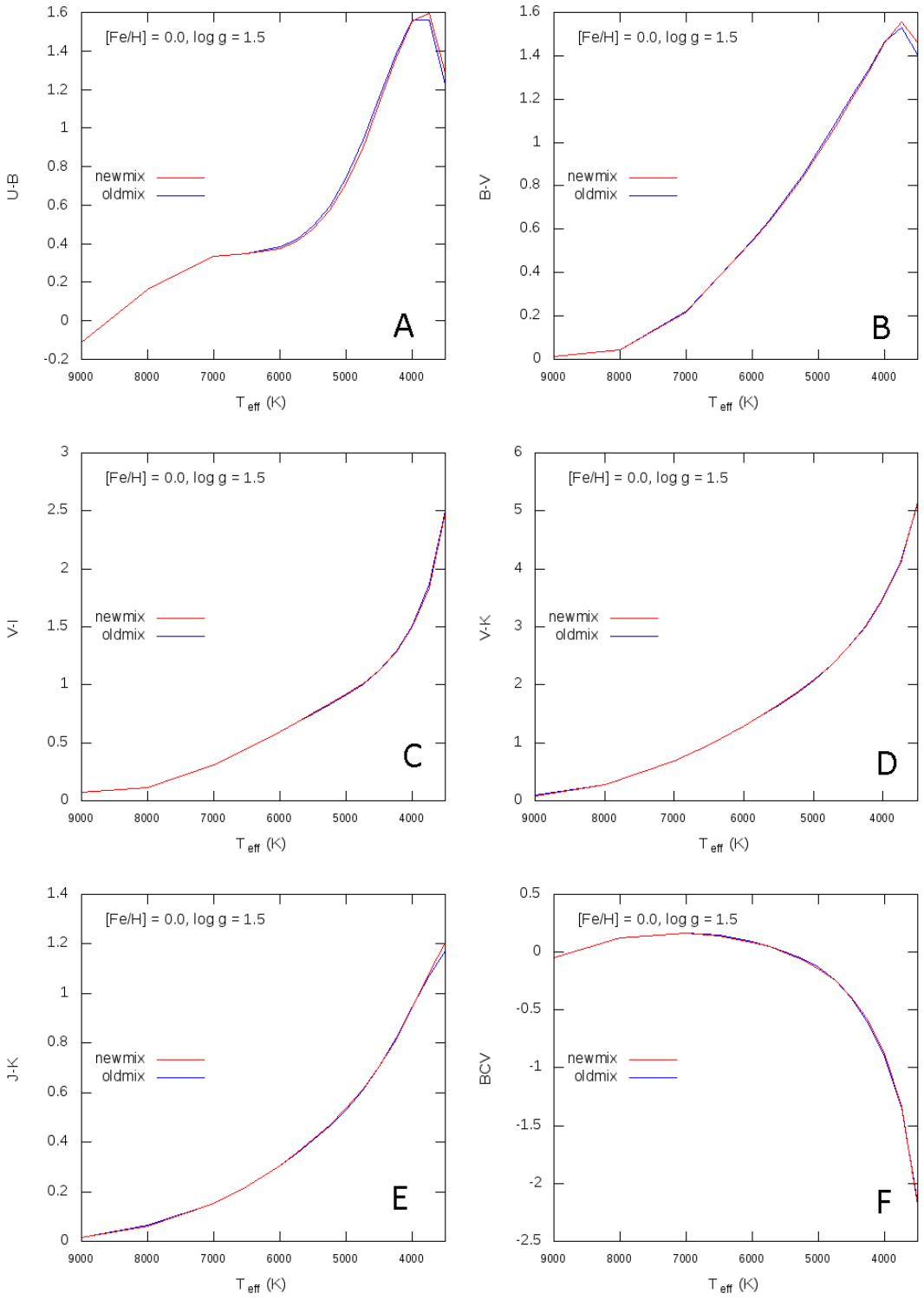

Figure 4.2.4 T_{eff}-colour relations for logg=1.5 and [Fe/H]=0.0 showing old-ODF models (blue) and new-ODF models (red) for five Johnson-Cousins-Bessell colour indices (A: U-B, B: B-V, C: V-I, D: V-K, E: J-K) and F: the bolometric correction in V.

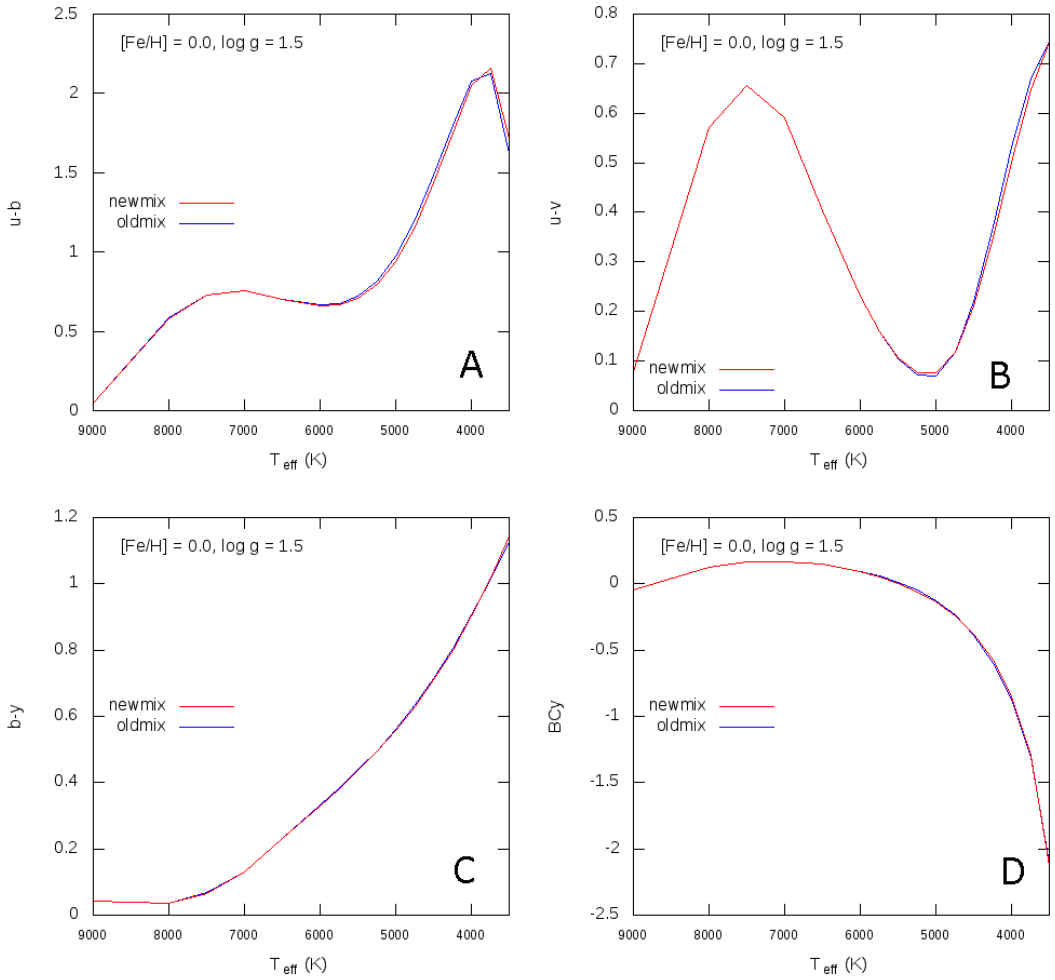

Figure 4.2.5 T_{eff}-colour relations for logg=1.5 and [Fe/H]=0.0 showing old-ODF models (blue) and new-ODF models (red) for three Strömgren colour indices (A: u-b, B: u-v and C: b-y) and D: the bolometric correction in y.

The Strömgren colour relations for giant stars (figure 4.2.5) show a similar pattern to the Johnson colour relations, with the new model producing u-b colours that are redder below 4250K, and bluer between 4250K and 6000K. The u-v colours show the opposite effect, the new model producing redder colours between 4750K and 6000K, and bluer colours below this temperature range. There is no difference in the b-y colour or the bolometric corrections in y or for the f300w UV filter (figure 4.2.3B).

4.3 Comparisons with empirical data

Worthey and Lee (2011) produced a collection of empirically derived data that was used to create colour-colour relations from Johnson/Cousins photometry, producing a table of colours and the V-band bolometric correction as a function of T_{eff}, [Fe/H] and log g. Worthey and Lee used this empirical data to produce an interpolation programme that can provide the values for colours for any input based on the empirically derived data (Worthey & Lee, 2011). This programme was used to create colour and bolometric corrections matching the parameters used to create the synthetic spectra with the Asplund *et al.* (2009) abundances. Figures 4.3.1 to 4.3.12 show the effective temperature colour relations for the scaled solar and alpha enhanced models at [Fe/H] = 0, -1 and -2 for four different gravities (log g 4.5, 3.0, 1.5 and 0.0), showing the calculated theoretical colour-temperature relations for U-B, B-V, V-I, V-K and J-K, along with the colour-bolometric correction for V, hereafter referred to as the 'computed' values and shown in blue for the scaled solar spectra and green for the alpha enhanced. These are compared with the empirical data obtained from the interpolation programme provided by Worthey and Lee (2011), hereafter referred to as the 'empirical' data and plotted with purple circles in the figures that follow.

4.3.1 T_{eff} U-B relations

Figures 4.3.1A – 4.3.4A shows the plots of U-B against T_{eff} for [Fe/H] = 0 for four different log g values. For log g 4.5 stars of T_{eff} above 8000K, the computed values agree with the empirical data within the error limits, but between 4750K and 8000K the computed values are redder than the empirical data, with a discrepancy of around 300K. Below 4750K the computed and empirical values diverge more, with a constant difference of 0.3 in U-B. With decreasing gravity, the computed values of U-B deviate from the empirical ones further. At log g of 3.0, the computed and empirical values agree within the error limits at 5250K to 6000K, but for hotter stars the computed values are bluer, and for cooler stars they are

redder. The computed values begin to show better agreement at temperatures above 10,000K, although this is outside of the parameters calculated for the lowest gravities. The computed values for log g 0.0 show the most deviation at 6000K, with a difference of up to 0.5 in the U-B values.

At a constant log g of 4.5, the computed values become more accurate at lower metallicities, (compare figures 4.3.1A, 4.3.5A and 4.3.9A), being within the error limits of the empirical data at temperatures above 4500K, and with only a discrepancy of around 200K at temperatures below this. However, figure 4.3.5A and 4.3.9A do show two other differences between the empirical and computed data. The computed relation for U-B at [Fe/H] = -1 and -2 does not show the same turn off at 3500K that the empirical data (and the computed data for [Fe/H] = 0) does, and the computed U-B value for stars at 9000K is significantly redder than the empirically derived value, and outside the uncertainty range.

At lower values of log g (3.0, 1.5 and 0.0) the divergence between the computed and empirical values does not change with decreasing metallicity; the values agree within the error limits at around 5250K, but for hotter stars the computed values are bluer, and for cooler stars they are redder (figures 4.3.2A, 4.3.3A, 4.3.4A, 4.3.6A, 4.3.7A, 4.3.8A, 4.3.10A, 4.3.11A, 4.3.12A).

4.3.2 T_{eff} B-V relations

Figures 4.3.1B – 4.3.4B shows the plots of B-V against T_{eff} for [Fe/H] = 0 for four different log g values. At a log g of 4.5 between 6000K and 7000K the computed values are within the error margins of the empirical values, and below this temperature range there is a discrepancy of around 200K, with the empirical values being hotter. At temperatures above 7000K, the empirical values become cooler than the calculated ones, by up to around 1000K (figure 4.3.1B).

Unlike for the U-B relations, there is no pattern between the discrepancies at different gravities for [Fe/H] = 0. At a log g of 3.0, the empirical values give a consistently redder colour in B-V than the computed ones, except at between 6000K and 800K where the computed values are within the error bars (figure 4.3.2B). At a log g of 1.5, the empirical data and computed values show good agreement (figure 4.3.3C), but this does not continue at log g of 0.0, where the empirical values are consistently around 250K cooler. There is no change in the B-V relation for log g 4.5 (figures 4.3.5B and 4.3.9B) or log g 3.0 (figures 4.3.6B and 4.3.10B) with decreasing metallicity, although the discrepancy becomes less for the very coolest stars (<4000K) at the lowest metallicity. This is also true at log g 1.5 (figure 4.3.7B and 4.3.11B) but not at log g 0.0 (figure 4.3.8B and 4.3.12B).

4.3.3 T_{eff} V-I relations

Figures 4.3.1C – 4.3.4C show the plots of V-I against T_{eff} for [Fe/H] = 0 for four different log g values. At a log g of 4.5 the computed values are within the error margins of the empirical values, and the computed and empirical values are in better agreement than either the U-B or B-V values. The only discrepancy occurs in stars above 12000K where the empirical values for V-I are around 0.1 bluer. The fit is equally good for log g of 3.0 (figure 4.3.2C) and log g of 1.5 (figure 4.3.3C), although at a log g of 0.0 (figure 4.3.4C) at temperatures above 5500K, the computed values are around 250K cooler than the empirical data. There is no change with decreasing gravity in the difference between the empirical and computed values for each log g value for the V-I; and the values remain in good agreement (figures 4.3.5C – 4.3.12C) except for the very coolest stars (3500K) where the empirical values have a V-I value around 0.3 greater.

4.3.4 T_{eff} V-K relations

Figures 4.3.1D – 4.3.4D show the plots of V-K against T_{eff} for [Fe/H] = 0 for four different log g values. In general, at a log g of 4.5 the synthetic colours are in good agreement with the empirically derived data, especially within the 4500K to 9000K range. This is to be expected

as the V-K colour is very insensitive to the metal abundance (Worthey & Lee, 2011). However, there are some small differences between the computed and derived values. Below 4500K the computed values are around 100K hotter than the corresponding empirical value at the same V-K. Above this range, however, the computed values give a cooler value than the empirical data, by up to 1000K. At the very hottest star plotted (20000K), however, the computed and empirical data are in good agreement (figure 4.3.1D).

There is no change in the V-K comparison between the computed and empirical data at log g 3.0 (figure 4.3.2D) and log g 1.5 (figure 4.3.3D) but at the lowest gravity log g 0.0 (figure 4.3.4D) there is only good agreement at 3750K; in all other cases the effective temperatures given by the computed data are about 150K cooler. The behaviour of the V-K relation does not change with decreasing metallicity for gravities of log g 4.5, 3.0 or 1.5, but at log 0.0 there are some differences. At lower metallicities the temperature at which the computed and empirical data are in agreement changes (3750K at [Fe/H]=0, 4250K at [Fe/H]=-1, and 4750K at [Fe/H]=-2) with the computed V-K values being bluer at temperatures below this.

4.3.5 T_{eff} J-K relations

Figures 4.3.1E – 4.3.4E show the plots of J-K against T_{eff} for [Fe/H] = 0 for four different log g values. At log g of 4.5 (figure 4.3.1E) the empirical and computed data are in close agreement, although below 5000K where the computed J-K values are redder and above this temperature they are slightly bluer. This pattern remains the same with decreasing gravity (figures 4.3.2E, 4.3.3E and 4.3.4E), and metallicity (figures 4.3.5E to 4.3.12E).

4.3.6 T_{eff} Bolometric Correction in V relations

Figures 4.3.1F – 4.3.4F shows the plots of BCV against T_{eff} for [Fe/H] = 0 for four different log g values. At log g of 4.5 (figure 4.3.1F) the empirical and computed data are in good

agreement at temperatures below 6000K, and again at temperatures between 10000K and 12000K. Between these ranges, the computed BCV values are around 0.07 greater than empirically derived ones and above 12000K the computed values are approximately 0.2 greater. There is no change in this relationship with decreasing gravity, although at log g 3.0 (figure 4.3.2F) above 10000K the computed values give a smaller BCV rather than a larger one.

There is also very little change with decreasing metallicity; at log g of 0.0 the computed values at [Fe/H] = -2 fit the empirical data slightly better than at [Fe/H] = 0, but not at other gravities.

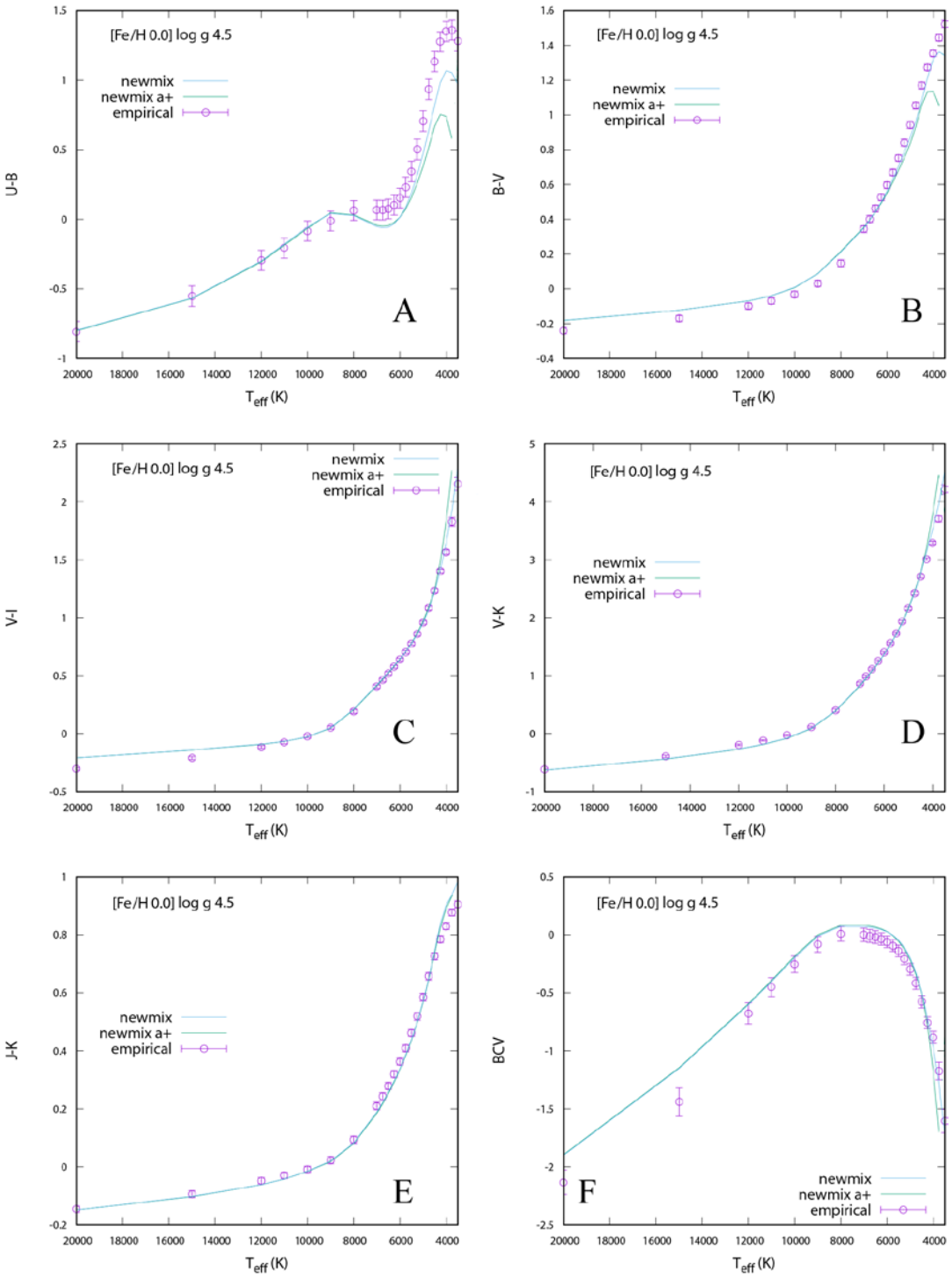

Figure 4.3.1 T_{eff}-colour relations for logg=4.5 and [Fe/H]=0.0 showing new-ODF models (blue lines), new alpha enhanced ODF models (green lines) and empirical data (purple circles) for five colour indices (A: U-B, B: B-V, C: V-I, D: V-K, E: J-K) and F: the bolometric correction in V.

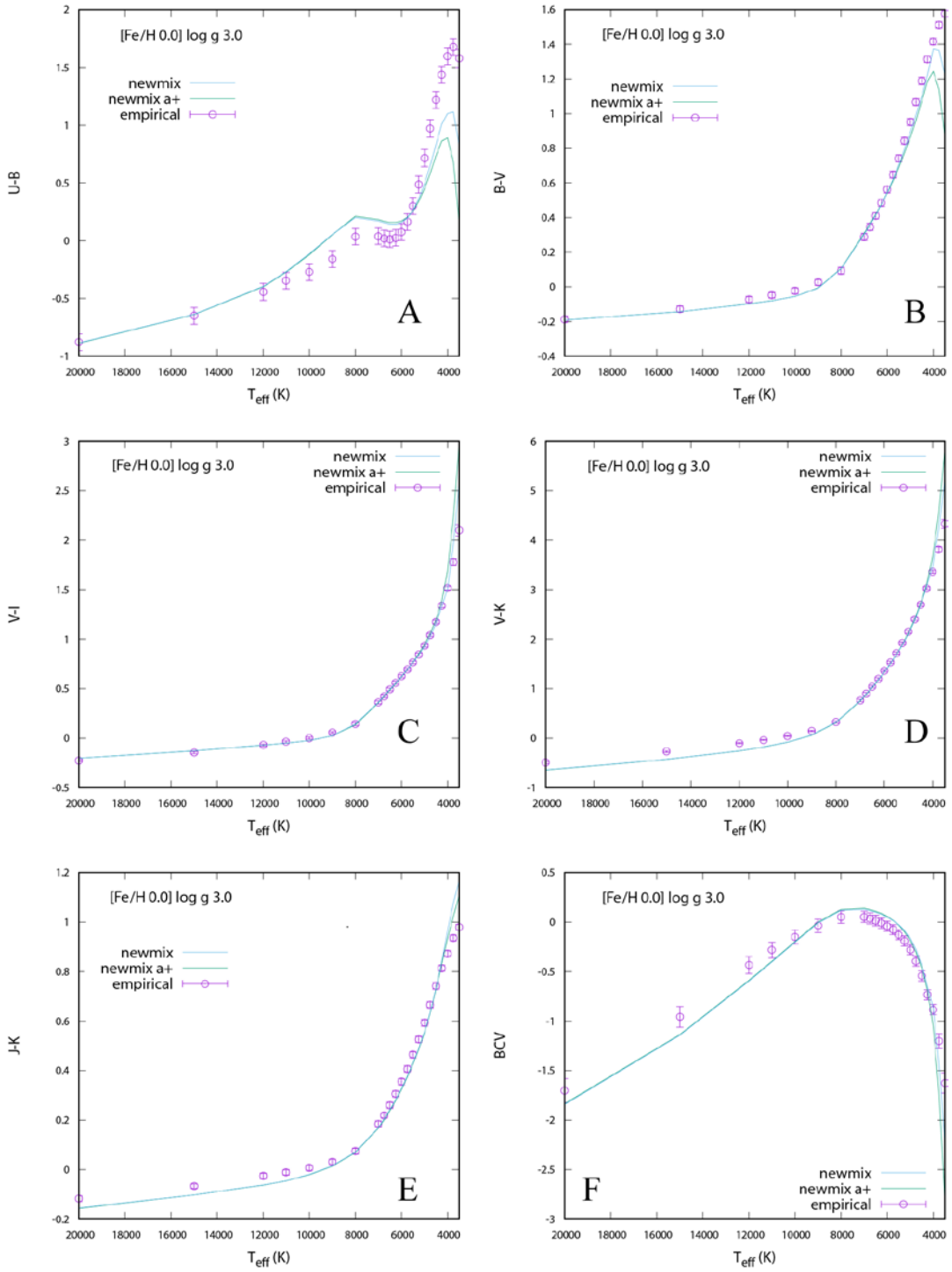

Figure 4.3.2 T_{eff}-colour relations for logg=3.0 and [Fe/H]=0.0 showing new-ODF models (blue lines), new alpha enhanced ODF models (green lines) and empirical data (purple circles) for five colour indices (A: U-B, B: B-V, C: V-I, D: V-K, E: J-K) and F: the bolometric correction in V.

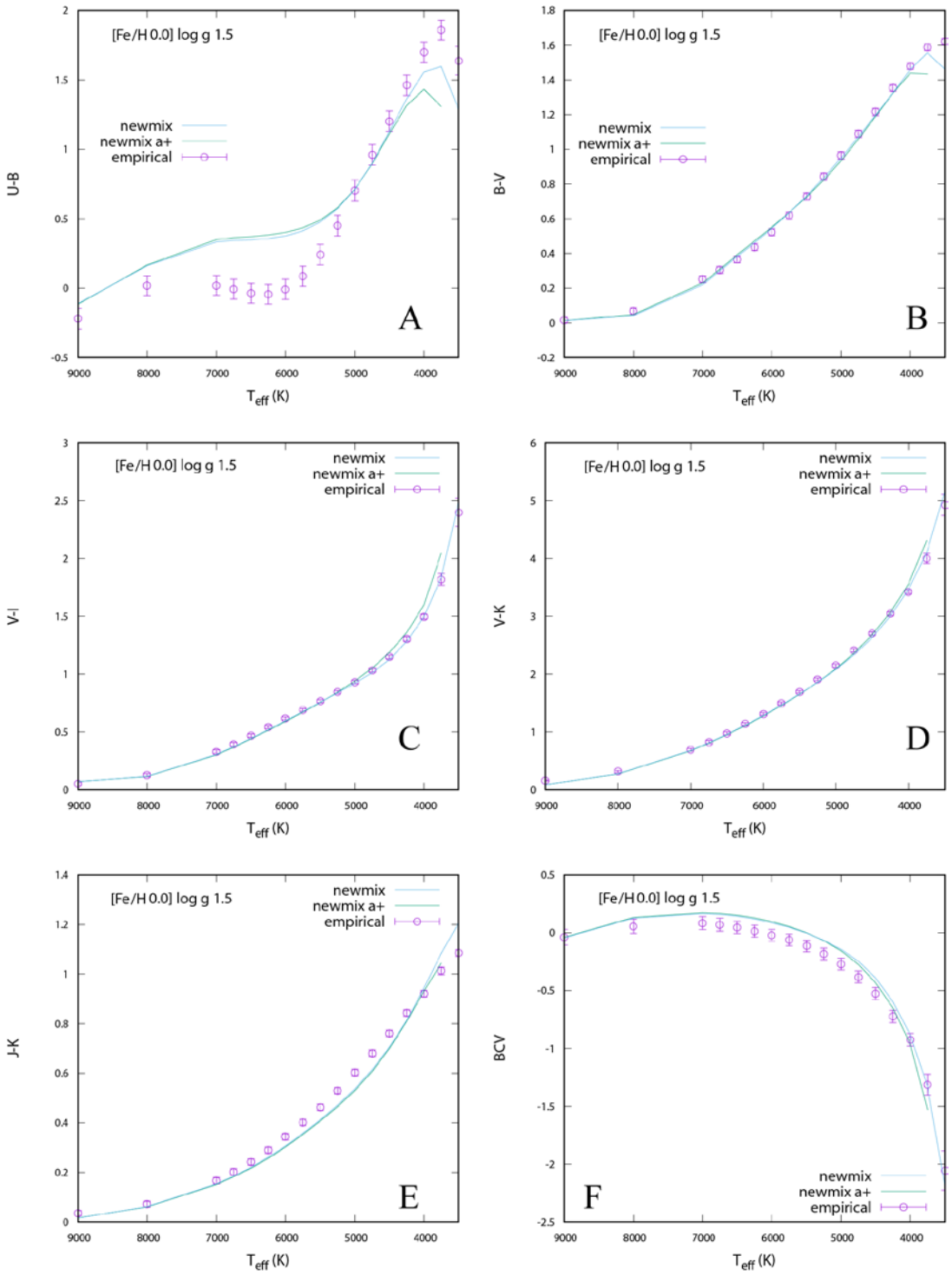

Figure 4.3.3 T_{eff}-colour relations for logg=1.5 and [Fe/H]=0.0 showing new-ODF models (blue lines), new alpha enhanced ODF models (green lines) and empirical data (purple circles) for five colour indices (A: U-B, B: B-V, C: V-I, D: V-K, E: J-K) and F: the bolometric correction in V.

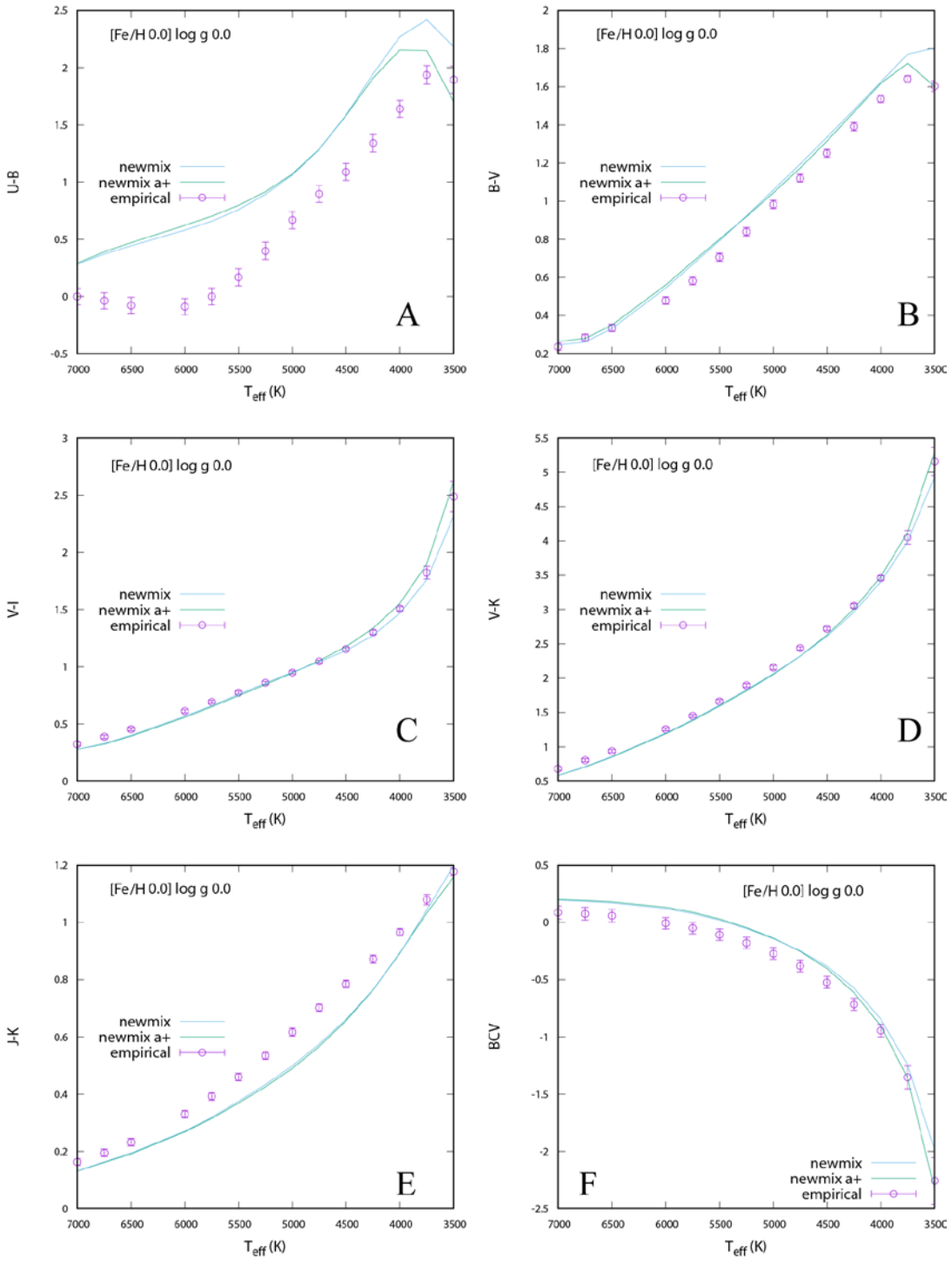

Figure 4.3.4 T_{eff}-colour relations for logg=0.0 and [Fe/H]=0.0 showing new-ODF models (blue lines), new alpha enhanced ODF models (green lines) and empirical data (purple circles) for five colour indices (A: U-B, B: B-V, C: V-I, D: V-K, E: J-K) and F: the bolometric correction in V.

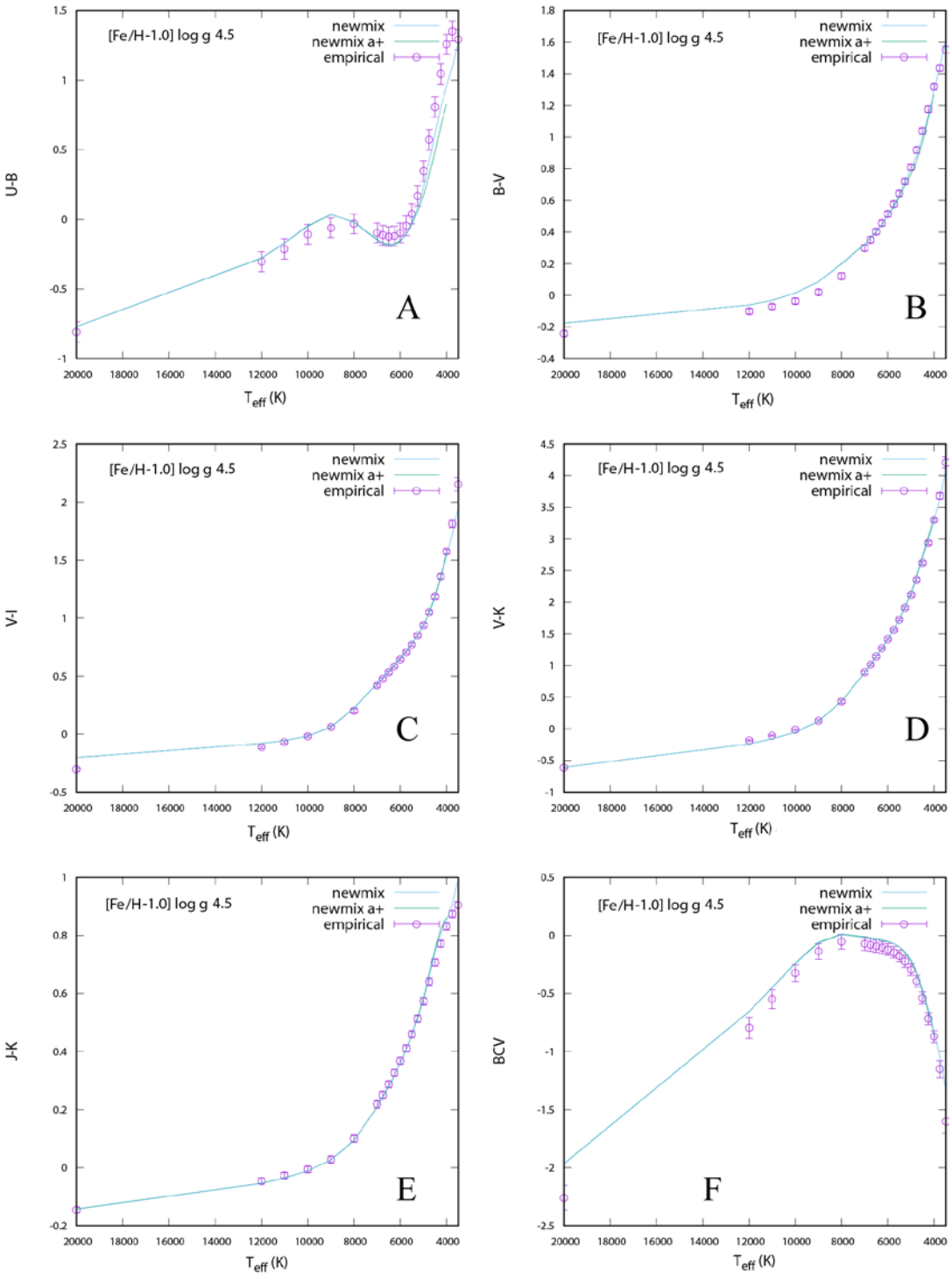

Figure 4.3.5 T_{eff}-colour relations for logg=4.5 and [Fe/H]=-1.0 showing new-ODF models (blue lines), new alpha enhanced ODF models (green lines) and empirical data (purple circles) for five colour indices (A: U-B, B: B-V, C: V-I, D: V-K,E: J-K) and F: the bolometric correction in V.

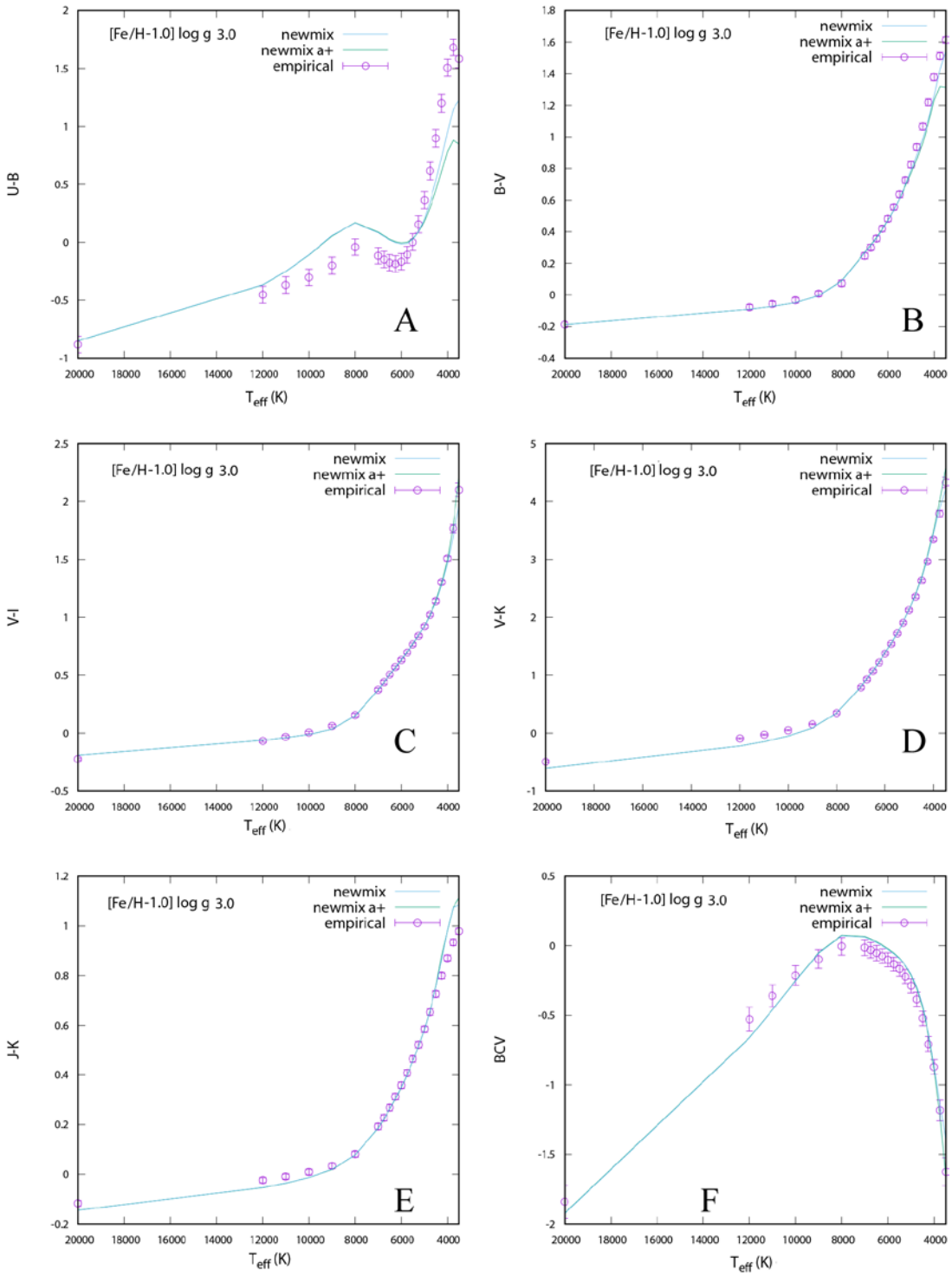

Figure 4.3.6 T_{eff}-colour relations for logg=3.0 and [Fe/H]=-1.0 showing new-ODF models (blue lines), new alpha enhanced ODF models (green lines) and empirical data (purple circles) for five colour indices (A: U-B, B: B-V, C: V-I, D: V-K,E: J-K) and F: the bolometric correction in V.

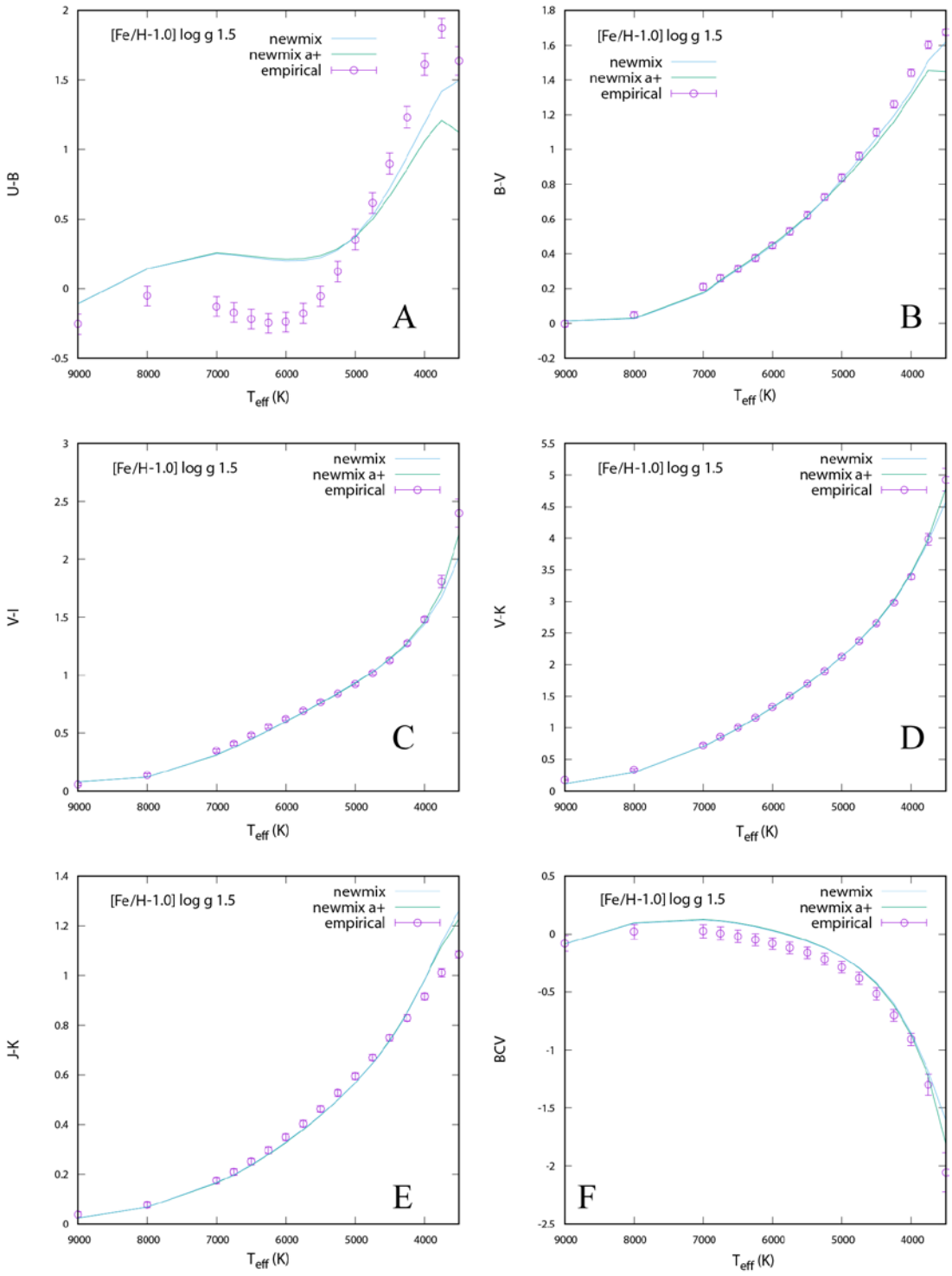

Figure 4.3.7 T_{eff}-colour relations for logg=1.5 and [Fe/H]=-1.0 showing new-ODF models (blue lines), new alpha enhanced ODF models (green lines) and empirical data (purple circles) for five colour indices (A: U-B, B: B-V, C: V-I, D: V-K,E: J-K) and F: the bolometric correction in V.

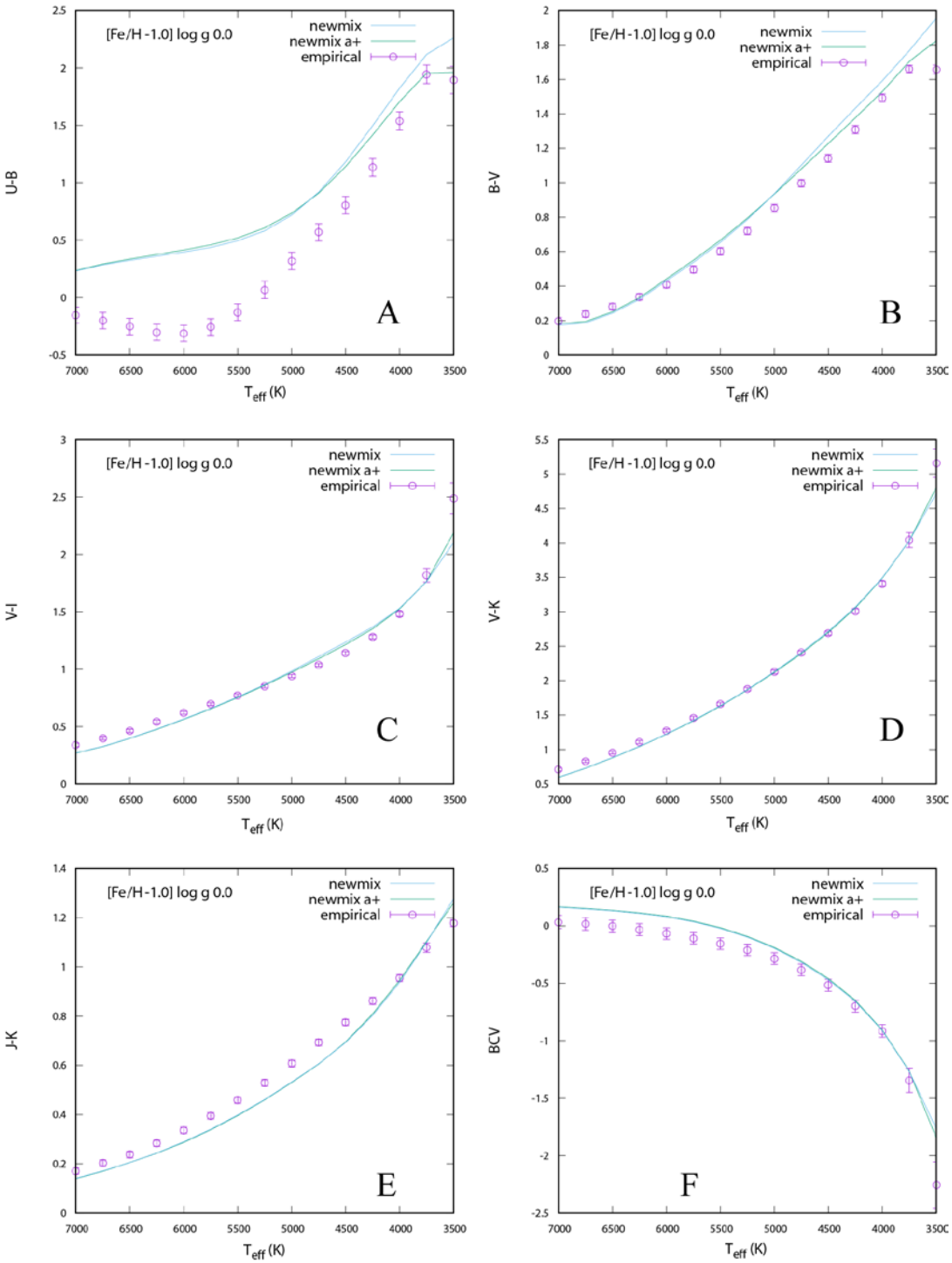

Figure 4.3.8 T_{eff}-colour relations for logg=0.0 and [Fe/H]=-1.0 showing new-ODF models (blue lines), new alpha enhanced ODF models (green lines) and empirical data (purple circles) for five colour indices (A: U-B, B: B-V, C: V-I, D: V-K,E: J-K) and F: the bolometric correction in V.

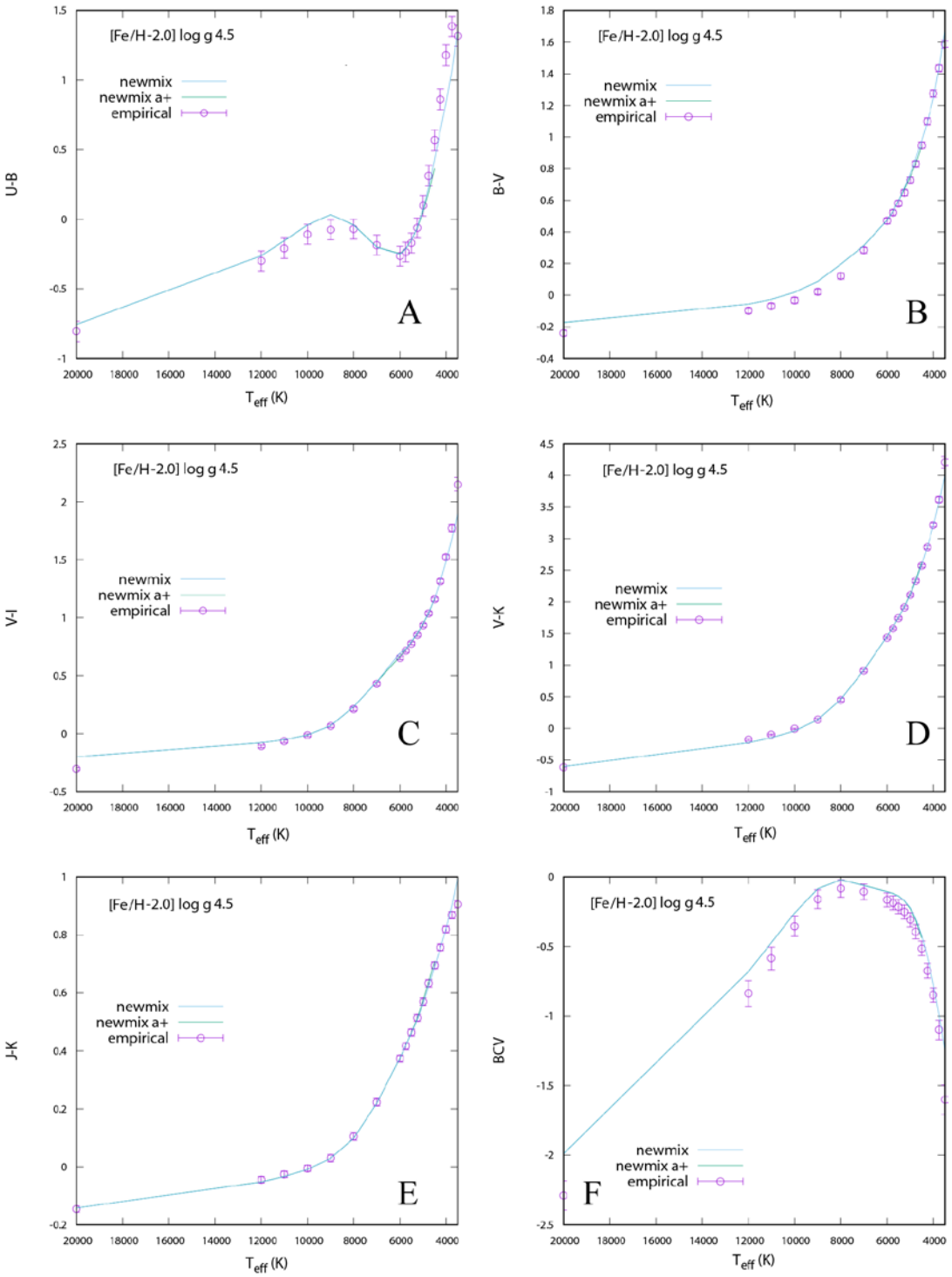

Figure 4.3.9 T_{eff}-colour relations for logg=4.5 and [Fe/H]=-2.0 showing new-ODF models (blue lines), new alpha enhanced ODF models (green lines) and empirical data (purple circles) for five colour indices (A: U-B, B: B-V, C: V-I, D: V-K,E: J-K) and F: the bolometric correction in V.

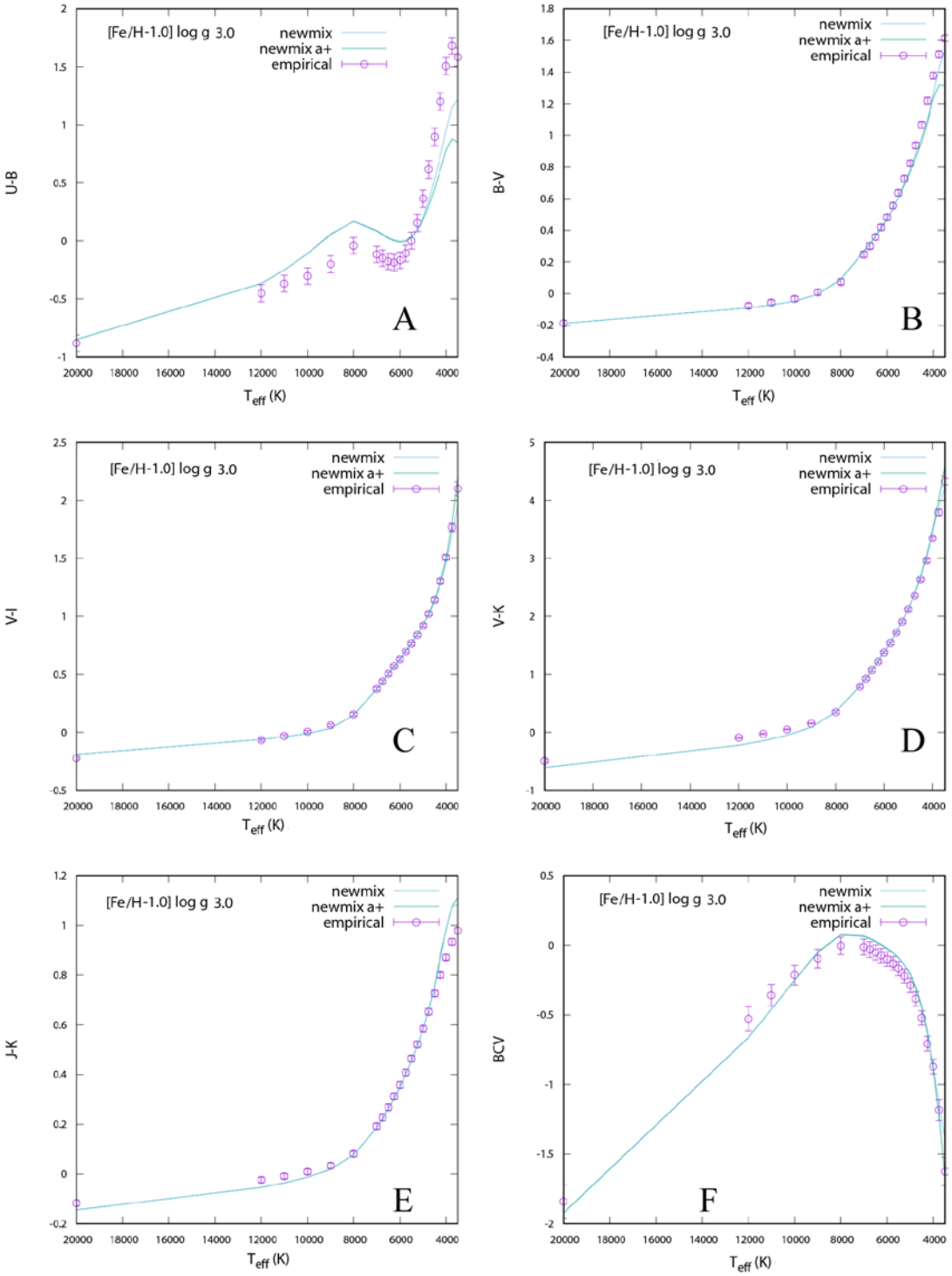

Figure 4.3.10 T_{eff}-colour relations for logg=3.0 and [Fe/H]=-2.0 showing new-ODF models (blue lines), new alpha enhanced ODF models (green lines) and empirical data (purple circles) for five colour indices (A: U-B, B: B-V, C: V-I, D: V-K,E: J-K) and F: the bolometric correction in V.

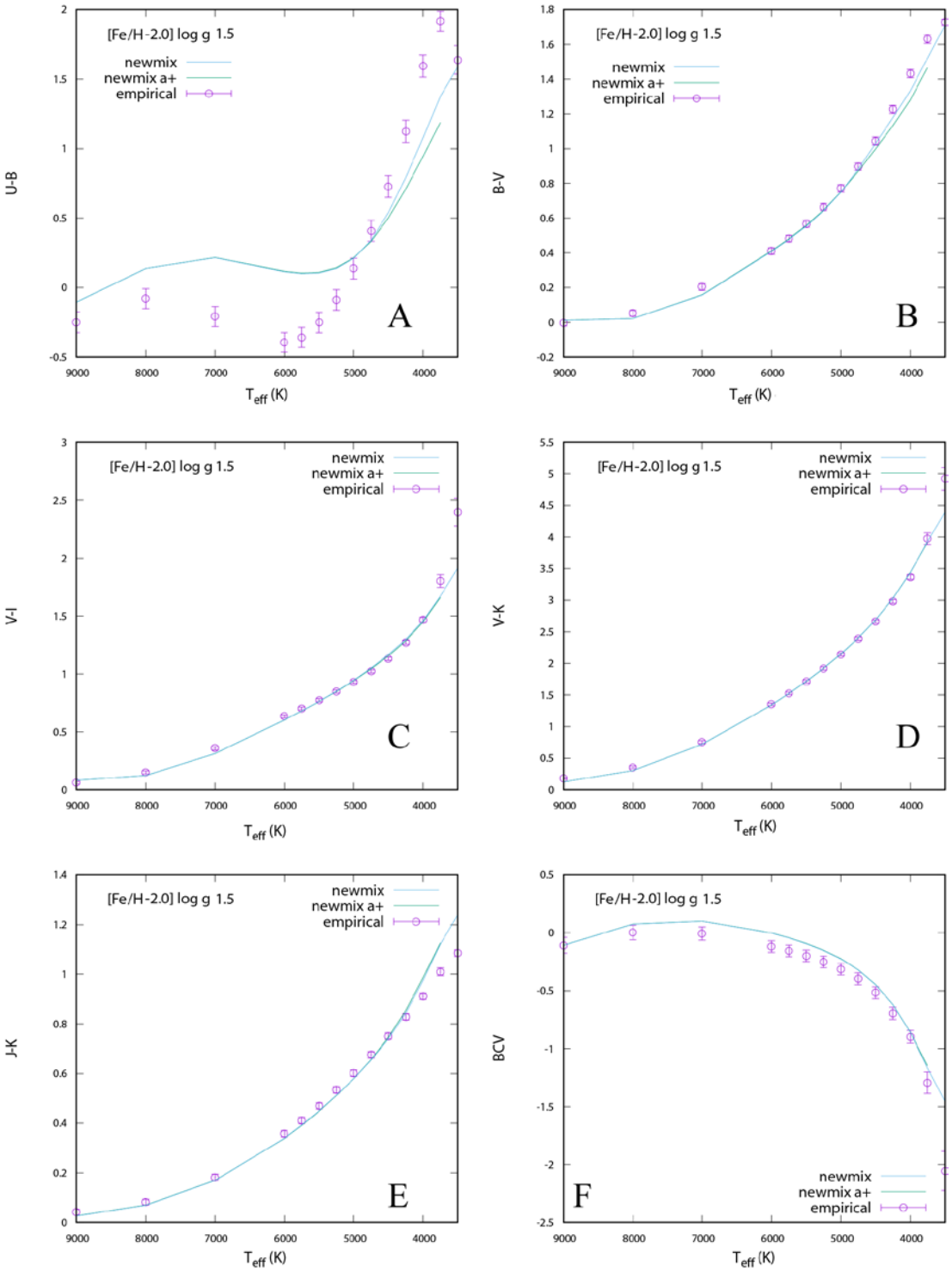

Figure 4.3.11 T_{eff}-colour relations for logg=1.5 and [Fe/H]=-2.0 showing new-ODF models (blue lines), new alpha enhanced ODF models (green lines) and empirical data (purple circles) for five colour indices (A: U-B, B: B-V, C: V-I, D: V-K,E: J-K) and F: the bolometric correction in V.

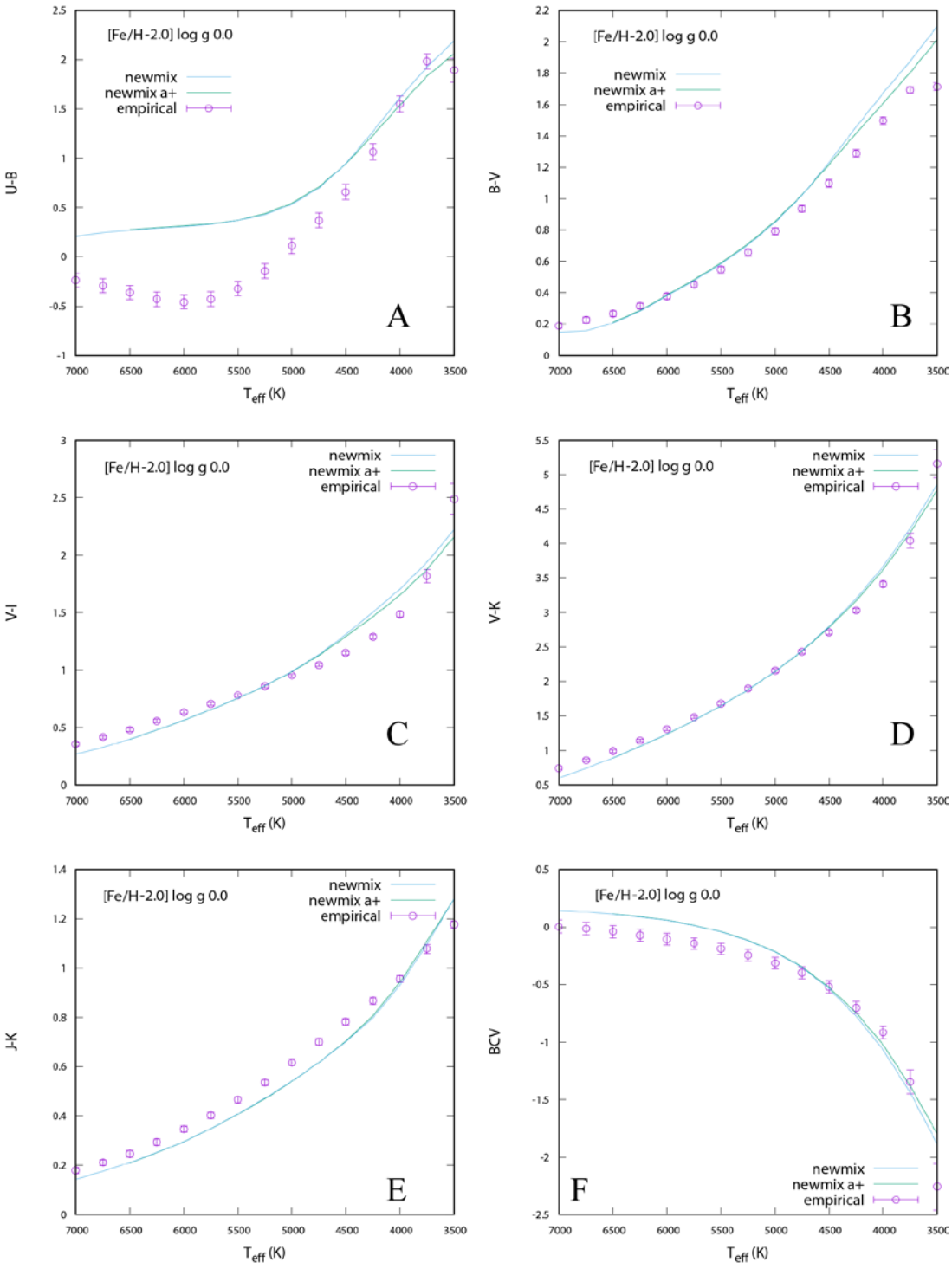

Figure 4.3.12 T_{eff}-colour relations for logg=0.0 and [Fe/H]=-2.0 showing new-ODF models (blue lines), new alpha enhanced ODF models (green lines) and empirical data (purple circles) for five colour indices (A: U-B, B: B-V, C: V-I, D: V-K,E: J-K) and F: the bolometric correction in V.

4.4 Comparisons between scaled solar and alpha enhanced colour transformations and bolometric corrections

While the scaled solar models of heavy element abundances are appropriate for use in many cases, there are certain populations of stars, such as globular clusters and field stars in the Galactic Halo, where it is more accurate to use the alpha enhanced models (Cassisi *et al.*, 2005). Cassisi *et al.* (2005) investigated the effects of using alpha enhanced theoretical model atmospheres (using the Grevesse and Sauval (1998) abundance values) on the colour transformations and bolometric corrections, and found that for low [Fe/H] values (~2) the scaled solar and alpha enhanced models were in good agreement, but as metallicity and temperature increase, the B-V and U-B alpha enhanced colours become progressively bluer than the equivalent scaled solar ones.

In this project, the calculated theoretical colour-temperature relations for U-B, B-V, V-I, V-K and J-K, along with the colour-bolometric correction for V, have been produced for both scaled solar spectra (blue) and alpha enhanced [α/Fe] = 0.4 (green), based on the models created with the Asplund *et al.* (2009) abundances. As can be seen from figures (4.3.1 – 4.3.12) the differences between the calculated scaled solar and alpha enhanced values are much less than the differences between the calculated scaled solar and empirically determined values.

4.4.1 T_{eff} U-B and B-V relations

Figures 4.3.9A – 4.3.12A shows the plots of U-B against T_{eff} for [Fe/H] = -2.0 for four different log g values. At this low metallicity, the values for the scaled solar and alpha enhanced models are identical at temperatures above 5000K, and below this value the alpha enhanced colours become bluer with decreasing temperature. This effect is seen regardless of the log g of the model, although unfortunately, the ATLAS9 programme did

not produce acceptable models at the lowest temperatures for [Fe/H] = -2.0, log g 4.5 or log g 1.5 (see table 2.4.2).

With increasing metallicity at [Fe/H] = -1.0 (Figures 4.3.5A – 4.3.8A) and [Fe/H] = 0.0 (Figures 4.3.1A – 4.3.4A, the differences in the U-B colour become more pronounced, with the alpha enhanced models being significantly bluer at temperatures below 5000K. However, at lower gravities (log g 1.5 and log g 0.0) there is a region between 5500K and 7000K where the alpha enhanced values are slightly redder than their scaled solar equivalent, and this discrepancy increases with decreasing gravity (see figures 4.3.8A and 4.3.12A).

Comparing the scaled solar and alpha enhanced values for the B-V colours shows a similar pattern to the U-B colours; the two colour values are identical above 5000K and differences only appear below this value, with the alpha enhanced colours being bluer than the equivalent scaled solar one. The differences in colour increase with decreasing effective temperature, and with decreasing gravity (figures 4.3.1B – 4.3.12B).

4.4.2 T_{eff} V-I, V-K and J-K relations

In the other colour bands investigated (V-I, V-K and J-K) there is a much less of a difference between the scaled solar and alpha enhanced colours, which is expected as these colours only have a weak dependence on the metal content of the mixture (Cassisi *at al.,* 2005). However, there are some differences at the lowest effective temperatures (<4000K) with the alpha enhanced colours being slightly redder than the scaled solar ones in the V-I and V-K colours, and slightly bluer in J-K. This difference increases with increasing metallicity and decreasing gravity (figures 4.3.1C – 4.3.1F).

Chapter 5

Conclusions and Further Work

Comparisons between the synthetic spectra and the colour transformations of the stellar atmosphere models produced by the Asplund *et al.* (2009) abundances, and those produced by the Grevasse and Sauval (1998) abundances, have shown that the different solar abundances do not affect the models to any great degree. There are only any significant differences in the energy distribution of the spectra at the coolest temperatures of stars studied (3500K – 4500K), although changes in the depth of some specific spectral lines can be seen at higher temperatures.

For models with an effective temperature less than 4500K, the colour indices U-B, B-V and u-b produced by using the new abundance values are redder than the indices produced by the old values, but there is little difference in the other indices studied. Comparisons between the colour indices calculated using the new abundances and the empirically derived values show a good general agreement for main sequence stars regardless of the metallicity, but this agreement is less for giant stars.

The full grid of models and synthetic stellar spectra calculated with the Asplud *et al.* (2009) abundances will be made publicly available, and can be used in stellar evolution and population synthesis databases. Further work can be done in future by calculating models with different microturbulence velocities; Casagrande and VandenBerg (2014) state that supergiant stars can have values of up to $\xi = 5 kms^{-1}$, and this could be worth investigating to see whether the atmospheric models and colour transformations produced for giant stars with higher microturbulence values are more similar to the empirically derived values.

Additionally, the solar metal abundance is being constantly revised as new work is done (e.g Scott *et al.,* 2014), and as new, more accurate, values of the abundance of each

element is determined, it is important to continually check if these changes to the solar abundances have any significant effects when used as inputs to stellar models.

References

Allard, F., Hauschildt, P. H., and Schwenke, D. *TiO and H_2O Absorption Lines in Cool Stellar Atmospheres.* The Astrophysical Journal, 540. 1005-1015. **2010.**

Anders, E. & Grevesse N. *Abundances of the elements: Meteoric and solar.* Geochimica et Cosmochimica Acta, Vol 53, pp 197-214. **1989.**

Asplund, M., Grevesse, N. and Sauval, A. *The Solar Chemical Composition.* Astronomical Society of the Pacific Conference Series, 366. 25. **2005**.

Asplund, M., Grevesse, N., Jacques Sauval, A. and Scot P. *The Chemical Composition of the Sun.* Annual Review of Astronomy and Astrophysics, 47: 481-522, **2009**.

Bessell, M.S., Castelli, F. and Plez, B. *Model atmospheres broad-band colors, bolometric corrections and temperature calibrations for O – M stars.* Astronomy and Astrophysics, 333, 231-250, **1998.**

Bessell, M. S. *Standard Photometric Systems.* Annu. Rev. Astron. Astrophys. 43: 293-336. **2005.**

Caffau, E., Ludwig, H-G., Steffan, M., Freytag, B. and Bonifacio, P. *Solar Chemical Abundances Determined with a CO5BOLD 3D Model Atmosphere.* Solar Physics, 268: 2: 255-269, **2011**.

Casagrande, L. and VandenBerg, D.A. *Synthetic Stellar Photometry – I. General considerations and new transformations for broad-band systems.* MNRAS. **2014.** arXiv:1407.6095v2

Cassisi, S., Potekhin, A. Y., Pietrinferni, A., Catelin, M. and Salaris, M. *Updated Electron-Conduction Opacities: The Impact on low-mass stellar models.* The Astrophysical Journal, 661:1094-1104, **2007**.

Cassisi, S., Salaris, M., Castelli, F. and Pietrinferni, A. *Color Transformations and Bolometric Corrections for Galactic Halo Stars a-enhanced versus Scaled-Solar results.* Astrophysical Journal, 616, 498-505, **2004**.

Castelli, F. *Kurucz's models, Kurucz's fluxes and the Atlas code.* Osservatorio Astronomico di Trieste. Pubblicazione O.A.T. N. 1164, **1998.**

Castelli, F., Gratton, R.G., and Kurucz, R.L. *Notes on the convection in the ATLAS9 model atmospheres.* AStron. Astrophys. 318, 841-869. **1997.**

Castelli, F. *Synthetic photometry from ATLAS9 models in the UBV Johnson system.* Astronomy and Astrophysics. 346, 564-585, **1999**.

Castelli, F. *DFSYNTHE: how to use it.* Mem. S.A.It Suppl. Vol 8, 34. **2005.**

Castelli, F. and Kurucz, R. *Model atmospheres for Vega.* Astronomy & Astophysics, 281, 817-832. **1994**.

Castelli, F. and Kurucz, R. *New Grids of ATLAS9 Model Atmospheres*. **2004**. arXiv:astro-ph/0405087v1

Cordier, D., Pietrinferni, A., Cassisi, S. and Salaris, M. *A Large Stellar Evolution Database for Population Synthesis Studies. III. Inclusion of the full asymptotic giant branch phase and web tools for stellar population analyses.* The Astronomical Journal, 133: 468-478, **2007**.

Dotter, A. *MESA isochrones and Stellar Tracks (MIST) 0: Methods for the Construction of Stellar Isochrones.* The Astrophysical Journal Supplement Series, Volume 222, Issue 1, article id. 8, 11 pp. **2016**.

Girardi, L., Bertelli, G., Bressan, A., Chiosi, C., Groenewegen, M.A.T., Marigo, P., Salasnich, B. and Weiss, A. *Theoretical isochrones in several photometric systems.* Astronomy and Astrophysics 391, 195-212, **2002**.

Grevesse, N., and Sauval, A.J. *Standard Solar Composition*. Space Science Reviews, 85, 1-2, 161-174, **1998**.

Gustafsson, B., Edvardsson, B., Eriksson, K., Jorgensen, U. G., Nordlund, A. and Plez, B. *A grid of MARCS model atmospheres for late-type stars I. Methods and general properties*, **2008**. arXiv:0805.0554

Hubeny, I. and Lanz, T. *A brief introductory guide to TLUSTY and SYNSPEC,* **2017.** arXiv:1706.01859

Hubeny, I. and Mihalas, D. *Theory of Stellar Atmospheres. An Introduction to Astrophysical Non-equilibrium Quantitative Spectroscopic Analysis.* **2015.** Princeton. ISBN: 9780691163291.

Husser, T-O., Wende-von Berg, S., Dreizlert, S., Homeier, D., Reiners, A., Barman, T. and Huschildt, P. H. *A new extensive library of PHOENIX stellar atmospheres and synthetic spectra*, **2013**. arXiv:1303.5632

Kirby, E. *Grids of ATLAST9 Model Atmospheres and MOOG Synthetic Spectra*. **2011.** arXiv:1103.1385v1

Kramida, A., Ralchenko, Yu., Reader, J. and NIST ASD Team (2018). NIST Atomic Spectra Database (ver. 5.5.6), [Online]. Available: https://physics.nist.gov/asd [2018, September 16]. National Institute of Standards and Technology, Gaithersburg, MD.

Kurucz, R. L. ATLAS: A computer program for calculating model stellar atmospheres. SAO Special Report 309. Smithsonian Institution. **1970.**

Kurucz, R. L. *Model Atmospheres for Population Synthesis.* In The Stellar Populations of Galaxies (225-232). Barbuy B. and Renzini, A. (eds). IAU. **1992**.

Kurucz, R. L. *Diatomic Molecular Data for Opacity Calculations.* Revista Mexicana de Astronomia y Astrofisica, 23, 45. **1993**.

Kurucz, R. L. *Status of the ATLAS12 Opacity Sampling Program and of New Programs for Rosseland and for Distribution Function Opacity.* M.A.S.S.; Model Atmospheres and Spectrum Synthesis ASP Conference Series, Vol 108; 1996; ed. S. J. Adelman, F. Kupka and W. W. Weiss. **1996.**

Kurucz, R. L. *Model Atmosphere Codes: ATLAS12 and ATLAS9.* **2005A**. http://kurucz.harvard.edu/ papers/wroclawcodes/atlas9atlas12.pdf

Kurucz, R. L. *How to build a model atmosphere.* **2005B.** http://kurucz.harvard.edu/papers/ wroclawhowto/howtosv.pdf

Kurucz, R. L. *Atlas12, Synthe, Atlas9, Width9, et cetera.* Memorie della Società Astronomica Italiana Supplement, v.8, p.14 **2005C.**

Lanz, T. and Hubeny, I. *A Grid of non-LTE linked blanketed model atmospheres of O-type stars.* The Astrophysical Journal Supplement Series, 136:417-441. **2003.**

Jørgensen, U.G. *Sampling Methods.* Rev. Mexicana Astron Astrof, 23, 195-202. **1992**.

Meszaros, Sz., Allende Prieto, C., Edvardsson, B., Castelli, F., Garcia Perez, E., Gustafsson, B., Majewski, S.R., Plez, B., Schiavon, R., Shetrone, M. and de Vicente, A. *New ATLAS9 and*

MARCS model atmosphere grids for the apache point observatory galactic evolution experiment (APOGEE). Astronomical Journal, **2012**.

Pietrinferni, A., Cassisi, S., Salaris, M. and Castelli, F. A *Large Stellar Evolution Database for Population Synthesis Studies. I. Scaled Solar models and isochrones.* The Astrophysical Journal, 612: 168-190, **2004.**

Pietrinferni, A., Cassisi,S., Salaris, M. and Castelli, F. *A Large Stellar Evolution Database for Population Synthesis Studies. II. Stellar models and isochrones for an [el]enhanced metal distribution.* The Astrophysical Journal, 642: 797-812, **2006**.

Pietrinferni, A., Cassisi, S. and Salaris, M. *The impact of an updated $^{14}N(\rho,\gamma)^{15}O$ reaction rate on advanced evolutionary stages of low-mass stellar models.* Astronomy and Astrophysics, 522, A76, 7, **2010**.

Salaris, M. and Cassisi, S. *Evolution of Stars and Stellar Populations.* **2005.** John Wiley & Sons, Ltd.

Salaris, M., Cassisi, S., Pietrinferni, A., Kowalski, P. M. and Isern J. *A Large Stellar Evolution Database for Population Synthesis Studies, VI. White Dwarf Cooling Sequences.* The Astrophysical Journal, 716, 1241-1251, **2010**.

Salaris, M., Percival, S., Cassisi, S. and Pietrinferni, A. *Population synthesis models and the VO.* Memorie della Società Astronomica Italiana, v.80, p.387, **2009.**

Sbordone, L., Bonifacio, P. *Atlas Cookbook.* **2005.** http://atmos.obspm.fr/index.php/documentation/7

Sbordone, L., Bonifacio P. and Castelli, F. *Atlas 9 and Atlas 12 under GNU-Linux.* Convection in Astrophysics, Proceedings IAU Symposium No. 239, **2006**. F. Kupka, I. W. Roxburgh and K. L. Chan (eds). doi:10.10.17/S1743921307000142

Scott, P., Grevesse, N., Asplund, M., Sauval, A.J., Lind, K., Takeda, Y., Collet, R., Trampedach, R. and Hayek, W. *The elemental composition of the Sun. I. The intermediate mass elements Na to Ca.* Astronomy and Astrophysics, **2014**. arXiv:1405.0279v1

Scott, P., Asplund, M., Grevesse, N., Bergemann, M., and Sauval, A.J. *The elemental composition of the Sun. II. The iron group elements Sc to Ni.* Astronomy and Astrophysics, **2014**. arXiv:1405.0287v1

Smalley, B. *Teff and log g Determinations.* **2005.** arXiv:astro-ph/0509535

VandenBerg, D. A., Bergbusch, P.A., Dotter, A., Ferguson, J. W., Michaud, G., Richer, J. and Proffitt, C.R. *Models for Metal-Poor stars with Enhanced Abundances of C, N, O, Ne, Na, Mg, Si, S, Ca, and Ti, in turn, at Constant Helium and Iron Abundances.* The Astrophysical Journal, 755, 1. **2012.**

VandenBerg, D. A. *The effects of physics and chemical-abundance uncertainties on the properties of lower-mass stars that are used as standard candles.* Advancing the Physics of Cosmic Distances Proceedings IAU Symposium No. 289, **2012.**

Worthey, G. and Lee, H-c. *An Empirical Color-Temperature Calibration for Stars*. Astrophys.J.Suppl. 193:1, **2011**. arXiv:astro-ph/0604590.